uOttawa

L'Université canadienne
Canada's university

FACULTÉ DES ÉTUDES SUPÉRIEURES ET POSTOCTORALES

uOttawa

L'Université canadienne
Canada's university

FACULTY OF GRADUATE AND POSDOCTORAL STUDIES

Shirine Jeradi

AUTEUR DE LA THÈSE / AUTHOR OF THESIS

M.Sc. (Cellular and Molecular Medicine)

GRADE / DEGREE

Department of Cellular and Molecular Medicine

FACULTÉ, ÉCOLE, DÉPARTEMENT / FACULTY, SCHOOL, DEPARTMENT

Understanding the Role of the *shha*-expressing Cells During Zebrafish Caudal Fin Regeneration

TITRE DE LA THÈSE / TITLE OF THESIS

Marie-Andrée Akimenko

DIRECTEUR (DIRECTRICE) DE LA THÈSE / THESIS SUPERVISOR

CO-DIRECTEUR (CO-DIRECTRICE) DE LA THÈSE / THESIS CO-SUPERVISOR

Anne-Gaëlle Rolland-Lagan

Max Hincke

Gary W. Slater

Le Doyen de la Faculté des études supérieures et postdoctorales / Dean of the Faculty of Graduate and Postdoctoral Studies

Understanding the role of the *shha*-expressing cells during zebrafish caudal fin regeneration

Shirine JERADI

Thesis submitted to the Faculty of Graduate and Postdoctoral Studies in partial fulfillment of the requirements for the degree of

Master of Science

In Cellular and Molecular Medicine

Department of Cellular and Molecular Medicine
Faculty of Medicine
University of Ottawa

Your file Votre référence
ISBN: 978-0-494-79700-6
Our file Notre référence
ISBN: 978-0-494-79700-6

Cette thèse est dédiée à 'Jeddi', mon grand-père, qui a consacré sa vie à sa famille et au savoir, et à mon frère, Mahmoud, pour qui je serai toujours présente.

Abstract

Zebrafish is able to regenerate its fins following amputation. We are interested in elucidating the cellular and molecular events that are underlying regeneration of the bones of the fin rays. Previous studies from our laboratory showed that genes involved in the Hedgehog Hh pathway are re-expressed during fin regeneration. In addition, gain and loss of function experiments previously showed that Hedgehog signalling might be involved in regenerate outgrowth and osteoblasts differentiation and patterning. Two members of the *hedgehog* gene family are expressed during fin regeneration: *ihha* (*Indian Hedgehog*) is expressed in the newly differentiated osteoblasts, while *shha* (*Sonic Hedgehog*) is expressed in a small domain of the basal epidermal layer in the differentiation zone.

To understand the specific role of the *shha*-expressing cells, we precisely monitored these cells during the process of branching morphogenesis, using the transgenic line *2.4shha:GFPABC#15*. We subsequently defined 3 stages that are successively taking place during the formation of the branches in the regenerating fin ray. We also assessed the expression profile of genes that might be involved in potential cross-talks between HH/FGF signalling during fin ray regeneration.

Shh has been shown to play a role during branching morphogenesis in different organs that branche, through inducing cell proliferation. We analysed the cell proliferation profile during branching morphogenesis in the regenerating fin rays, and we suggest that *shha*-expressing cells might regulate the proliferation rate during branching morphogenesis.

Previous results obtained from laser ablation experiments, where the transgenic line *2.4shha:gfp:ABC*#15 was used to specifically but transiently ablate the *shha*-expressing cells using a laser beam showed that the transient absence of the *shha* –expressing cells from the regenerating ray results in a branching delay. Based on this finding, along with our results from cell proliferation analysis, and the time course analysis of the *shha*-expressing cells during branching morphogenesis, we propose a model for branches formation during fin regeneration, in which the splitting of *shha* –expressing cells govern branches formation.

We also elaborated a new approach based on the generation of a transgenic line expressing the nitroreductase in the *shha*-expressing cells, through which we aim to conditionally ablate these cells in the fin regenerate by addition of the prodrug, metronidazole. This will allow us to maintain the absence the *shh*-expressing cells long enough to observe the long term ablation effects and to better understand the role of these cells during caudal fin regeneration.

Table of contents

List of figures

List of abbreviations

AEC: Apical Epidermal Cap

BCC: Basal Cell Carcinoma

bmp2b: bone morphogenetic protein 2 b

BrdU: Bromo-2'-deoxy-uridine

BSA : Bovin Serum Albumin

Ci: Cubitus interruptus

CFP: Cyan Fluorescent Protein

Col10a: type X collagen

Col2a1: type II collagen

Cos2: Costal 2

Dhh: Desert Hedgehog

dpa : day post amputation

dpf: day post fertilization

E12.5: Embryonic day 12.5

E8: Embryonic day 8

Fgf: Fibroblastic Growth Factor

Fgfr: Fibroblastic Growth Factor Receptor

Fu: Fused

GFP: Green Fluorescent Protein

Hh: Hedgehog

Hhip: Hedgehog interacting protein

hpa: hours post amputation

Ihh: Indian Hedgehog

ihha: indian hedgehog a

ISH: *In Situ* Hybridization

kb: kilo base-pairs

MTZ: Metronidazole

N-Shh: N-terminal peptide of Shh

NTR: Nitroreductase

osx: osterix

PBS: Phosphate buffer saline

PBST: Phosphate buffer saline/0.1% Tween-20

PCNA: Proliferating cells nuclear antigen

PFA: Paraformaldehyde

ptc1: Patched 1

RA: Retinoic Acid

RAR: Retinoic Acid Receptor

Shh: Sonic Hedgehog

shha: sonic hedgehog a

smo: smoothened

tRNA: transfer RNA

ZPA: Zone of Polarizing Activity

Acknowledgments

I wish to express my deep and sincere gratitude to my supervisor, Dr. Marie-Andrée Akimenko, for her guidance, full support and trust during these two years. It has been a great privilege to work in her lab. Also, I would like to thank my advisory committee members, Dr. Marc Ekker and Dr. Anne-Gaëlle Rolland-Lagan, for always providing me their valuable suggestions. Thanks to Jing for her friendship, her great advices, for helping me in everything I needed help with, and for her time all along the way. I wish you all the best. Special recognition is also given to Dr. Melanie Debiais for her kindness and help. Thanks to my friends and colleagues Leona, Nadir, Yanwei and Vishal, for their support and for all the fun times. Thanks also to all the lab members and colleagues, for their endless encouragement and support throughout the whole period. To my parents, Kamil Jeradi and Claudine Le Bouthillier-Jeradi, thank you for your trust, your undoubtfull faith, your love and for supporting me in making my own choices. To my grand-parents, to Le Bouthillier and Jeradi families, especially Yves Le Bouthillier, Louise Shaugnessy, Maude and Sam and to all of my friends, thank you so much for your continuous support. Finally, Alhamdoulillah, for everything.

Introduction

I. Regeneration

1. Overview

Regeneration is a morphogenetic event that allows the partial or complete replacement of a lost organ/tissue. It can occur following an injury (reparative regeneration) or can be a constitutive event that is involved in the maintenance of the organism integrity (physiological regeneration). Based on the cellular mechanisms that are involved, regeneration can be classified as morphalaxis (when it does not involve cell proliferation; the lost tissue is regenerated through structural and cellular remodeling of the remaining part of the organ) or epimorphosis (when it requires an active cell proliferation, and blastema formation (Morgan, 1901)). While regeneration is widely spread among non-vertebrate species (planarian, hydra...), very few adult vertebrate species are able to regenerate lost parts of their body. Some tetrapod species were shown to be able to regenerate parts of their body at a given stage of their life cycle, notably during embryonic development, but their regeneration capacity at the adult stage seems to be very limited following injury (Han et al., 2005; Yokoyama, 2008). Following injury, non-regenerative tetrapod species heal through repair, which involves an inflammatory response and results in a scar (Broughton et al., 2006). Regeneration, in contrast, does not involve an inflammatory response.

To date, the exact molecular mechanisms that are underlying regeneration are not fully understood. While embryonic and neonatal mice still have the ability to

regenerate their digits (Reginelli et al., 1995; Han et al., 2003), adult mice are unable to do so. The same observation was made in human where children have the ability to regenerate fingertips, a faculty that is completely lost in adults (Vidal and Dickson, 1993; Han et al., 2005). Why is the regenerative ability lost with age in mammals? Do we still have the molecular machinery that is necessary to induce regeneration? Is it a matter of regulation, environment? And is it possible to enhance an organism regenerative capacity? These are among the numerous questions that remain unsolved in the regeneration field.

Recently, a new branch of medical research has emerged, called regenerative medicine. It seeks to understand the process of regeneration in species that are able to do so, in order to apply it to humans (reviewed in (Andersson and Lendahl, 2009)). This new discipline will be of benefit for people that are suffering from limb amputation, major burn, muscle failure... etc. However, in order to make regeneration possible for human, we first have to identify and understand the fundamental mechanisms that are involved during regeneration, and, later, find a way to control these processes and induce them in non-regenerative tetrapod species. Once these requirements are met, one can reasonably hope that regeneration for human will be possible.

2. Urodele amphibians as a model to study regeneration

Urodele amphibians are the most widely used vertebrate model to study regeneration. In contrast to anurans (frogs and toads) that have a very limited capacity to regenerate

their limbs after amputation, urodeles (axolotls and salamanders) are able to regenerate their limbs as well as other structures correctly and at any time of their life cycle (Yokoyama, 2008).

Regeneration of urodele limbs was first reported in 1768 by Spallanzani who first described the salamander limb regeneration process. Limb regeneration process involves: (i) the formation and thickening of the wound epithelium to eventually form the Apical Epidermal Cap (AEC), (ii) the dedifferentiation of cells located under the amputation plane, that will migrate and proliferate under the AEC to form a cluster of undifferentiated cells termed 'blastema', and (iii) a re-development phase where the undifferentiated cells start to re-differentiate to give rise to all cell types that are necessary to form the lost limb (Bryant et al., 2002; Gardiner et al., 2002).

Although regeneration studies using urodeles allowed gaining insights into the epimorphic regeneration process, especially at a cellular level, urodele amphibian models present several limitations. Beside the fact that urodeles are neotenic organisms, meaning that they retain some of their embryonic characteristics when they reach sexual maturity, axolotls and salamanders are hardly amenable to transgenesis (even though transgenesis is possible (Sobkow et al., 2006)). The internal fertilization and the relatively long generation time (several years in the wild to reach sexual maturity for the newts) make it very hard to create a stable transgenic line. Overall, these models offer a limited amount of genetic tools that would allow the dissection of the regeneration process at a molecular level (Raya et al., 2004).

To overcome these limitations, the complementary use of other vertebrate models to understand the regeneration process becomes urgent. Recently, the zebrafish has joined the urodeles as another popular and informative vertebrate model to study

regeneration (Poss et al., 2003).

3. The Zebrafish model

Zebrafish (*Danio rerio*) is a small freshwater teleost fish of the cyprinid family and belonging to the class of the actinopterygii (ray finned fish). Zebrafish has emerged as a valuable animal model to study both developmental biology as well as human disease since the early 1980s, when methods were developed to allow genetic analyses in this species. Since then, zebrafish has been widely used as an animal model to assess different problematics.

An amazing combination of features makes the zebrafish a particularly attractive vertebrate model. These include low maintenance cost, small size of the fish which allows maintaining a large pool of animals in a relatively small facility, their robustness, high fertility (each pair can lay 100 to 200 eggs per day throughout the year), and the short generation time. Fertilization is external and embryos undergo rapid and synchronous development and are optically transparent, allowing *in vivo* imaging of the developing organs.

Multiple tools have been developed for the zebrafish model. Reverse genetic approaches include the use of antisense morpholinos, to transiently knock down gene functions, and TILLING to introduce mutations in a gene of interest. The zebrafish genome sequencing was undertaken by the Sanger institute and annotated sequences are available on Ensembl (http://www.ensembl.org/Danio_rerio/Info/Index). A more complete annotation is undertaken in collaboration with the ZebraFish Information Network (ZFIN) and can be accessed through the Vegadatabase (http://vega.sanger.ac.uk/Danio_rerio/index.html).

Methods have been developed to allow the generation of stable transgenic lines, expressing fluorescent reporters under the control of tissue specific promoters, which allows *in vivo* imaging (Brittijn et al., 2009).

Besides being a good model for developmental studies, zebrafish is widely used as a model to study regeneration. In fact, teleosts species are among the very few vertebrates that are able to regenerate, at adult stage, several organs. They are able to regenerate scales, optic nerves, heart, spinal cord, brain, pancreas, liver and all fins.

II. Zebrafish fin regeneration

1. Zebrafish fin morphology

Zebrafish possesses five sets of fins: two paired fins, pectoral and pelvic, and three unpaired fins, dorsal, anal and caudal fins (Fig 1-A). The caudal fin has been used as a model to study regeneration because it is the most accessible one. Its amputation does not impair the animal life and it presents an almost perfectly symmetrical shape. This bi-lobular shape allows the use of one of the lobes as the control, reducing the amount of variation between the experimental samples and their controls.

The zebrafish caudal fin harbors a relatively simple structure. The major exoskeleton components of the adult fins are the dermal bony rays, called lepidotrichia. They are articulated *via* ligament on the internal endoskeleton made of endochondral bones. Each lepidotrichium is composed of two hemirays that are concave dermal bones,

facing each other. They are enclosing a loose, vascularized and innervated mesenchyme and are surrounded by a multilayered epithelium. Each hemiray consists in a succession of segments (Akimenko et al., 2003). The successive addition of segments ensures the longitudinal growth of the hemirays (Fig 1-C).

In the caudal fin, there are 18 lepidotrichia (ray). Each ray can form successive bifurcations as the fin grows, increasing the fin surface and thus probably facilitating swimming. The two lateral rays never form branches (Quint et al., 2002) (Fig 1-B).

At the distal tip of each lepidotrichia are clusters of small rigid fibrils called actinotrichia. They extend distally as straight, unbranched spicules (Becerra et al., 1983). Actinotrichia are un-mineralized structures, made of elastoidin, which is composed of collagen and actinodin (Zhang et al. 2010).

Fin amputation at the level of the dermal bony rays is followed, in 100% of cases, by a quick regeneration of these rays (three weeks at 28 °C, Fig 2-A). However, fins amputated at the level of endochondral bones regenerate at a very low speed (about 51 days at 24 to 29 °C), and the regeneration is observed only in 50% of the cases (Fig 2-B) (Shao et al., 2009).

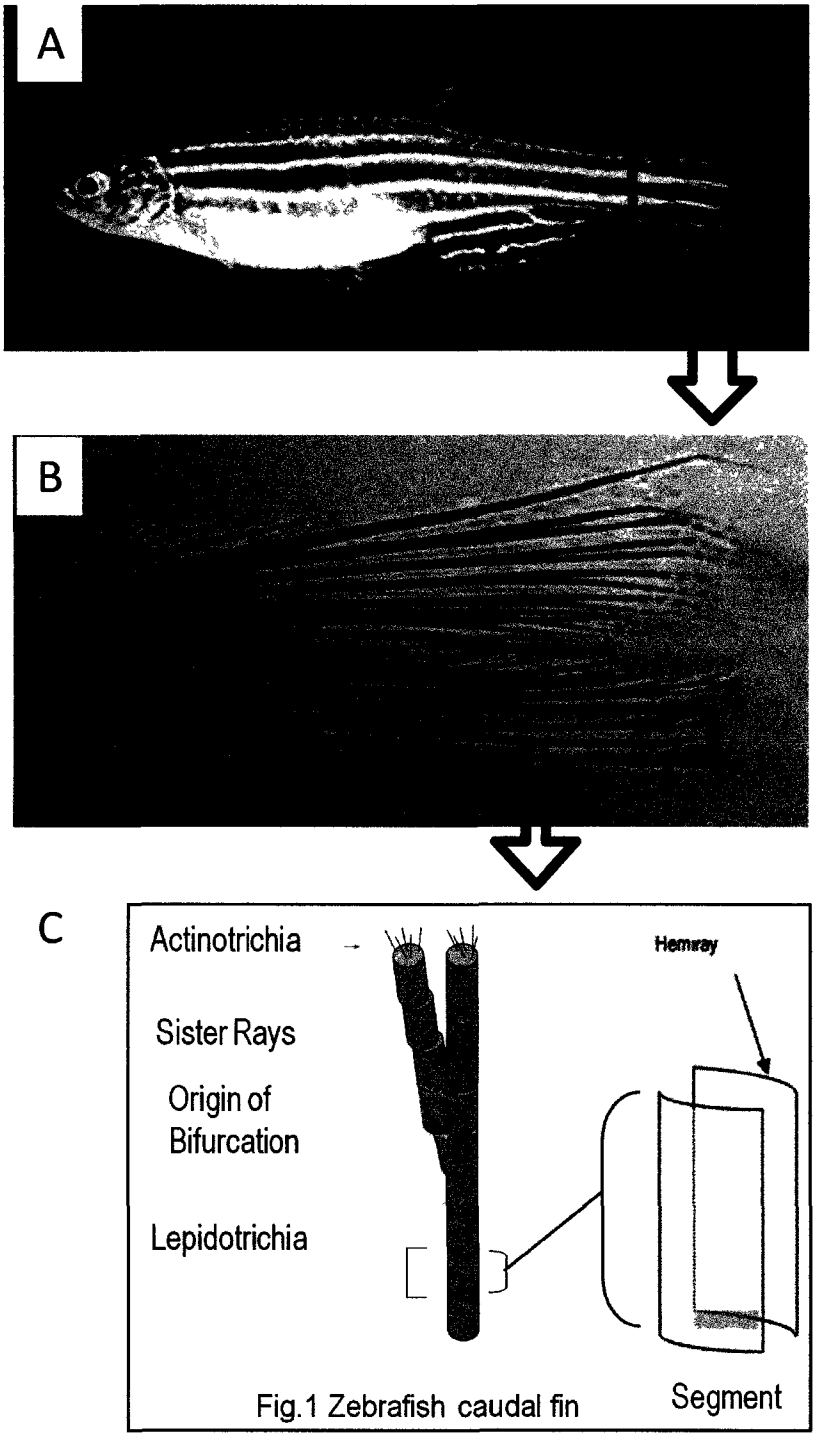

Figure 1. : The zebrafish caudal fin

Figure 1: The zebrafish caudal fin (A) An adult zebrafish possesses two sets of paired fins (pectoral and pelvic), and three sets of unpaired fins (dorsal, anal and caudal); (B) the bony skeleton of the zebrafish caudal fin, stained with alizarin red. The elongated structures are the dermal bony rays called lepidotrichia, and constitute the exoskeleton, along with the actinotrichia. Lepidotrichia are articulated on the endochondral endoskeleton (yellow box); (C) schematic representation of a single bifurcating ray. Each lepidotrichium consists of two symmetrical, parenthesis-shaped hemirays filled with connective tissue. Each hemiray is made of successive segments. 16 out of 18 rays are bifurcating.

2. Zebrafish caudal fin regeneration: an overview of the regeneration process

Fin regeneration in zebrafish is a rapid process that allows re-development of the lost structure following amputation at the exoskeleton level within 3 weeks at 28.5 °C (Fig 2A). Three main steps take place during fin regeneration: 1) wound healing, 2) blastema formation and 3) Regenerate outgrowth (Fig 3A-C). In the following part, we will discuss in further details the main cellular events that are taking place during fin regeneration, through the lens of these three main regeneration steps.

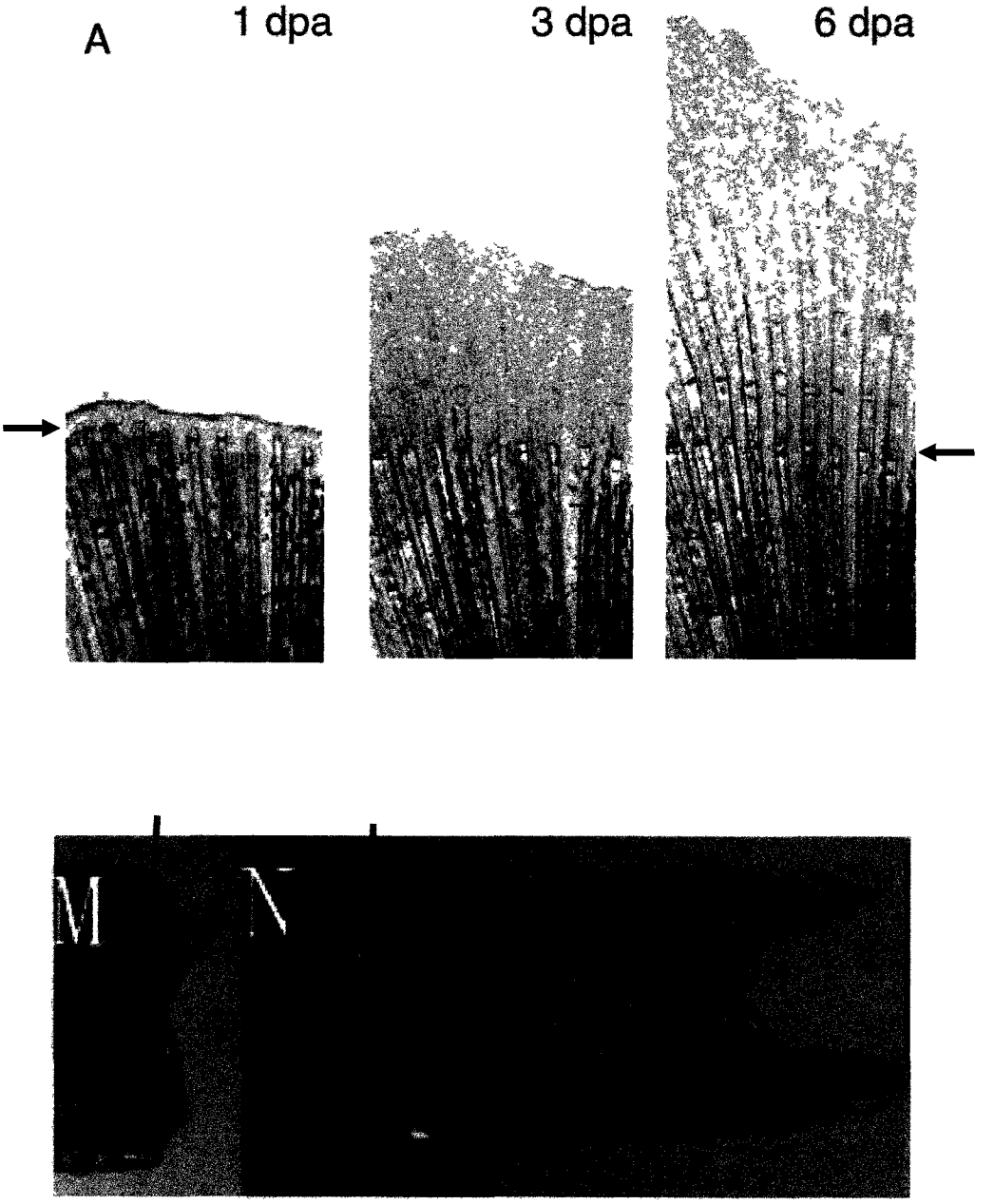

Shao & al. 2009

Figure 2: Regeneration of the zebrafish caudal fin

Figure 2: Regeneration of the zebrafish caudal fin.

(A) Regeneration after amputation at the level of the exoskeleton (red arrow). At 6 days post amputation (dpa), a nicely formed fin regenerate, with differentiated epidermis and newly synthesized bone is observed (only part of the regenerate is shown). The whole structure will be restored after about 3 weeks at 28.5 °C.

(B) Only 50% of the tails regenerate following amputation at the level of the endoskeleton (red arrow). Regeneration takes about 51 days at 28.5 °C. Adapted from (Shao et al., 2009), permission to reproduce obtained from publisher.

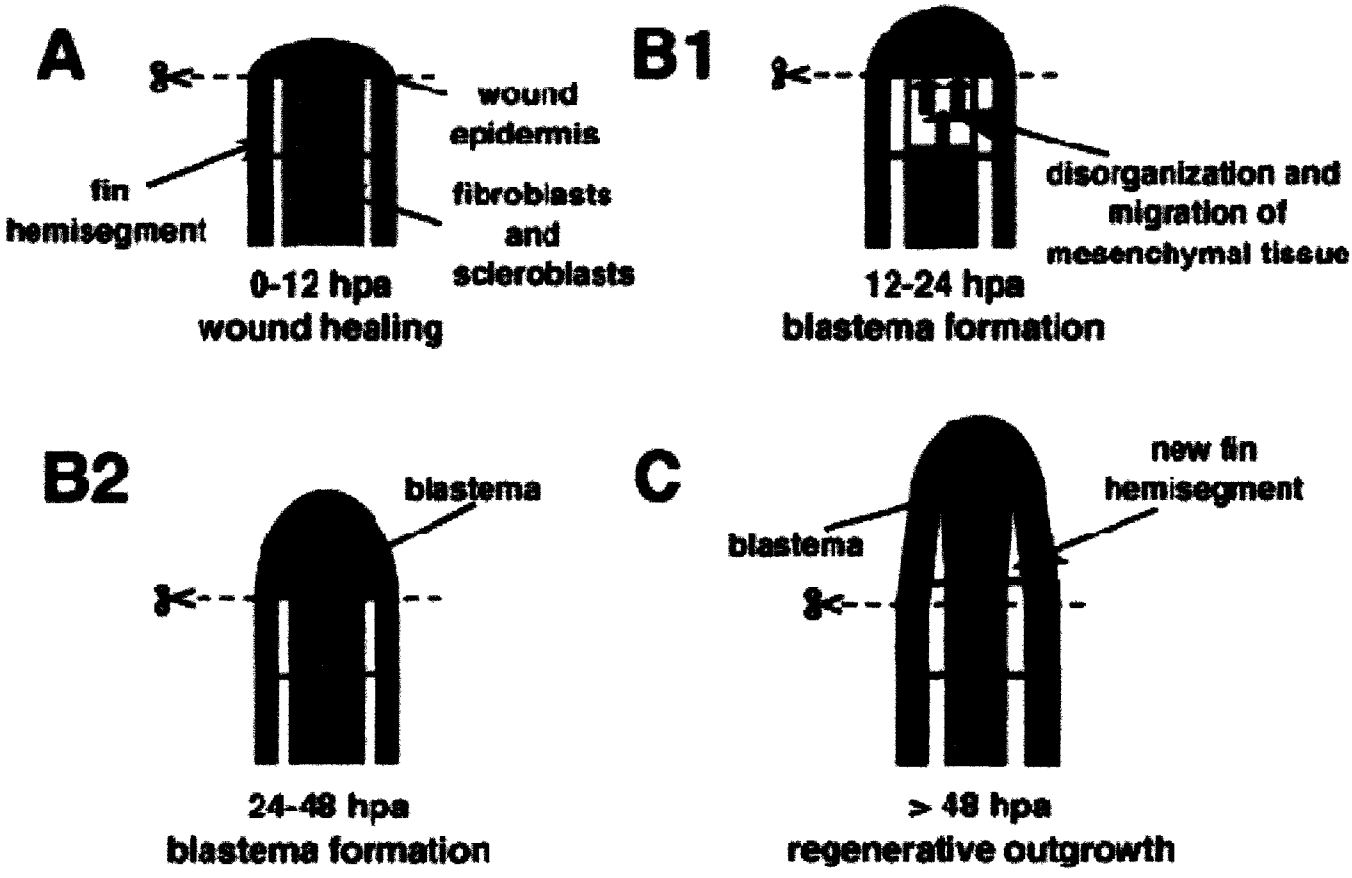

Figure 3: The regeneration process of the caudal fin

Figure 3: The regeneration process of the caudal fin.

(A-C) Schematic representations of longitudinal sections across a single ray (top is distal; bottom is proximal) at different stages during fin regeneration. (A) During the first 12 hours post amputation (hpa), epidermal cells migrate to cover the wound to form the mature wound epidermis. (B1) Parallel to the thickening of the wound epidermis, the underlying mesenchymal tissue located 1-2 segments below the amputation plane is loosened, and loses its organization, which allows the subsequent mesenchymal cell migration. (B2) The mesenchymal cells undergo de-differentiation and proliferation to form a cluster of un-differentiated cells called blastema. Starting from 48 hpa, the blastema is formed and is located underneath the epidermal cap. (C) During the growth of the regenerate, blastema cells divide, leave the blastema to enter the differentiation zone and differentiate to restore the lost organs. This time course represents the regenerative events at 33 °C. Adapted from (Poss et al., 2003), permission to reproduce obtained from publisher.

a. Wound healing

Following amputation, very little bleeding is observed This is probably due to blood vessels rapid closure, along with the quick migration of surrounding epithelial cells, to cover the wound A thin epidermal layer is established within 1 to 3 hours post amputation (hpa) This step does not involve any cell proliferation, as shown *via* BrdU incorporation experiments (Poleo et al , 2001) During the next 12 hpa, the wound epidermis undergoes a 'maturation phase', during which it thickens and becomes multilayered *via* continuous cell migration (Poss et al , 2003) Parallel to the thickening of the epidermis, the underneath mesenchymal tissue is disorganized and loosened (between 12-24 hpa) allowing cell movements (Fig3 A, B1) This disorganization and cell migration is thought to result from the reception of signals (growth factors) secreted by the mature wound epidermis The wound epidermis is required for the regeneration process as it is was shown to be necessary for the establishment of the blastema In fact, impairment of AEC formation in the fin regenerate, through inhibiting cell migration (small molecule treatment inhibiting the Phosphoinositide 3-kinase PI3K pathway) inhibits blastema formation and the fin fails to regenerate (Nakatani et al , 2008)

b. Blastema formation and maturation

Once the multilayered wound epidermis has developed, the mesenchymal tissue located underneath the epidermis becomes loose and disorganized, and cell movement can be observed Various cell types will migrate and accumulate under the wound, most likely to undergo de-differentiation Although there is no evidence for the existence of progenitor stem-like cells that might contribute to the un-differentiated

cells, the existence of such a population is not to be excluded. The cluster of un-differentiated cells that is formed is called blastema. The establishment of the blastema around 24 hpa is required for the regeneration to occur (Fig3 B2).

As it gets to the maturity, the blastema can be divided in two compartments: the proximal blastema is constituted of dense and highly proliferative cells, while the distal blastema is composed of slowly cycling cells.

c. Regenerate outgrowth

In addition to the distal and proximal blastema, a third compartment called "differentiation zone" will appear in the regenerate. As they leave the proximal blastema, un-differentiated cells enter the differentiation zone where they undergo re-differentiation to give rise to different cell types that form the lost organ. Whether or not the blastema cells are completely multipotent (able to give rise to all cell types constituting the fin), or are submitted to cell lineage restriction, remains unclear.

The differentiation zone is maintained during the whole regeneration process and is always located below the proximal blastema. It is in the differentiation zone that the newly differentiated osteoblasts appear (Fig 3 C).

The fin rays are composed of bones from dermal origin, called dermal or intramembranous bone, as opposed to endochondral bone. Intramembranous ossification starts from mesenchymal condensation, during which mesenchymal progenitor cells differentiate directly into osteoblasts that secrete a bone matrix that will mineralize to form the dermal bone.

During the regeneration of the dermal bony rays, osteoblast differentiation occurs in

the mesenchymal part of the differentiation zone, in a proximo-distal manner More distal osteoblasts express early markers of differentiation (such as transcription factors *runx2a* and *runx2b*) while more proximal osteoblasts express markers of fully differentiated cells (such as *osterix* (*osx*) and the matrix gene *bone sialoprotein 1* (*spp1*)) These different markers were shown to characterize different stages of osteoblast differentiation during fin regeneration (Brown et al , 2009) (Fig 4 C, F, I, L, N)

Two members of the Hedgehog (Hh) family are also re-expressed during caudal fin regeneration in the differentiation zone *indian hedgehog a (ihha)* in the newly formed osteoblasts (Fig 5 A, C) (Avaron et al , 2006), and *sonic hedgehog a (shha)* in a subset of basal epithelial cells at the limit between the blastema and the differentiation zone (Fig 5 C) The Hh ligand receptor and Hh transcriptional downstream target, patched 1 (ptc1), is expressed in both newly differentiated osteoblasts and the basal layer of the epidermis, at the level of the differentiation zone The same domain of expression is observed for the Hh transcriptional target *bmp2b* (Laforest et al , 1998) The domain of expression of all these markers (*shha*, *ihha*, *bmp2b* and *ptc1*) split into two before a ray bifurcation can be detected

The detailed expression pattern as well as functional analysis of both *shha* and *ihha* will be described later

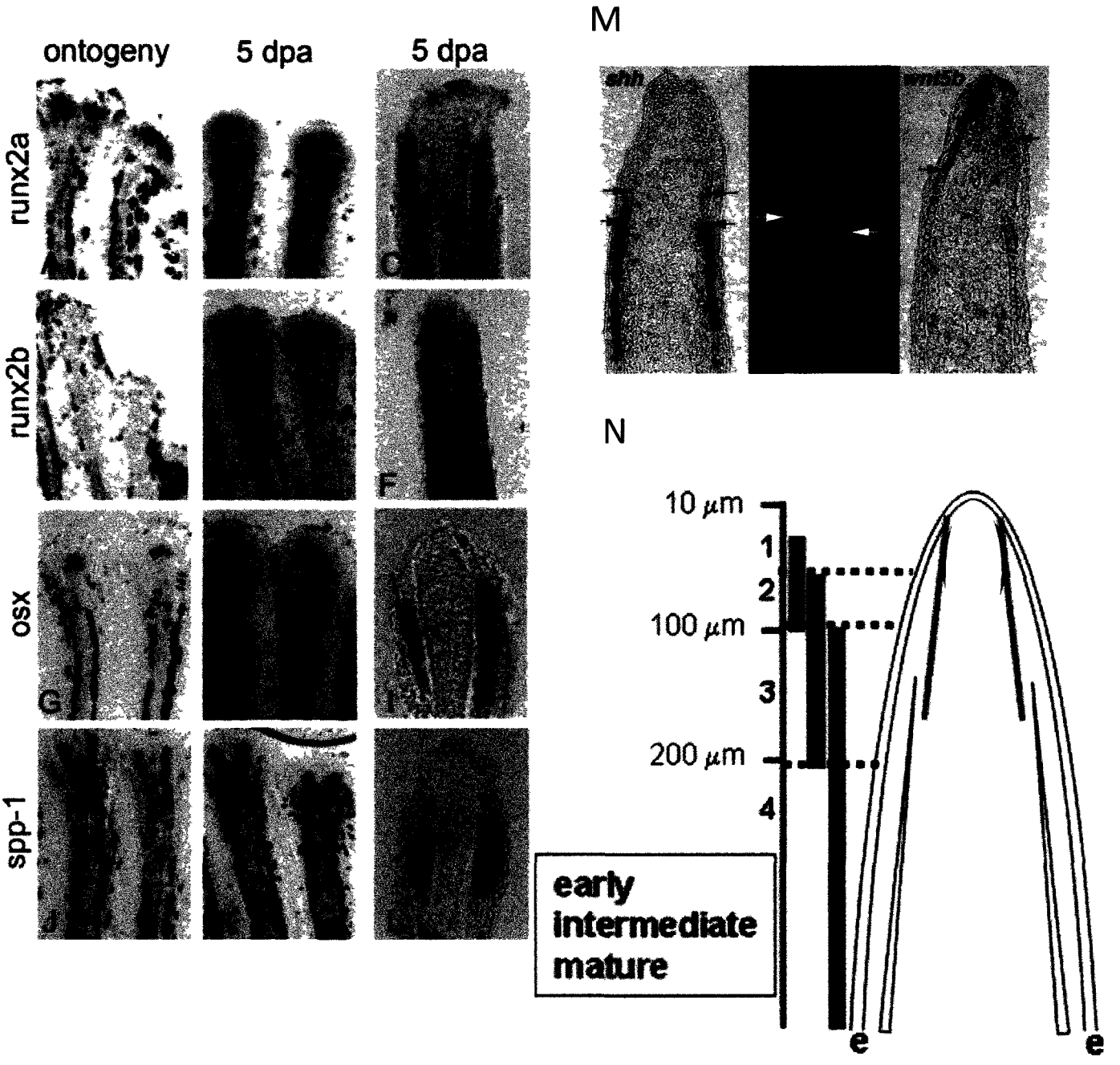

Figure 4: Analysis of the expression pattern of molecular markers characterizing different stages of differentiation of osteoblasts

Figure 4: Analysis of the expression pattern of molecular markers characterizing different stages of osteoblast differentiation. (A-L) *In situ* hybridization on whole mount (A,B,D,E,G,H,J,K) and on longitudinal sections of fins (C,F,I,L) during ontogeny (A,D,G,J) and regeneration (B,E,H,K). All the markers were exclusively expressed in the newly differentiated osteoblasts. Adapted from (Brown et al., 2009). (M) ISH for *shha* and *wnt5b* and antibody staining for Zns-5 in a single ray show that the distal limit of *shha* domain of expression starts at the same level as the Zns-5+ cells. *shha* is expressed in the basal layer of the epidermis while Zns-5+ cells consist in fully mature, functional osteoblasts. White and black arrows indicate the distal tip of the strong expression domain of both *shha* and Zns-5. The red arrow indicates a weak signal, more distal, still similar between *shha* and Zns-5. Adapted from (Lee et al., 2009), permission to reproduce obtained from publisher.

(N) Analysis of the distance between the tip (most distal part) of the regenerate and the beginning of the expression domains of different markers allowed proposing a model for osteoblast differentiation. The 'status' of osteoblast differentiation is represented on the left of the schematic, with an 'early domain' (*runx2* and *osx*) partially overlapping with an 'intermediate domain' (*ssp1*), itself partially overlapping with mature, Zns-5 positive osteoblasts (Brown et al., 2009), permission to reproduce obtained from publisher.

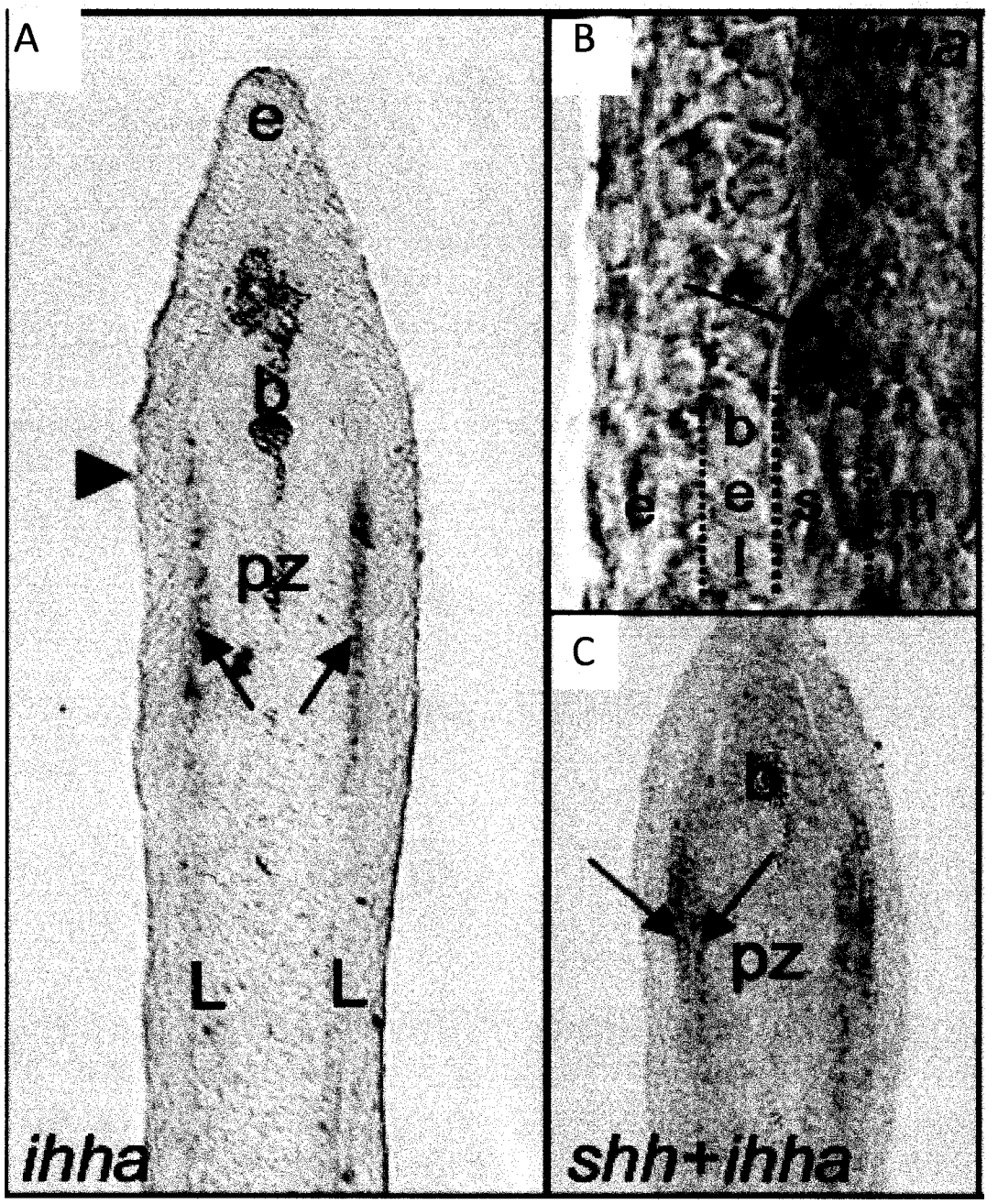

Figure 5: Expression pattern of *hedgehog* genes during dermal bony ray regeneration

Figure 5 Expression pattern of *hedgehog* genes during dermal bony ray regeneration

(A, B) *ihha* is expressed in the newly differentiated osteoblasts, (C) and its expression pattern seems to co-localize with *shha* along the proximal-distal axis, in the newly differentiated osteoblasts and the basal layer of the epidermis, respectively Adapted from (Avaron et al , 2006), permission to reproduce obtained from publisher

d. Ray branching morphogenesis

As mentioned earlier, the caudal fin is composed of 18 bony rays called lepidotrichia. All of these rays, except the two lateral-most rays, are undergoing successive bifurcations (1-2 bifurcations *per* ray). Therefore, the two lateral rays will be called non-bifurcating rays, as opposed to the other bifurcating rays. The cellular and molecular events that trigger the branching morphogenesis in the branching fin rays remain largely unknown.

It has been demonstrated that ray-interray interactions are required for the correct patterning of the fin rays during caudal fin regeneration of the goldfish and zebrafish (Mari-Beffa et al., 1999). The importance of the surrounding tissue for ray patterning is well demonstrated by the next two sets of experiments. For example, when one single bifurcating fin ray is amputated in the caudal fin, while neighboring rays remain intact, the regenerating ray is surrounded by non-regenerating interray tissue. The two surrounding, non-amputated rays heal together, sealing the empty space where the amputated ray should normally grow. The regenerating ray can then either grow outside of the fin plane, or grow in the sealed, well-differentiated interray tissue. While it exhibits a good regenerative potential, the amputated ray does not show a correct pattern of bifurcation, as it does not bifurcate. The same abnormal patterning was observed following continuous isolation of a single ray during the regeneration process: the caudal fin was completely amputated to 30%, and then during regeneration, a single ray was daily separated from its neighboring regenerating rays *via* scissor incision. The treatment resulted in the abolishment of fin bifurcation that could be restored upon cessation of the treatment (Mari-Beffa et al. 1999).

Supporting the hypothesis of the requirement of a ray-interray tissue interaction for a

correct patterning of the fin rays, ray grafting experiments consisting in grafting the lateral-most, non-bifurcating ray in a bifurcation-prone environment (in-between two bifurcating rays) followed by fin amputation can induce bifurcation of the non-bifurcating ray (Murciano et al , 2002)

The establishment of a correct fin ray pattern during regeneration is also depending on the amputation level along the proximo-distal axis of the fin rays This was demonstrated following amputation of the ray at different levels 'short cut', just distal to the ray bifurcation point, and 'high cut', at least 2 segments distal to the bifurcation point While the high cut amputation results in a normal branching morphogenesis establishment, short cut exhibits an abnormally patterned ray regenerate In the short cut ray regenerate, the two regenerating sister rays undergo fusion and keep regenerating as a ray that has not undergone bifurcation yet The sister rays fusion correlates with an abnormal diffuse expression pattern of *shha* *shha* is expressed in two diffuse domains (one *shha* expression domain per sister ray) that are very close, somehow communicating (Laforest et al , 1998) This suggests that the Shh signaling may be interpreted as a unique source, which characterizes the non-bifurcating ray, leading to the fusion of the sister rays (see **'IV. Hedgehog signaling: Expression and functional analysis of *shha* and *ihha* during fin regeneration'** for detailed description of *shha* expression pattern in regenerating ray)

The fin ray branching patterning has also been shown to be disrupted following Retinoic Acid treatment (RA) At 2dpa, *rar gamma* (*Retinoic Acid Receptor gamma*) is expressed in the distal blastema (White et al , 1994) Treatment of the 2 dpa regenerates with RA leads to a branching delay, without affecting the length of the ray The delayed branching morphogenesis correlates with the inhibition of *shha* and *ptc1*

expression in the regenerate (Geraudie et al., 1995; Laforest et al., 1998). These results introduce the idea of interactions between the blastema and differentiation zones, as disruption of RAR expression in the distal blastema results in the disruption of the expression of *shha* and its receptor *ptc1* in the differentiation zone. This interaction seems to be required for the correct patterning of the fin ray regenerate, and further suggests a role for the Hh pathway during branching morphogenesis.

III. Hedgehog signaling

1. Review of the pathway

The Hedgehog (Hh) pathway was first identified in *Drosophila melanogaster* and largely studied in this species (Nusslein-Volhard and Wieschaus, 1980). Hh is a secreted protein and is acting on the target cells through the 12-pass transmembrane protein Patched (Ptc). In *Drosophila melanogaster*, in the absence of Hh ligand, Hh receptor Ptc is inhibiting a 7-pass transmembrane protein called Smoothened (Smo). When Smo is inhibited, it is located in the cytoplasm of the cells, and the zinc finger transcription factor Cubitus interruptus (Ci) is forming a complex with Costal2-Fused (Cos2-Fu). This leads to the phosphorylation and processing of Ci. Ci N-terminal fragment accumulates and enters the nucleus to act as a transcriptional repressor. In such case, the target genes of the Hedgehog pathway are not transcribed and the pathway is turned 'off'. When Hh is present, the binding of Hedgehog to its receptor Ptc leads to the internalization of Ptc. Smo is no longer inhibited by Ptc and its cytoplasmic tail will be phosphorylated by PKA and CKI. This phosphorylation leads to the activation and accumulation of Smo on the cell surface. Membranous Smo

interacts with Cos2-Fu-Ci cytoplasmic complexes, to recruit Cos2-Fu complexes away from the zinc finger transcription factor Ci (Ho and Alman 2010). The full length Ci is no longer phosphorylated and processed to its N-terminal inhibiting form, and is now able to translocate to the nucleus under its full length version, thus acting as a transcriptional activator. The Hedgehog target genes are then transcribed and the pathway is turned 'on' (Fig 6).

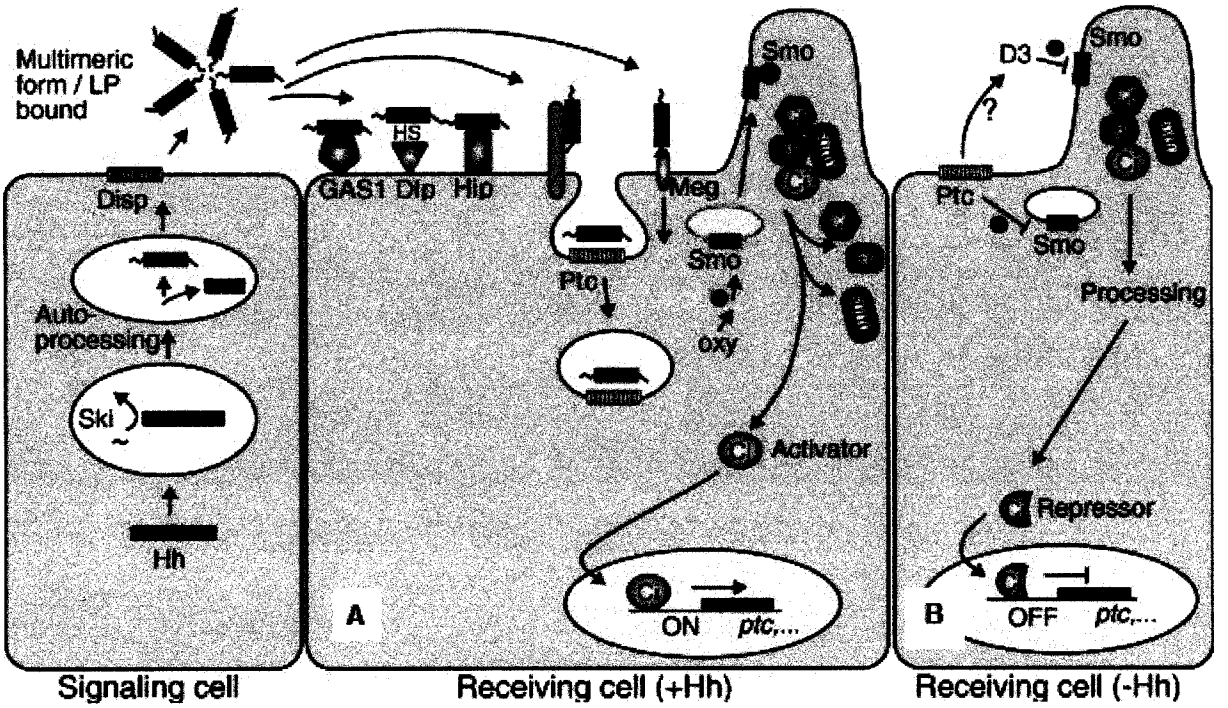

Figure 6: A simplified model of the Hedgehog pathway, based on data from both *Drosophila* and mammals

Figure 6: A simplified model of the Hedgehog pathway, based on data from both *Drosophila* and mammals. (A) The Hedgehog protein is synthesized and released through Dispatched (Disp) in the extracellular environment. It then diffuses as a multimeric complex and reaches the target cells. When Hh protein is received by the target cell that is expressing Ptc, the interaction Hh-Ptc leads to the internalization of the receptor Ptc that is no longer exerting its inhibiting action on Smo. Smo can translocate to the plasma membrane, or, in mammals, to the primary cilium. Smo is phosphorylated and activates the Hh signaling. In *Drosophila*, the activation of the Hh pathway occurs by releasing the transcription factor Ci from the complex it makes with the kinesin-like molecule Costal2 (cos2), Fused (Fu) and Suppressor of Fused (SuFu). The full length Ci released from the cos2-Fu-SuFu complex can then enter the nucleus as its full length version, and activate the Hh target genes. (B) In the absence of Hh, Ptc is inhibiting Smo, that is no longer phosphorylated. In this case, Ci is sequestered in the Cos2-Fu-SuFu-Ci complex and Ci is not able to enter the nucleus; it is cleaved by Cos2 and the Ci fragment acts as a transcriptional inhibitor. The Ci homologous proteins in mammals are Gli1, Gli2 and Gli3. There is no Cos2 and Fu homologs in mammals, instead, Su(fu) is playing a more prominent role in inhibiting the pathway. Adapted from (Burglin, 2008), permission to reproduce obtained from publisher.

In mammals, there are three Hedgehog homologs: Sonic Hedgehog, Indian Hedgehog and Desert Hedgehog, respectively *Shh*, *Ihh* and *Dhh* (Echelard et al., 1993). Even though the regulation of Smo localization by Ptc1 seems to be conserved between vertebrate and non-vertebrate species, a slight difference is observed in the cellular localization of Ptc1 and Smo in vertebrates, compared to *Drosophila*: when the pathway is not activated, Ptc1 is localized at the base of the primary cilia, which are cellular extensions found in most vertebrate cells and thought to be involved in sensing the external environment. This Ptc1 localization prevents Smo from entering and accumulating in the cilia. When the pathway is activated, Ptc1 is removed from the cilia. This allows Smo to enter and to accumulate in the cilia, and to activate the Hedgehog pathway (Rohatgi et al., 2007). In zebrafish, the link between cilia localization and Hedgehog pathway activation was just recently made, showing that the importance of cilia is also conserved in zebrafish (Kim et al. 2010).

The vertebrate Hedgehog proteins control gene expression through the processing of the vertebrate homologs of Ci: the Gli transcription factors. Gli2 and Gli3 both act in a similar way as Ci, being either stabilized under their full-length form to act as transcription activators, or being cleaved to act as transcriptional repressors (Sasaki et al., 1999). Gli1, however, is lacking the proteolytic cleavage site and can only act as a transcriptional activator (Hynes et al., 1997; Aza-Blanc et al., 2000).

The *Hh* genes share a high degree of homology which predicts at least a partial redundancy of function. However the Hedgehog proteins show different patterns of expression and play different roles during development (Ho and Alman 2010).

2. Role of Hedgehog signaling during embryonic development

a. Sonic hedgehog (Shh) and its role during development

Sonic hedgehog (Shh) is the most widely studied Hedgehog family member It is also the most broadly expressed in mammals its expression pattern during early embryogenesis includes the notochord, the floor plate and the Zone of Polarizing Activity (ZPA) in the developing limbs (Varjosalo and Taipale, 2008) It is a secreted protein, first synthesized as a precursor protein of 45 kDa Mature Shh protein is produced following multiple processing steps described herein

The precursor protein first undergoes autoproteolytic activity resulting in an N-terminal peptide (N-Shh) of 20 kDa, and a C-terminal peptide The C-terminal peptide is responsible for the autoproteolytic activity and has no other known biological activity The N-Shh contains a signal peptide and the biological activity A cholesterol molecule is added to the carboxyl terminus of N-Shh, allowing the binding of Shh to the external plasma membrane Subsequent to this binding, a palmitic acid molecule is added to the N-terminus of the N-Shh This palmitoylation is thought to enhance the signaling activity of Shh, as the non-palmitoylated form of Shh has been shown to be less able to activate the Hedgehog pathway than palmitoylated Shh (Chamoun et al , 2001) The resulting 20 kDa N-Shh protein presenting a cholesterol-added C-terminus and a palmitic acid-added N-terminus constitutes the mature, functional Shh protein Despite the presence of a pseudo-catalytic site that is critical for signal transduction (through binding to Ptc1 and also interaction with the natural Hh antagonist Hhip), no enzymatic activity has been reported for the N-Shh so far (Fuse et al , 1999, Maun et al 2010)

Shh can have a short range and a long range action, as it forms a gradient and acts in a dose dependent manner on the target cells. Shh has been shown to be active in a distance of up to 300 micrometers from its secretion point in the vertebrate limb buds (Zhu and Scott, 2004). The mechanisms through which Shh travels to exert its long range action are not fully understood, however, it is thought that several N-Shh signal peptides are able to multimerize through their cholesterol groups, and to diffuse as a multimere complex to create the gradient (reviewed in (Farzan et al., 2008)).

Shh is an important morphogen, playing a crucial role during embryonic development. It was first studied for its role in limb development where *Shh* is expressed in a cluster of cells located in the posterior mesenchyme of the tetrapod limb buds, a region called the Zone of Polarizing Activity (ZPA). The secretion of Shh by the ZPA cells leads to the establishment of a gradient along the anterior-posterior axis of the limb bud. Depending on the dose of Shh that they receive, and the exposure time that they experiment, the cells of the bud will acquire different identities, allowing the establishment of a correct digit pattern (Scherz et al., 2007) (Fig 7).

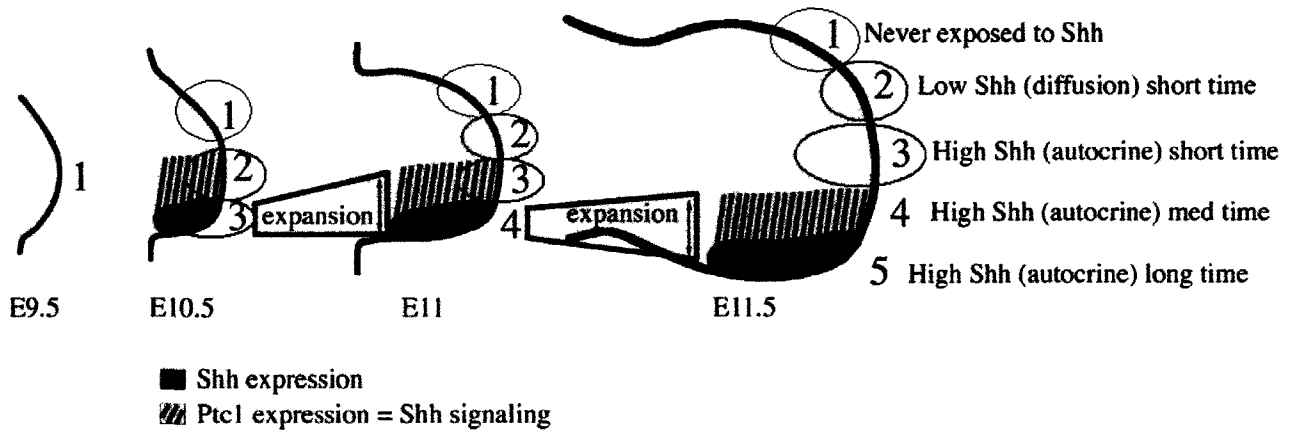

Figure 7: Shh role during cell fate specification in the mice limb bud

Figure 7: Shh role during cell fate specification in the mice limb bud is essential to the correct digit patterning along the anterior-posterior axis. In red the cells that never expressed, and were never exposed to, Shh. In this region, cell fate determination is Shh-independent. In blue, cells that never expressed, but that were exposed to, Shh. In orange, cells that expressed Shh (used to be part of the ZPA), but migrated away from the ZPA and are not expressing Shh anymore. These cells were briefly exposed to autocrine Shh, but also (for longer period) paracrine Shh once they left the ZPA. Cells in the region '4' are the cells that stayed longer in the ZPA, so they were exposed to longer Shh in comparison to region '3'. The cells in region '5' are the cells that remain in the ZPA at E11.5. They are cells that are exposed to autocrine and paracrine Shh actions for the longest period. The cumulative Shh dose received by these cells is the highest among all the cells of the bud. Adapted from (Scherz et al., 2007), permission to reproduce obtained from publisher.

Shh is also involved in cell fate specification in other organs such as the central nervous system in mice, where Shh was shown to be necessary for the determination of interneuron fate (Xu et al.2010), the establishment of progenitor domains in the neural tube (Dessaud et al., 2008), and the floor plate specification (Ribes et al.2010).

In *in vitro* experiments, Shh has been shown to be able to induce angiogenesis (Dohle et al.2010), as well as differentiation of osteoblast (Yuasa et al., 2002). It has been proposed that Shh is able to induce osteoblasts differentiation through a Runx2-independent pathway (Zunich et al., 2009).

Besides its role in cell fate specification during development, Shh has been proposed to play a role in cell proliferation. The ZPA of the limb bud, in addition to producing a morphogen, has been suggested to produce a growth factor that controls the size of the growing digits. Recently, it has been shown that Shh is mediating this proliferating effect (Towers et al., 2008).

Unsurprisingly, in the light of its mitotic, pro-survival potential, aberrant activation of Shh pathway has been linked to several types of cancer, such as basal cell carcinoma (BCC), which is one of the most frequent cancers in humans. Loss-of-heterozygosity of *Ptc1*, or activating mutation of the *Smo* gene leading to the constitutive activation of the Hedgehog pathway are found in most cases of BCC, in sporadic or inherited forms (Johnson et al., 1996; Xie et al., 1998).

Shh is a patterning protein; its role during limb outgrowth and its importance in patterning the anterior-posterior axis of the limb bud have been discussed above. It is also very important for branching morphogenesis in several organs, such as the

salivary gland, the prostate and the lung (Affolter et al., 2009). This aspect of Shh role during embryonic development will be developed later in '**c. Shh in branching morphogenesis**'.

b. Indian hedgehog (Ihh) and its role during development

Ihh is another member of the Hedgehog protein family. One of its major roles in mammalian development is to control the endochondral bone formation.

Endochondral ossification begins with mesenchymal cell condensation. These cells will differentiate into chondroblasts, and eventually into chondrocytes (cartilage cells). Chondrocytes rapidly multiply to form columns of highly proliferative cells, become pre-hypertrophic, and then hypertrophic chondrocytes. The hypertrophic chondrocytes further differentiate and become mature, mineralize their surrounding matrix, and undergo apoptosis. In parallel, perichondrial cells (bone matrix-secreting cells) differentiate at the periphery of the cartilage, neighboring the mineralized hypertrophic chondrocytes. The mineralized cartilaginous matrix will, later, be invaded by vascular tissue and degraded by chondroclasts. Osteoblasts coming in with vascular tissue will deposit bone matrix onto the degraded mineralized cartilaginous matrix to form the bone (Mackie et al., 2008).

Proper endochondral ossification requires the activation of several genes. Among these, *Ihh*, which interferes with several aspects of endochondral bone formation. In fact, functional analysis in mouse embryos has shown that Ihh slows down the differentiation of proliferative chondrocytes into hypertrophic chondrocytes in a feedback loop involving the parathyroid hormone related peptide 1 PTHrP1 (Vortkamp et al., 1996).

Ihh signaling has also been shown to regulate chondrocyte proliferation and differentiation (pre-hypertrophic to hypertrophic chondrocyte transition) and is required for osteoblast development in endochondral bones (St-Jacques et al., 1999).

In addition, blocking Ihh function during gastrulation in mouse embryos inhibits vasculogenesis and hematopoiesis, and Ihh-/- mice have smaller and fewer blood vessels in the yolk sac than wild type mice (Dyer et al., 2001; Byrd et al., 2002). This suggests a role for Ihh in both blood vessel formation and hematopoiesis.

Recently, *Ihh* was also shown to be expressed during dermal cranioskeleton formation in chick and mouse embryos, challenging the classical notions of endochondral and dermal bones (Abzhanov et al., 2007)

3. Sonic hedgehog role during branching morphogenesis

a. Shh and lung branching morphogenesis

The tetrapod lung develops from the anterior foregut, which give rise to the two primary lung buds at around E9.5 in mice embryos. Once formed, the primary lung buds extend into the surrounding mesenchyme and begin the process of branching morphogenesis, which extends between E9.5 and E16.5 (pseudo-glandular stage). Branching morphogenesis ends by giving a complex tree-like structure (Morrisey and Hogan 2010).

Initiation of the branching process in the mammalian lung has been proposed to be mediated through Shh/Fgf cross-talks. In the growing bud, the genes coding for Fibroblastic growth factor receptor 2 (*Fgfr2*) is expressed in epithelial cells located at

the tip of the growing bud. *Fgf10* is expressed in the overlying mesenchyme and acts on the bud endoderm through Fgfr2. Together; they ensure the bud elongation in the mesenchyme (Abler et al., 2009). Ectodermal cells are attracted to the Fgf10 source and migrate towards it, most likely to ensure the elongation during lung bud initiation (Park et al. 1998). Fgf10, through Fgfr2, activates the expression of several genes, among which *Shh* and its receptor *Ptc1* (Abler et al., 2009).

Shh is expressed in epithelial cells, and necessary for branching morphogenesis, as highlighted in Shh null mice that shows lung branching failure (Pepicelli et al., 1998). *Ptc1* is expressed in the overlying mesenchyme, with higher level of expression at the distal tip of the branch.

Shh downregulates *Fgf10* when expressed at high doses (Bellusci et al., 1997b). In the medial ectodermal region of the lung bud, where *Shh* is highly expressed, a negative feedback loop takes place, leading to the downregulation of *Fgf10* by Shh in the central region of the bud. This central inhibition impairs further unnecessary elongation of the bud, and restricts Fgf10 expression to the lateral sides of the tip of the bud (Kim et al., 2009). As Shh concentration on the lateral sides of the bud is low, it does not inhibit *Fgf10* laterally. Ectodermal cells are now attracted to the two lateral sides of the bud (sources of Fgf10) ensuring the branching.

As a morphogen, it is possible that Shh induces different target genes depending on the concentration of Shh to which the cell is exposed, and depending on the exposure time as it has been shown in the developing limb bud. At high dose, Shh induces the expression of *Hhip* at the tip of the bud. Hhip down-regulates Shh in the central region of the bud, inducing a reduction of cell proliferation in the tip region (Chuang et al., 2003). To summarize, *Shh* is expressed all-over the bud epithelium, with a

higher concentration at the tip that i) inhibits *Fgf10* at the tip, restricting it to the lateral sides of the tip of the bud and ii) activating *Hhip* and *Ptc1* expression at the tip, thus down-regulating itself at the tip of the bud.

Shh also stimulates *Bmp4* and *Wnt2* in the lung mesenchyme ((Pepicelli et al., 1998), reviewed in (Morrisey and Hogan 2010)). In the lung bud, Bmp4 has been shown to play a role in cell proliferation and cell survival (Eblaghie et al., 2006). During branching morphogenesis, at E12.5, BrdU incorporation is increased in the distal, *Shh*-expressing epidermis, compared to the proximal epidermis. Increased cell proliferation correlates with branching morphogenesis in the developing bud. As proliferative cells co-localize with Shh expression in the bud epithelium, it might indicate a role for Shh in branches formation through promoting cell proliferation (Okubo et al., 2005). Consistently, over-expression of *Shh* in the distal epithelium of the lung bud only (using a mouse transgenic line expressing *Shh* under the control of a specific promoter of the tip epithelial cell) increases the rate of cell proliferation in both epithelial and mesenchymal cells, suggesting a mitogenic activity of Shh at E16.5 (Bellusci et al., 1997a). Shh has also been shown to induce *cycD* in the bud, and to promote cell proliferation.

In an attempt to understand the cellular and molecular events that underlie branches formation in the lung, Kim & al. designed a transgenic mouse model expressing the gene coding for a mutant, constitutively active, pro-apoptotic Bax protein under the control of the Surfactant Protein C (SP-C) promoter. This promoter induces the expression of the transgene in the distal bud epithelium (Kim et al., 2009). The transgene was cloned downstream of the Tetracycline Response Elements (TRE). This line was then crossed with SPC-rtTA mice, which express the reverse tetracycline transactivator (rtTA) in lung epithelial cells under the human SP-C promoter.

Treatment of the pregnant mice with Doxicycline (added to the drinking water) allowed inducible and specific ablation of the epithelial cells at the distal tip of the developing lung bud of the pups. This ablation led to the impairment of branching morphogenesis in the developing lung. In accordance with the role of Fgf10 and its interaction with Shh that was discussed above, Fgf10 showed an increased expression in the ablated lung mesenchyme, with a broader domain of expression, highlighting the importance of the Shh-expressing cells in restricting the Fgf10 domain and the requirement of a Shh/Fgf cross-talk to ensure a correct branching pattern.

b. Shh involvement in salivary gland branching morphogenesis

The mice salivary gland arises from a thickening of the oral epithelium that buds in a neural crest-derived condensed mesenchyme at around E12. Epithelial bud progression in the mesenchyme is ensured by epithelial cell proliferation at the tip of the bud.

In the bud epithelia of the salivary gland, Shh is detected at the terminal bud, along with its receptor Ptc1. While treating salivary gland explants with exogenous Shh peptides enhances branches formation, abrogation of Shh signaling (through cyclopamine treatment) leads to a decrease in branching morphogenesis. This effect could be over-passed by Fgf8 treatment (Jaskoll et al., 2004).

Fgf10 is abundantly expressed in the mesenchyme (Tucker, 2007) where it stimulates epithelial salivary gland bud elongation in the mesenchyme, through promoting cell proliferation. Fgfr1 and Fgfr2 are expressed in epithelial cells (Patel et al., 2006). Fgf10+/- mice present a salivary gland hypoplasia (Entesarian et al., 2005) and histological analysis revealed that Fgf10-/- mice and Fgfr2-/- mice salivary gland at

E12 5 present a single epithelial bud which degenerate by E13 5, a stage at which branching morphogenesis normally begins in the gland Fgf10+/- and Fgfr2+/- , however, revealed a gland with fewer ducts and fewer terminal buds (Jaskoll et al , 2005)

Inhibition of Fgf signaling using the SU5402 chemical inhibitor in the mouse salivary gland explants leads to a clear reduction in branches formation that correlates with a reduction of cell proliferation, normally concentrated in the epithelial cells of the terminal buds (Hoffman et al , 2002)

Thus, Fgf signaling could be mediating branching morphogenesis through inducing directed cell proliferation

In salivary gland, Fgfr inhibitor treatment resulted in the reduction of cell proliferation, correlating with an increased level of Bmp4 and Fgf10, pointing to a potential cross talk between BMP signaling and Fgf signaling (Hoffman et al , 2002)

4. The Hedgehog signaling in *Danio rerio*

In zebrafish, because of the additional genome duplication that occurred after divergence of the teleost lineage from the tetrapod lineage, there are five members of the Hedgehog protein family *sonic hedgehog a* (*shha*) and *shhb* (previously named *tiggy-winkle hedgehog* (*twhh*)) are both orthologs of the mammalian *Shh* gene, *indian hedgehog a* (*ihha*), and *ihhb* (previously named *echnida hedgehog* (*ehh*)) are both orthologs of the mammalian *Ihh* gene, and *desert hedgehog (dhh)* (Roelink et al , 1994, Ekker et al , 1995, Currie and Ingham, 1996, Avaron et al , 2006)

Shh: Expression pattern of *shha* in zebrafish embryos was described by (Krauss et al ,

1993) Using *in situ* hybridization on whole mount embryos, *shha* transcripts were detected as early as 8 hours post-fertilization (hpf) At 11 5hpf, *shha* was detected in the hindbrain, notochord and floor plate cells of the neural tube *Shhb* however, is restricted to the floor plate cells of the neural tube (Ekker et al , 1995) Following floor plate induction, *shha* expression in the notochord is progressively lost, and the signal fades progressively from rostral to caudal At 24 hpf, only the most rostral part of the notochord is still expressing *shha* At that same stage, the expression in the floor plate is still clear *shha* expression is also detected in the pectoral fin buds (Krauss et al , 1993) Overall, the *shh* pattern of expression is similar to what is observed in tetrapod embryos, as *Shh* is expressed in the three key signaling centers notochord, floor plate of the neural tube and ZPA In mouse, frog, chick and fish, *Shh* regulates the ventral polarity of the neural tube and the anterior-posterior polarity in the limb/fin (Ingham and McMahon, 2001)

Ihha: Similar to the expression of *Ihh* in tetrapods, the zebrafish *ihha* is detected in a few cells of the parachordal cartilage in embryos at 4 days post fertilization (dpf) These cells are relatively large and are also expressing the cartilaginous matrix gene *col10a1* suggesting that they correspond to pre-hypertrophic or early hypertrophic chondrocytes At 6 dpf, *ihha* and *ihhb* are expressed in several cartilage elements, consistent with their role during endochondral ossification in tetrapods

ihha was detected in the forming scales of zebrafish larvae (Avaron et al , 2006) During caudal fin regeneration in adult fish, *ihha* was also detected in the newly differentiated osteoblasts in each of the fin rays that also are dermal bones (Avaron et al , 2006)

As mentioned earlier, expression of Ihh during dermal bone formation was also reported during chick embryos craniofacial skeleton formation (Abzhanov et al., 2007).

IV. Hedgehog signaling during zebrafish caudal fin regeneration: Expression and functional analysis of *shha* and *ihha*

During fin regeneration, both *shha* and *ihha* are expressed in the regenerate. Treatment of the fish with cyclopamine, which is an Hh signaling pharmacological inhibitor, was shown to induce a growth arrest of the regenerate (Quint et al., 2002). This growth arrest results from the inhibition of both shha and ihha signaling, as the cyclopamine interacts with Smo, the signal-transducer of the Hedgehog pathways. The growth defects demonstrate a role of *shha* and/or *ihha* in cell proliferation and blastema maintenance of the regenerate and highlight the importance of the Hedgehog pathway during regeneration. However, cyclopamine treatment does not allow distinguishing the specific role of Shha and Ihha during caudal fin regeneration.

Back in 1998, Laforest et al. were reporting the expression of the *shha* gene during caudal fin regeneration in zebrafish, starting at 30 hpa, in a few dispersed cells at the distal end of each fin rays. As the regenerate grows, *shha* expression gets stronger and is maintained in a subset of basal epidermal cells immediately adjacent to the newly formed bone matrix (Fig 8-B). A strong expression of *shha* is detected in the regenerate around 48 hpa, in a few basal epithelial cells located in the differentiation zone. This subpopulation of cells specifically expresses *shha* throughout the regeneration process and remains confined to the distal end of the regenerate, underneath the blastema (Fig 8-C) (Laforest et al. 1998).

Shha and Ihha receptor, Ptc1, is expressed in a pattern that partially overlaps with

shha but extends to the newly formed osteoblasts that express *ihha* (Avaron et al , 2006) *bmp2b*, a member of the TGF beta family that is induced in many tissues in response to SHH signaling, was shown to be expressed in a pattern similar to the one of *ptc1* in the basal epidermal layer, in the differentiation zone as well as in the newly differentiated osteoblasts This indicates an activation of the Hedgehog pathway in both cells of the basal epidermal layer and in newly differentiated osteoblasts

The expression pattern of *shha* during regenerate outgrowth is very dynamic In fact, at 2dpa, a single set of *shha*-expressing cells is detected in the regenerate (Fig 8-B) When a unique group of *shha*-expressing cells is present, it is located in the center of the hemiray in the differentiation zone Around 3 5dpa, the *shha*-expressing cells separate into two subpopulations of cells When two groups of cells express *shha*, they are located on the lateral limits of the hemiray (Fig 8 B) This division of the domain of expression is soon followed by the formation of a bifurcation of the ray (Fig 8-A) Following a bifurcation, each sister ray presents a single set of *shha*--expressing cells that is maintained until a second bifurcation occurs This pattern of expression is also observed for *ptc1* and *bmp2b*, both targets of the Hedgehog pathway Sixteen rays out of eighteen do present this dynamic expression pattern, the only two exceptions are the two lateral rays that never bifurcate This expression pattern of *shha* may indicate a role of the *shha*-expressing cells in the branching morphogenesis of the regenerating rays

Supporting this hypothesis, amputation of the caudal fin immediately after a branching point will result in sister ray fusion The fusion correlates with a single set of *shha*-expressing cells in the ray, and seems to result from a disruption of the separation of the *shha*-expressing cells This indicates that a correct distribution of the

shh-expressing cells is required for branching formation (Laforest et al , 1998)

Consistently, ectopic expression of *shha* between sister rays (through transfection with a *shha*-expressing plasmid), where *shha* is not normally expressed, leads to fusion of the branches (Quint et al , 2002) (Fig 9) Alcian blue staining allows the detection of glycosaminoglycans in the lepidotrichia matrix and shows that the sister ray fusion results from ectopic bone deposition in the transfected rays Thus, *shha* appears to be able to drive ectopic bone secretion by mesenchymal cells in the regenerate (Fig 9-B) (Quint et al , 2002)

Thus, in the fin regenerate, *shha* seems to be involved in patterning the branches formation and/or inducing osteoblast differentiation

ihha is also expressed in a subpopulation of cells in the regenerate, the newly differentiated osteoblasts in the differentiation zone, adjacent to, but not overlapping with, *shha*-expressing cells (Fig 8-C) This expression domain is maintained throughout the regeneration process and remains confined to the distal tip of the regenerate It also obeys to an apparent cyclic expression pattern, alternating between a single domain of expression per ray and division of the expression domain into two populations of cells, announcing a bifurcation (Avaron et al , 2006)

As *Ihh* is known for its role during the endochondral bone formation, it is most likely playing a role during osteoblasts differentiation in the regenerate This presumed role is in accordance with its expression pattern

ihha and *shha* are highly conserved in vertebrates In zebrafish, they present a high degree of homology Thus, one can expect a partial redundancy in the function of these two genes However, the targeted expression domain that never overlaps during

fin regeneration would suggest a different role for *shha* and *ihha* during regeneration.

In order to determine what are the respective roles of the *shha*- and *ihha*-expressing cells during caudal fin regeneration, specific deletion and/or loss-of-function experiments for each of them is required.

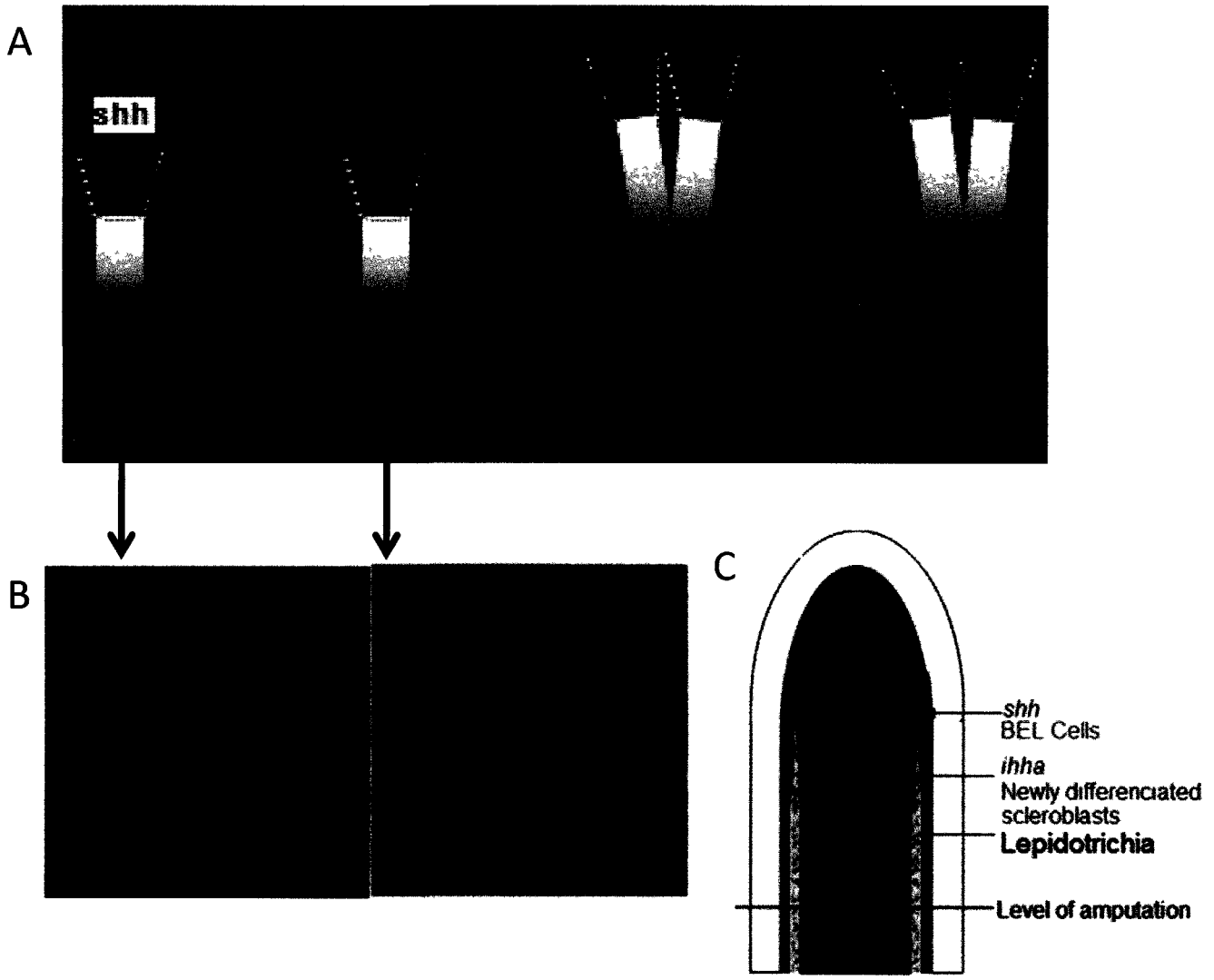

Figure 8: Schematic representation of *shha* expression pattern during branching morphogenesis (A) , *shha* ISH on transverse section(B) and schematic representation of *shha* and *ihha* expression in fin ray lateral section

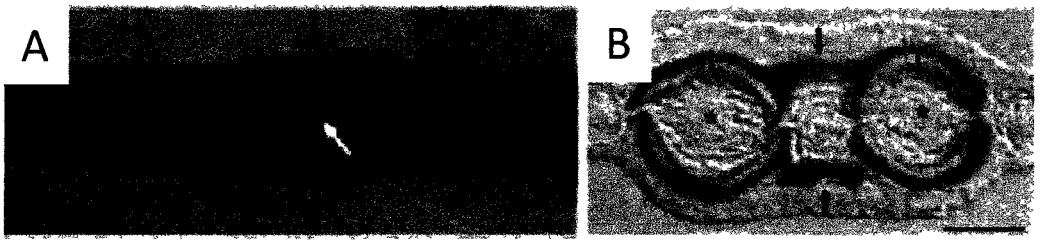

Figure 9: Ectopic expression of *shha* leads to ectopic bone formation

Figure 8: (A) The *shha*-expression pattern (in pink) during fin ray regeneration is very dynamic. When a single ray is growing, a single subset of *shha*-expressing cells exists in the regenerate. Before a bifurcation occurs, the single domain of *shha*-expressing cells separates into two domains, located on the lateral sides of each fin ray. This separation seems to announce a future bifurcation. (B) *shha in situ* hybridization on transverse sections, showing the separation of the *shha*-expressing cells. (C) Schematic representation of a single blastema, *shha* and *ihha* expressions are shown in pink and in orange, respectively.

Figure 9: Ectopic expression of *shha* in between the sister rays (white arrow in A) leads to ectopic bone formation (B) and sister rays fusion. Adpted from (Quint et al. 2002), permission to reproduce obtained from publisher.

V. Background information related to the project

1. Characterization of the *shha* regulatory elements

In order to characterize *shha* regulatory elements, Dr. Uwe Strähle's group used a transient transgenesis approach. They made several constructs containing genomic fragments of the 2.4kb promoter sequence along with either intron1 or intron2 of the *shha* gene, and this cassette was inserted upstream of the *LacZ* reporter gene. These constructs were injected in one-cell stage zebrafish embryos, which were screened for *LacZ* expression at later stages to reveal the regulatory activity of the genomic fragments. Thus, they could isolate three regions within intron1 and intron2 able to drive *LacZ* expression in the embryos: ar-A and ar-B in intron1, and ar-C in intron2. While ar-A and ar-C drive *LacZ* expression mostly in the notochord and floor plate cells, ar-B induces an expression only in the floor plate. The promoter alone is sufficient to drive expression of the reporter in the hindbrain (Muller et al., 1999).

2. The transgenic line *2.4shh:gfp:ABC*#15

Based on the above findings, Dr. Uwe Strähle's group created a stable transgenic line *2.4shh:gfpABC*#15, that expresses the GFP protein under the control of the 2.4kb *shha* promoter associated to the ar-A, ar-B and ar-C enhancers. In this line, *gfp* expression recapitulates the *shha* endogenous expression in the brain, floor plate and notochord during embryonic development. However, the regulatory elements that were used do not contain the sequence that is necessary for the expression in the pectoral fin buds since no GFP could be observed in the fin buds of transgenic embryos. This construct, however, drives the expression of the GFP protein in the *shha*-expressing cells during caudal fin regeneration.

3. Laser ablation of the *shha*–expressing cells

In an attempt to determine the role of the *shha*-expressing cells during zebrafish caudal fin regeneration, Jing Zhang, a former M.Sc. student in Akimenko's lab performed a laser ablation of the *shha*-expressing cells in 3 dpa regenerates. Jing Zhang used the *2.4shh:gfpABC*#15 transgenic line kindly provided by Dr. Uwe Strähle, which is expressing GFP in the *shha*-expressing cells during caudal fin regeneration (see '5.b. Transgenic line *2.4shh:gfpABC*#15'). Using a laser beam, GFP+ cells were removed from the regenerate at 3dpa. Fins were examined at 6dpa.

In the rays in which the *shha* –expressing cells were ablated, branching morphogenesis patterning was disturbed: after 3 days post-amputation, the branches formation in these rays cells was delayed, compared to their non ablated counterparts on the opposite lobe of the same fin. The ray branching morphogenesis was considered as delayed when the branching occurred at least two segments more distal than the control. This delay was observed in 48% of the ablated rays vs. 0.07% in non ablated rays, showing that the delay is resulting from the transient absence of the *shha*-expressing cells in the regenerate. A very slight growth delay may also occur in the ablated rays but it was not large enough to be quantified (Zhang, unpublished data). Thus, these results suggest that *shha*-expressing cells may regulate branching morphogenesis during fin ray regeneration.

However, the method of laser ablation presents several limitations: beside the fact that it is tedious and time-consuming, it does not allow to keep the *shha*-expressing cells absent from the regenerate for longer than 9 hours. This is due to the quick regeneration that leads to the rapid restitution of the lost cells. We think that the lapse

of time during which the *shha*-expressing cells are absent from the regenerate is not sufficient to observe the complete effect of a long-term ablation of this cell population

Because of this limitation, we decided to use a different approach to determine the effect of the long-term ablation of the *shha*-expressing cells on the regeneration For this, we used the Nitroreductase/Metronidazole ablation system to achieve cell ablation in an easy, targeted and inducible way in a stable transgenic line

4. Background information on the targeted ablation system: Nitroreductase/Metronidazole

Gene Directed Enzyme/Prodrug Therapies (GDEPT), also termed in the literature as Suicide Gene Therapies (SGD), Virus Directed Enzyme Prodrug Therapies (VDEPT) or Gene Prodrug Activation Therapies (GPAT) are approaches used in the cancer research field in an attempt to develop cancer gene therapy (Altaner, 2008) They are all based on the ability of a foreign enzyme to convert its substrate into a cytotoxic agent The treatment consists in two main phases, 1) the transgene that is coding for the foreign enzyme (bacterial, viral or yeast) is delivered in the tumor cells *via* different ways, 2) a low toxicity drug is systemically administered and will be converted by the enzyme into its cytotoxic product, in the tumor cells only When administered *in vivo*, not all tumor cells will receive the gene coding for the enzyme However, the cytotoxic form of the prodrug can get out of the transduced cells and kill not only the tumor cells in which it is synthesized, but also neighboring tumor cells in a solid tumor This process is termed 'bystander effect' (Altaner, 2008) Bystander effect was proposed to be dependent on GAP junctions for the

Enzyme/Prodrug ablation system Thymidine kinase/Ganciclovir, which allows transferring the active drug from transfected cells to untransfected cells (Mesnil et al., 1996).

Nitroreductase/CB1959 is one of these GDEPT that was developed to kill a specific cell population (tumor cells) through the conversion of CB1959 into its cytotoxic form (Bridgewater et al., 1995).

Nitroreductase is a bacterial enzyme which is synthesized by E.coli, coded by the *nfsB* gene. It has the ability to reduce its substrates, CB1954, Nitrofurantoin (NFT) and Metronidazole (MTZ) into cytotoxic agents that bind to the DNA, induce double strand break and lead to apoptosis (Fig. 10 A). In 1997, Bridgewater et al. tested the ability of Nitroreductase to reduce several of its substrates and assessed the bystander effects of each of them. Thus, they were able to show that, in contrast to the reduced form of CB1954, reduced MTZ does not have any bystander effect (Bridgewater et al., 1997). This was explained by the fact that reduced MTZ is unstable in normal oxygen conditions, and thus, could not diffuse from the transfected to the untransfected neighboring cells.

In 2007, two groups, Curado and colleagues as well as Pisharath and colleagues, took advantage of the absence of the bystander effect observed when the Metronidazole is used as a substrate for the Nitroreductase, to develop a conditional targeted ablation system in zebrafish embryos (Curado et al., 2007; Pisharath et al., 2007). The two groups published their results at about the same time, and both group's results were similar. We will only further refer to the results described in Curado et al, as they described the ablation system in a wider panoply of tissue, in three different transgenic lines (cardiomyocytes, liver and beta-cells ablation), covering the cell type

that was addressed in Pisharath et al's results (beta-cells only).

Curado et al. created zebrafish stable transgenic lines in which *nfsB,* the gene coding for the *E.coli* Nitroreductase (NTR), was fused to the Cyano-Fluorescent Protein (CFP) gene. The fusion protein was specifically expressed in a targeted cell population, through the use of tissue-specific promoter. Three transgenic lines were created where CFP-NTR was expressed in the beta cells of the pancreas, the cardiomyocytes of the heart and the hepatocytes of the liver. The transgenic embryos were exposed to different concentrations of MTZ for different times. CFP expression disappeared in treated embryos after a specific time of exposure, and correlated with an increasing rate of apoptosis of the target cells. Even though some CFP+ cells remained in the embryos, a Caspase3 staining allowing the detection of apoptotic cells showed that these cells were undergoing apoptosis. Following the transfer of the embryos to clean water, the Metronidazole was washed out of the embryos and CFP+ cells later reappeared, showing that the ablation effects could be reversed (as long as the tissue can regenerate).

Therefore this system allows a conditional, spatially and temporally controlled, ablation of a cell population, as long as a specific promoter is available to target the desired cell population (Fig. 10 B). The only cells that are affected by the ablation in the presence of MTZ are the cells that are coding for NTR, as MTZ itself does not have any cytotoxic effects and the reduced MTZ is not stable enough to diffuse to surrounding cells (Curado et al., 2008).

A

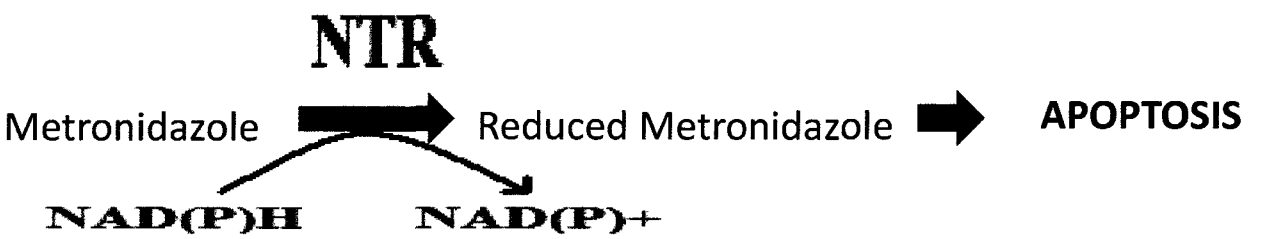

B

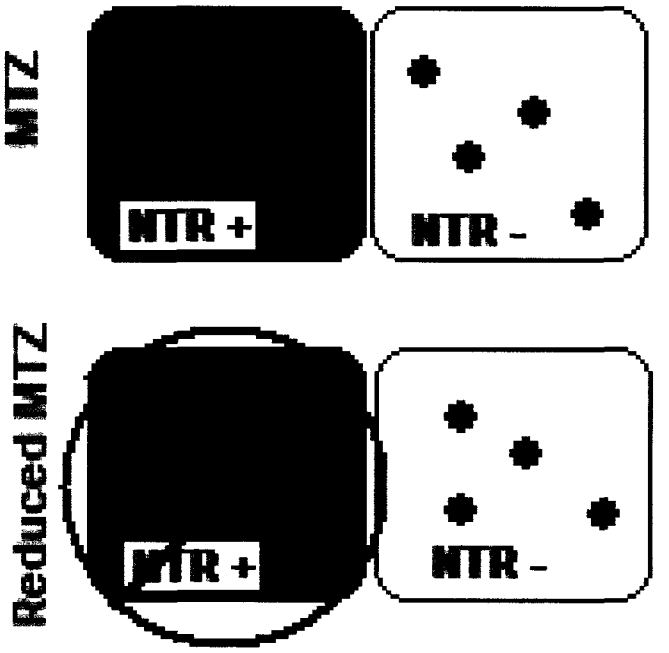

Figure 10: Nitroreductase/ Metronidazole ablation system

Figure 10: The NTR/MTZ system. (A) Following the reduction of the prodrug MTZ by the nitroreductase enzyme, MTZ is converted into a cytotoxic agent that induces apoptosis. (B) The use of the NTR/MTZ to ablate a targeted cell population. The blue cells are expressing the *cfp-ntr* fusion gene. Thus, following addition of MTZ to the medium, the blue cells convert the prodrug MTZ into the cytotoxic agent. Neighboring cells, represented in white, are unable to do so. Thus, the blue cells are the only cell population that will be ablated.

Since these initial studies, the NTR/MTZ ablation system has been used to efficiently ablate specific cell populations such as retinal cells (Zhao et al., 2009) and testis cells (Hsu et al. 2010) in zebrafish embryos, as well as retinal cells in adult zebrafish (Montgomery et al., 2010).

Hypothesis and objectives

The Hedgehog signaling pathway is active during zebrafish caudal fin regeneration. Two members of the *Hedgehog* family are expressed during caudal fin regeneration: *shha* and *ihha*. They are expressed in two neighboring, but non-overlapping cell populations in the differentiation zone.

shha is expressed in the basal layer of the epidermis in the differentiation zone. It has the ability to induce ectopic bone secretion.

Besides its potential involvement in bone formation, the Hh pathway is required to maintain the cell proliferation in the regenerate and ensure the regenerate outgrowth. A proliferative effect of Shh has also been proposed in the developing lung in mice embryos, where Shh is thought to regulate the branching morphogenesis process through inducing cell proliferation.

shha expression pattern suggests a role in branch formation during fin ray regeneration as well. It might be doing so by inducing cell proliferation in a way that is favorable to branches formation. Similar to other branching morphogenesis models, Hh signaling might also be involved in cross-talks with other pathways such as Fgf signaling, to induce the branching morphogenesis. The hypothesis of *shha*-expressing cell being required for a correct patterning of the rays is supported by data obtained from the transient deletion of the *shha*-expressing cells during regeneration (laser ablation). However, the transient characteristic of these ablations prevented us to examine the long-term effects of the ablation of the *shha*-expressing cells. Thus, the

exact role of the *shha*-expressing cells during regeneration remains unclear.

The purpose of this study is to determine the role of the *shha*-expressing cells during zebrafish caudal fin regeneration. We want to further understand the mechanism by which *shha*-expressing cells are influencing the branching morphogenesis process by:

1) Precisely characterize the behavior of *shha*-expressing cells during branch formation.

2) Study the detailed profile of cell proliferation, in regard to the behavior of the *shha*-expressing cells, during branching morphogenesis in the regenerate. This will allow us to better understand the dynamic of cell proliferation in relation to the branching morphogenesis steps, and identify a possible relation between *shha* expression and cell proliferation profile.

3) Analyze the expression profile of genes that are potentially involved in mediating potential Hh/Fgf cross-talk.

4) Undertake a different ablation approach, based on Nitroreductase-Metronidazole enzyme-prodrug system in a stable transgenic line, to observe the long-term ablation effects on the regeneration process.

In a larger perspective, this project will allow to further decipher the molecular cross-talks and cellular events that are taking place during zebrafish caudal fin regeneration, and provide insights into the branching morphogenesis process.

Materials and Methods

1. Animals

The zebrafish *2.4shh:gfpABC*#15 transgenic lines were kindly provided by Dr. Uwe Strähle. The Loeb Wild type fish were born and raised in the Loeb fish facility. Fish are maintained at 28.5°C with a photo-period of 14 hours of light and 10 hours of darkness, and fed regularly (Westerfield, 1995).

2. Fin amputation

Adult zebrafish of at least 12 weeks of age were anesthetized by immersion in system water containing 0.17 mg/ml tricaine (ethyl-aminobenzoate; Westerfield, 1995) to immobilize the fish and minimize possible pain and discomfort caused by the procedure. Caudal fins of adult fish were amputated, using a scalpel blade, one to two segments proximal to the first branching point of the lepidotrichia. Fish were then returned to their tanks where they rapidly recovered with very little bleeding and no sign of obvious pain. Afterwards at various time points, the fin regenerates were collected by cutting the regenerated part one segment proximal to the first amputation plane, using a scalpel blade.

3. Fluorescence imaging

A dissection microscope (Leica MZ FLIII) with integrated FLUOIII filter system was used to visualize the samples. A digital camera (Sony 3CCD Color Video Camera)

and AxioVision software were used to photograph the samples. Fluorescent pictures of whole-mount caudal fin require an average exposure time of 1sec. Bright-field pictures of the same fin require an exposure time of 6 msec.

4. Preparation of antisense RNA probes

Antisense RNA probes were synthesized *in vitro* from a linearized DNA template. The synthesis reaction contained 1 μg of linearized DNA template, 2μl NTP labelling mix (10mM ATP, 10mM CTP, 10mM GTP, 6.5mM UTP, 3.5mM DIG-11-UTP (Roche)), transcription buffer (40mM Tris pH 8.0, 6mM $MgCl_2$, 10mM DTT, 10mM NaCl, 2mM spermidine (Roche)), 20 units RNAsin (Fermentas), and 20 units of the appropriate RNA polymerase (Roche) (refer to Appendix I). Diethyl pyrocarbonate (DEPC) treated water was added to bring the total volume to 20μl. The reaction mixture was incubated at 37°C for two hours. The synthesized probe was then purified using the Sigma Spin Post-Reaction Clean up Columns (Sigma-Aldrich S5059-70E) according to the manufacturer instructions. To check the RNA concentration and quality, 1μl of probe solution was mixed with 1μl of 2xRNA loading dye and 5μl of Diethyl pyrocarbonate (DEPC) water. The mix was heated at 70 °C for 5 minutes and chilled on ice, before to be run on a 0.8% RNAse free agarose gel. To ensure a better preservation of the synthesized RNA, the remaining volume of the probe mixture (19μl) was mixed with 9μl of "RNA later" (Sigma) and 1μl of 0.5M EDTA. The average RNA probe concentration obtained following this protocol was about 120ng/μl.

5. Whole mount *in situ* hybridization

In situ hybridization experiments on whole mount fins were performed as described in Laforest et al., (1998). Fins were fixed overnight in a solution of PBS containing 4% paraformaldehyde (PFA) at 4°C. The samples were washed twice in PBS, twice in 100% methanol and were stored in methanol for at least 2 hours at -20°C. The samples were subsequently rehydrated in a series of 5-minute washes in dilutions of methanol and 1xPBS (75% MeOH:25% PBS, 50% MeOH:50% PBS, 25% MeOH:75% PBS). The samples were washed 3 times for 5 minutes each in PBST (1x PBS, 0.1% Tween-20). Fins were permeabilized in 20µg/ml proteinase K (Invitrogen) for 30 min. The samples were then washed twice for 5 minutes in PBST, fixed for 20 minutes in 4% PFA and washed twice for 5 minutes in PBST. Samples were then incubated in acetylation solution consisting of 125µl triethanolamine and 27µl acetic anhydride in 10ml of water for 10 minutes, followed by two 10-minute washes in PBST. Next, embryos were pre-hybridized at 65°C for 3-4 hours in a solution containing 50% deionized formamide, 5x SSC (20x SSC stock solution; 3.0M NaCl, 0.3M citric acid), 0.1% Tween-20, 50 µg/ml heparin, 9.2mM citric acid and 200 µg/ml yeast tRNA. After incubation for 3-4 hours, the hybridization solution was replaced with a fresh pre-hybridization solution containing 1 ng/µl DIG-labeled antisense RNA probe and the samples were allowed to hybridize overnight at 65°C.

The next day, the hybridized samples were washed at 65°C for 15 minutes in a series of dilutions of hybridization mix (1x salt, 50% Ultrapure Fromamide, 10% Dextran sulfate, 1mg/ml yeast tRNA, 1x Denhardts solution) and 2x SSC (75% hyb mix:25%

2x SSC, 50% hyb mix:50% 2x SSC, 25% hyb mix:75% 2x SSC and 100% 2x SSC). This was followed by two 30-minute washes in 0.2x SSC. The samples were successively washed at room temperature in serial dilutions of 0.2x SSC and PBST (75% 0.2x SSC:25% PBST, 50% 0.2x SSC:50% PBST, 25% 0.2x SSC:75% PBST and 100% PBST) for 10 minutes each. The samples were then pre-incubated for 1 hour at room temperature in PBST containing 10% calf serum and 40mg/ml BSA. Fins were subsequently incubated at room temperature for 2-4 hours in a solution consisting of a pre-absorbed anti-DIG antibody conjugated to Alkaline Phosphatase (AP) (Roche). Pre-absorption of the antibody was performed during the first day of the in situ hybridization where 2-3 of non-hybridized fins were placed in a solution containing 20µl calf serum, 20µl BSA, and 1µl anti-DIG AP antibody and 960µl PBST for 2-4 hours at room temperature and then placed at 4°C overnight. Following incubation with the pre-absorbed anti-DIG AP antibody the hybridized embryos were washed twice for 5 minutes and then placed at 4°C overnight.

The hybridized fins were subsequently washed 6 times for 15 minutes each in PBST. Prior to the chromogenic reaction, the fins were equilibrated in three 5-minute washes in equilibration buffer (100mM Tris pH 9.5, 50mM $MgCl_2$, 100mM NaCl) plus 0.1% Tween-20. Fins were stained in a solution containing 0.175 mg/ml 5-Bromo-4-Chloro-3-Indolyl phosphate (BCIP) and 0.337mg/ml Nitro Blue Tetrazodium (NBT) in the staining buffer at room temperature until a suitable color was visualized. After staining, the samples were washed in PBST and post fixed in 4% PFA for 2 hours. Fins were then washed in PBS and stored at 4°C in PBS containing 5mM EDTA. The entire *in situ* hybridization procedure was carried out in six well plates (NUNC Brand Products) with the fins placed in plastic "baskets". The pre-hybridization and hybridization steps were however performed in eppendorf tubes.

Fins were observed and photographed using a Leica microscope equipped with Eclipse software.

6. Sectioning of fin samples for *in situ* hybridization

Collected fins that were fixed in 4% PFA were rehydrated in a series of 5 minutes washes in dilutions of methanol and PBS (75% MeOH: 25% PBS, 50% MeOH: 50% PBS, 25% MeOH: 75% PBS). The samples were washed 3 times for 5 minutes each in PBST. Fins were then embedded in a melted embedding gel (1.5% agarose in 1xPBS and 5% sucrose). After solidification, a block enclosing the tissue to be sectioned was trimmed with a scalpel. These blocks were placed in a 30% sucrose PBS solution and stored at 4°C overnight. The blocks were mounted on the cryostat chuck in a layer of cryomatrix (VWR) and then frozen in 2-methyl butane (-80°C). Sections of 16μm thick were made using a cryostat sectioner (Leica CM3050S). Sections were collected on coated glass slides and stored at –20°C until used.

7. *In situ* hybridization on cryostat sections

The sections on slides were thawed at room temperature for at least 1 hour, and warmed up at 60°C for 10 minutes. Slides were then fixed for 5 minutes in 4% PFA in PBS, followed by 2 times 5 minutes washes in DEPC-PBS (pH7.4). Samples were incubated for 15 minutes in 0.3% Triton X-100/DEPC-PBS (pH7.4), and washed 2 times for 5 minutes with DEPC-PBS. The tissue was permeabilized in 20μg/ml proteinase K (Invitrogen) for 30 min. The samples were then washed twice for 5 minutes in DEPC-PBS. Samples were then incubated in acetylation solution

consisting of 500µl triethanolamine and 108µl acetic anhydride in 40ml of DEPC treated water for 5 minutes, and dehydrated in a series of 3-minute washes in dilutions of ethanol and DEPC-treated water (50% ethanol:50% DEPC-H2O, 70% ethanol:30% DEPC-H2O, 95% ethanol:5% DEPC-H2O, 100% ethanol). Next, slides were pre-hybridized at 60°C for 2-3 hours in pre-hybridization solution (50% deionized formamide, 1x Salt, 10% Dextran Sulfate, 1mg/ml yeast tRNA, 1x Denhardts solution, in DEPC-treated water). Each slide was covered with 500µl of the pre-hybridization solution, and pre-hybridization was made in a sealed plastic box containing a piece of brown paper soaked in 0.1xSSC and 50% formamide solution, to create a humidified chamber. After incubation for 2-3 hours, the hybridization solution was replaced with a fresh pre-hybridization solution containing 1 ng/µl DIG-labelled antisense RNA probe, previously denatured for 5-10 minutes at 70°C. The samples were allowed to hybridize overnight at 60°C.

The next day, the hybridized samples were washed at 60°C for twice 20 minutes in 2xSSC, twice 20 minutes in 1xSSC/50% formamide and twice in 0.2x SSC. This was followed by two 10-minute washes at room temperature in TBST (0.14M NaCl, 0.27mM KCl, 25mM Tris-HCl and 1% Tween-20). The samples were then pre-incubated for at least 1 hour at room temperature in TBST containing 10% calf serum. Absorption of the antibody was performed by adding 500µl of 1:2000 anti DIG AP antibody in blocking solution. This step was done overnight at 4°C, in a sealed plastic box containing a piece of brown paper soaked in water.

The next day, hybridized samples were subsequently put through 3 washes of 10 minutes each in TBST. Prior to the chromogenic reaction, the fins were equilibrated in 10-minute washes in NTMT equilibration buffer (100mM Tris pH 9.5, 50mM

$MgCl_2$, 100mM NaCl) Sections were stained in a solution containing 0 175 mg/ml 5-Bromo-4-Chloro-3-Indolyl phosphate (BCIP) and 0 337mg/ml Nitro Blue Tetrazodium (NBT) in NTMT equilibration buffer (100mM Tris pH 9 5, 50mM $MgCl_2$, 100mM NaCl) at room temperature until a suitable color was visualized After staining, the samples were washed in PBS containing 10mM EDTA and post fixed in 4% PFA for 20 minutes A quick wash with water preceded the mounting step Microscopy aquatex mounting medium was used to mount the slides

8. Cryostat sectioning of fin samples for anti-PCNA antibody staining

The same procedure as cryostat sectioning for *in situ* hybridization samples was followed, except that the fixation was done in 9 1 Formaldehyde (37%) Ethanol (95%) for overnight at 4°C

9. Anti-PCNA antibody staining

Slides were thawed at room temperature for at least 2 hours Samples were rehydrated in 1xPBS for 30 minutes, and blocked at room temperature for 2 hours (Blocking solution 0 2% Triton X-100 and 2% Calf Serum in 1x PBS) Rabbit anti-PCNA antibody (FL261, Rabbit Polyclonal, Santa Cruz Biotechnology) was diluted in blocking solution to 1 100, and slides were covered with 200µl of the primary antibody Sections were incubated overnight at 4°C in a sealed plastic box containing a piece of brown paper soaked in water, to create a humidifying chamber

The next day, samples were washed for at least 4x10 minutes at room temperature, in

1x PBS with 0.1% Tween-20. Sections were incubated for 4 hours at room temperature, with Fluorescent labeled secondary anti-rabbit antibody (Alexa Fluo 594, red Goat anti-rabbit IgG, cat.#A11012, and Alexa Fluo 488, green Goat anti-rabbit IgG, cat.# A11088) diluted to 1:500 in 1xPBS with 0.1% Tween-20. Samples were subsequently washed for at least 4x10 minutes at room temperature, in 1x PBS with 0.1% Tween-20, quickly washed in water and mounted, with either microscopy aquatex mounting medium, or DAPI staining mounting medium (Vector Laboratories, Inc.).

The same protocol was followed for anti-GFP antibody and anti-Zns-5 antibody (adapted from the protocol used in Dr. Vince Tropepe laboratory).

10. Cloning of the *GFP* gene

The *GFP* cDNA was PCR amplified from the *2.4shh:gfp:ABC* construct, kindly provided by Dr. Uwe Strahle. PCR product was inserted in pDrive MCS. Primer sequences are described in the Appendix II.

11. Subcloning of the *2.4shh:cfp-ntr:ABC* construct

The *2.4shh:cfp-ntr:ABC* construct was made by subcloning the *2.4shh* promoter from the *2.4shh:gfp:AC* construct (kindly provided by Dr. Uwe Strahle, and previously used to create the *tg2.4shh:gfp:ABC* #15) in pDrive. This was done by PCR amplifying the promoter using suitable primers (see Appendix II for all the primer sequences).

The promoter was subcloned upstream of the *cfp-ntr* fusion protein gene, in the Tol2-MCS-CFP-NTR construct (kindly provided by Dr. Didier Stainier. The fragment was inserted as an NheI/MluI fragment. This construct is called *2.4shh:cfp-ntr:tol2*

The ar-A and ar-C elements were also inserted in pDrive, through PCR amplification using suitable primers. ar-B was later inserted downstream of ar-A and upstream of ar-C, as an SpeI/SfiI fragment. This plasmid will be called ABCpDrive. The ABC fragment was excised from the ABCpDrive and inserted in a Tol2-carrying plasmid, the Tol2_sp72 (kindly provided by Dr. Marc Ekker), as a SalI/KpnI fragment.

Finally, the *2.4shh:cfp-ntr* was amplified from the *2.4shh:cfp-ntr:tol2* plasmid, inserted in pDrive and sub-cloned as a SalI fragment upstream of the ar-A, ar-B and ar-C sequence, in the Tol2:ABC_sp72 plasmid. The final plasmid is called *2.4shh:cfp-ntr:ABC.*

12. Transposase mRNA synthesis

The pCS-TP plasmid, containing the *transposase* gene downstream of the sp6 RNA polymerase promoter sequence, was linearized with NotI restriction enzyme. The RNA synthesis was done using the Ambion SP6 mMessage mMachine kit, according to the manufacturer instructions. The reaction was stopped and the RNA was precipitated by adding 30µl of nuclease free water and 30µl of LiCl precipitation solution (available with the kit). The mixture was kept at -20°C for at least 30 minutes, and then centrifuged at 4°C for 15 minutes, at 13000 rpm. The supernatant was carefully removed and the pellet was washed twice with 70% ethanol in DEPC-water, with 15 minutes centrifugation at 4°C in between. Finally, RNA was re-suspended in DEPC-treated water, to a final concentration of 100ng/µl, and stored as individual 1µl

aliquot at -80°C.

13. Microinjection

Injection mix was prepared just prior to the injection. The DNA was diluted to a final concentration of 100ng/µl along with Phenol Red 0.5%. For the *2.4shh:cfp-ntr:ABC*, 50ng/µl of *transposase* mRNA (one aliquot (1 µl) of 100ng/µl was used *per* injection day) was added to the injection mix. Final volume was adjusted with DEPC treated water. One-cell stage embryos were collected, treated with bleach and aligned in an agarose injection plate. Injection was done using 'NARISHIGE IM-300' microinjector, with a pressure of 102 psi and for 30 msec/injection.

14. Screening

Injected fish were screened at 24 hpf for cyan fluorescence. Only the embryos that showed a strong and complete expression pattern (recapitulating the GFP expression in the *2.4shh:gfp:ABC*#15 line) were kept to be raised. Three month old injected fish were bred and their progeny were screened at 24 hpf for cyan fluorescence. A couple was considered as 'screened-negative' whenever 300 of their off-springs were obtained and no fluorescence was observed.

15. Metronidazole treatment

The treatment was done on 24 hpf injected embryos previously screened for cyan fluorescent under UV light. Fluorescent embryos were transferred to either in embryo

medium containing 0.2% DMSO or in embryo medium containing 3, 5 and 10 mM MTZ in 0.2% DMSO. Treatment was done for 24 hours in the dark at 28.5 °C. The treated embryos were observed at 48 hpf (24 hours post treatment) for fluorescence signal strength/ fluorescent cells number.

Results

I. Characterization of the *2.4shha:gfp:ABC#15*

1. Analysis of the expression of GFP in the *Tg 2.4shha:gfp:ABC#15* during fin ray branching morphogenesis

In the introduction section **'IV. 3. Laser ablation of the *shha* –expressing cells'**, we were reporting a branching morphogenesis defect in the rays in which *shha* –expressing cells were temporarily removed The delay in branching formation observed in the laser ablated rays, along with previously reported *shha* expression pattern analysis, suggest that *shha*–expressing cells are directing the branching morphogenesis In order to better understand the behavior of the *shha*-expressing cells during fin ray branching morphogenesis, we used the *2 4shh gfp ABC#15* line to visualize these cells *in vivo* and precisely follow their fate during the branching morphogenesis process This line was kindly provided by Dr Uwe Strahle and has the *gfp* gene expressed under the control of the 2 4kb *shha* promoter fragment, associated to the ar-A, ar-B and ar-C *shha* enhancers GFP expression in the regenerating tail recapitulates the endogenous *shha* expression during this process and this line was previously used for the laser ablation experiments (see Introduction for more details)

However, before undertaking the description of the time course of the GFP expression pattern, during branching morphogenesis, I would like to quickly review the main components of a fin ray Also, I want to introduce a schematic representation of a single fin ray, before and after bifurcation This schema can be used as a reference to locate sections along the proximal-distal axis in the fin regenerate

The morphology of a transverse section of a fin regenerate is described in Fig R1. It represents a transverse section through two adjacent rays of a 6 dpa regenerate. The section was made at a very proximal level, where the bone matrix is very thick. This allows a better visualization of the bony structures, as well as other components of the fin. At this level, the different cell types are fully differentiated, which allows to observe a good organization of the different tissues. As we progress toward the distal edge of the regenerate, the bone matrix gets thinner to completely disappear at the distal-most extremity of the differentiation zone. The blastema is located at the distal tip of the ray. No bone matrix is observed at the blastema level, as no osteoblasts are present (not shown).

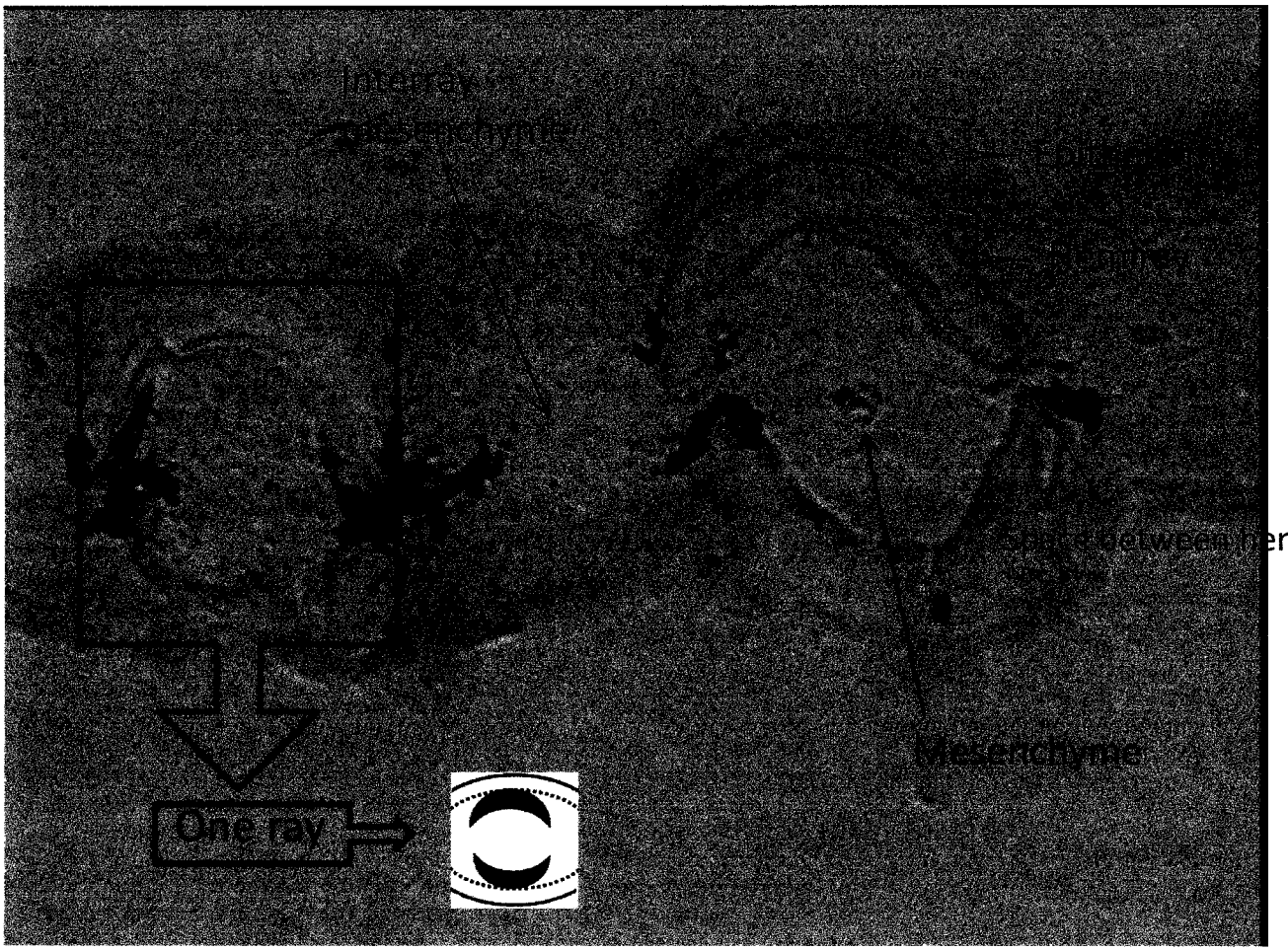

Description of a proximal 6dpa regenerate transverse section

Figure R1

Figure R1: Transverse section showing the morphology of two fin rays at 6dpa in the proximal part of the regenerate. Each ray is composed of two dermal bony hemirays (yellow), enclosing a loose mesenchymal tissue (blue arrow). The hemiray is surrounded by a multilayered epidermis (red). Each ray is composed of two concave hemirays facing each other, but the two extremities of the hemirays are not fused (cherry arrow). Hemirays are separated by mesenchymal tissue. The two adjacent rays are separated by an interray mesenchymal tissue (orange arrow). The green box represents a schema of transverse section of a ray.

A schematic representation of the process of branching morphogenesis, along with transverse sections across different levels of the regenerating ray is presented in Fig R2. In the figure R2 (A), a single ray that has not undertaken the bifurcation process yet is represented. As we progress from distal to proximal, the bone matrix appears and gets thicker (Fig R2 A1 to A3). Fig R2 A1 represents a transverse section through the blastema. At this level, no bone matrix is deposited. A2 represents a section that is made a bit more proximal in the ray. At this level, differentiated osteoblasts secrete a very thin bone matrix A3 represents a section at the very edge of the amputation level. The same description could be made regarding bone matrix thickness as we progress along the proximal-distal axis on the bifurcating ray represented in Fig R2 B. However, in the ray that is undergoing bifurcation, two blastemas are present. Each blastema belongs to one of the newly formed sister ray. Fig R2 B2 represents a section that is made slightly more proximally. Similarly to Fig R2 B1, two bone-deposition domains are present, representing the two sister rays. As we progress toward the level of amputation (proximal), the bone matrix gets thicker, and the two sister rays are not distinguished anymore. In fact, more proximally, a single ray is observed. Fig R2 B4 represents a very proximal section which belongs to the regenerated part at 5-6 dpa.

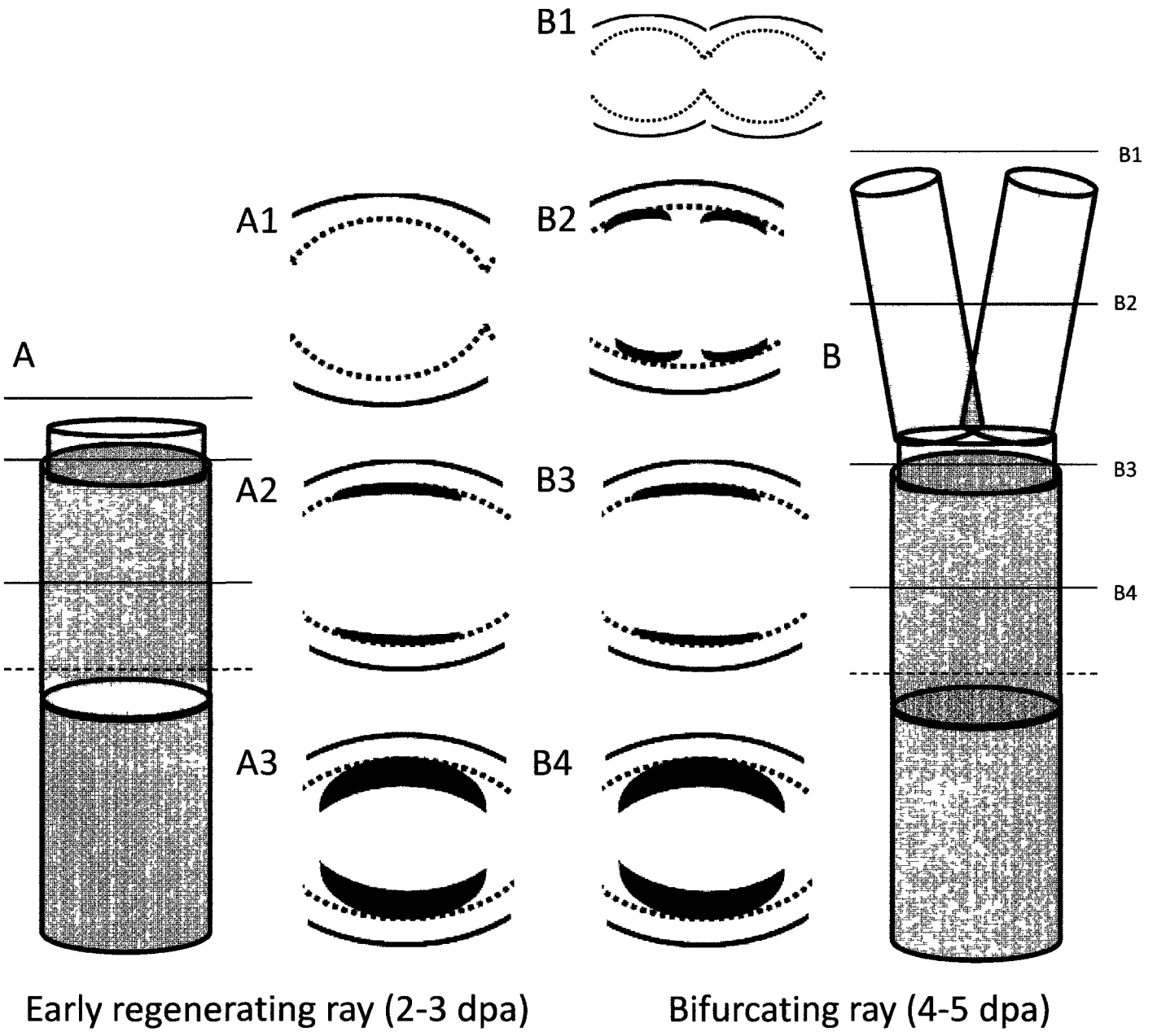
A
A1
A2
A3
B1
B2
B3
B4
B
B1
B2
B3
B4
Early regenerating ray (2-3 dpa)
Bifurcating ray (4-5 dpa)

Figure R2

Figure R2: Schematic representation of a single ray before (A) and after (B) bifurcation.

(A) Single ray regenerate at 2-3 dpa, before bifurcation: (A1) In the distal part of the regenerate, a single blastema cell population is localized in the central part of the ray. The blastema is surrounded by a multilayered epidermis. The red dotted line indicates the limit between the epidermis and the blastema. At this level along the proximal-distal axis, the only separation between the two cell types consists in basement membrane. (A2) At a more proximal location is the differentiation zone, where the newly differentiated osteoblasts are formed and start secreting bone matrix in the space between the epidermis and the mesenchyme. The layer of newly secreted bone matrix is very thin (represented as a dark blue crescent). (A3) At a more proximal level, closer to the amputation plane (shown in (A) as a red dashed line) the bone matrix is thicker.

(B) Single ray regenerate at 4-5 dpa, during/after bifurcation: (B1) In the very distal part of the regenerate, each lepidotrichia possesses two blastema, one blastema *per* sister ray. The two blastemas are linked through mesenchymal interray. (B2) In the differentiation zone, two sub-domains of bone matrix-secreting cells are present, within one fin ray. The two newly formed osteoblast domains are located lateral to the original hemiray. These two sets of osteoblasts direct the branching morphogenesis through lateral bone matrix deposition. (B3) In the proximal part of the regenerate, a single set of osteoblasts is present. (B4) At the more proximal level, closer to the amputation plane (shown in (B) as a red dashed line), the bone matrix is thicker. The section has the same morphology as the proximal section observed at 2-3 dpa (A3).

To precisely follow the fate of the GFP+ cells during branching morphogenesis, caudal fin amputation (one to two segments below the first bifurcation point) was performed on a group of twelve *2.4shha:gfp:ABC#15* adult fish. Caudal fin regeneration was monitored between 2 dpa and 10 dpa, at 28.5 °C, to examine the time course of *gfp* expression during regeneration (Fig R3).

Pictures were taken every 12h, starting at 2dpa, which is the time when GFP+ cells first appear in the regenerate. At this time point, *gfp*-expressing cells are detected in a single domain. The GFP signal is easily noticeable, even though it is weak. The signal is strengthened at 2.5 dpa and remains confined to a single domain of GFP+ cells, located in the center of each hemiray.

At 3dpa, the three lateral-most bifurcating rays (also called long rays) show two domains of *gfp*-expressing cells located on both sides on the growing ray, instead of the single central domain observed in the previous stages. However, these two domains remain related in the centre *via* GFP+ cells. At 3.5 dpa, this pattern was also observed in 10 out of the 16 other bifurcating rays. We therefore decided to define the stage observed at 3.5 dpa as 'early splitting', when the separation of the *gfp*-expressing domain into two independent domains is clearly noticeable in almost all fin rays. At this time point, in all the bifurcating rays, the two *gfp* expression domains still remain close to each other, with some *gfp* expression in between the two domains (Fig R3, 3.5 dpa, blue arrow).

Cell separation always seemed to be more pronounced in the proximal side of the GFP+ domain than at its distal side (Fig R3, 3.5 dpa, red arrow).

The distal part of the GFP+ domain also displayed a separation pattern, although less wide than in the proximal-most part (Fig R3, 3.5 dpa, asterisk). The GFP+ domain thus formed an H shape at 3.5dpa stage, with a bridge of GFP+ cells between the two

separating domains, and with a clear and deep cell separation in the proximal-most part and a less deep cell separation in the distal-most side (Fig R3, 3.5 dpa).

At 4.5dpa, all branching rays presented fully separated GFP+ domains. The two GFP+ domains are located on the lateral limits of each hemiray. At this stage, the overall shape of the two domains was reminiscent of a heart shape, the two domains being further apart at their distal most tip (Fig R3, 4.5 dpa, asterisk) but remaining closer in their proximal ends. Thus, we called this stage the 'heart-shaped' *shha*-expressing domain.

The 'Heart shape' is still observed at 5 dpa and 6 dpa, but the distance between the two domains is enlarged. As the regenerate grows, the two sister rays will progressively separate, leading to more pronounced GFP+ cell separation. At 10 dpa, the two sister rays are far away from each other, behaving as independent branched rays; the 'heart shape' is lost as each sister ray has its own set of GFP+ cells, that is fully separated from the neighboring one. The GFP+ domain that belongs to each of the newly formed sister rays is located in the central part of the ray.

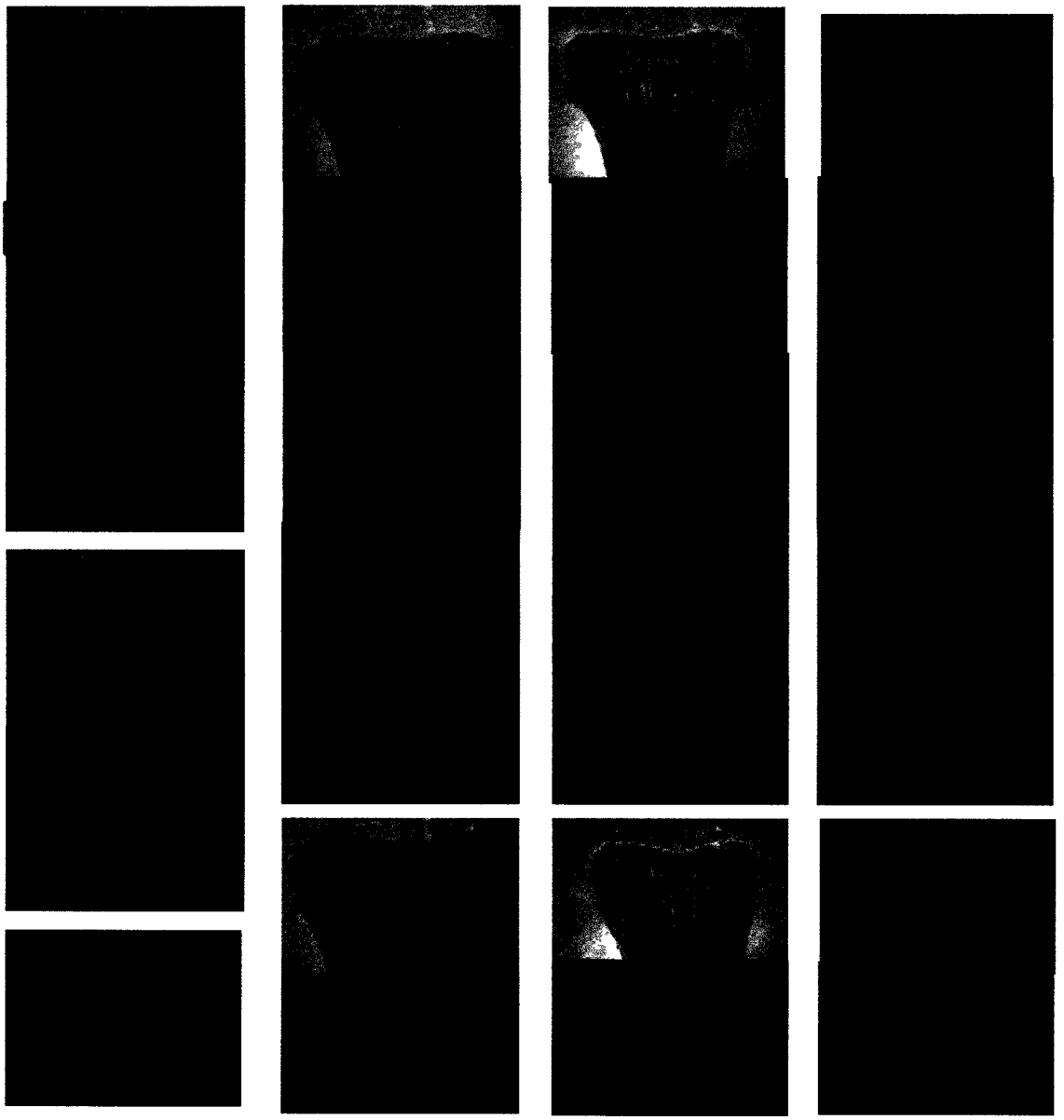

Figure R3

Figure R3: Time course of GFP expression in the *2.4shha:gfp:ABC#15* fin regenerate during branching morphogenesis. (2 dpa) GFP is first detected in the regenerate at 2dpa. (2.5 dpa) The GFP signal is strengthened at 2.5 dpa, but remains confined to a single domain. (3 dpa) By 3dpa, the 2-3 most lateral bifurcating rays (long rays) undergo the 'early splitting' stage (arrow head). However, 10-12 out of the 16 bifurcating rays in the regenerate are still expressing GFP in a single domain for each ray. (3.5 dpa) At 3.5 dpa, defined as 'Early splitting' stage, the GFP+ domain starts to separate into two distinct domains. The two GFP domains remain linked in the middle *via* a weak GFP signal (blue arrow). Notice that the separation of the GFP+ domain is deeper in the proximal-most GFP domain (red arrow) compared to the distal-most GFP domain (asterisk). (4 dpa) At 4 dpa, all branching rays present two subsets of non-communicating GFP+ domains, located on the lateral border of each ray. The cell separation at the level of the two distal-most extremities of the GFP+ domain is very clear (asterisk). (5 dpa) At 5 dpa, these separated domains are located further apart. (6 dpa) At 6 dpa, the two domains are completely separated, with one single GFP expression domain per newly formed sister ray. This situation is maintained at 10dpa, (10 dpa) where each sister ray grows independently and expresses one independent GFP domain. Notice that, in the two lateral most rays, that are known to be non-bifurcating rays, the *gfp* expression domain remains confined to a single set of cells and this domain does not undergo the separation that characterizes the branching rays.

Transverse sections through 6 dpa regenerates collected from the line *2.4shh:gfp:*ABC#15 show that GFP+ cells are restricted to the basal layer of the epidermis. The distal-most GFP+ cells are present in two distinct domains *per* hemiray. The two domains are located on a lateral border of the original hemiray, adjacent to the newly formed osteoblasts of each of the sister rays. As sections progress to the proximal-most extremity of the GFP+ domain, the distance that separates the two sets of fluorescent cells diminishes, consistent with the 'Heart shape' GFP domain observed on whole mount (Fig 4-D). We also observed a GFP signal in the blood vessels.

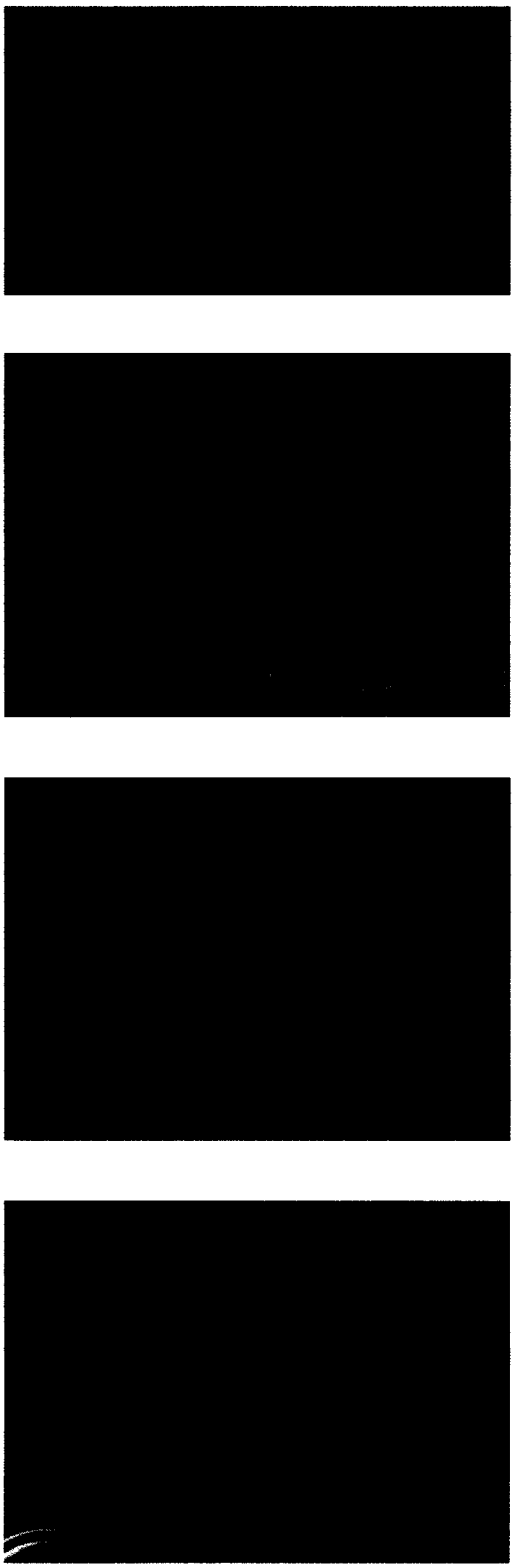

Figure R4

Figure R4: Transverse sections of a 6 dpa regenerate from *2.4shh:gfp:ABC#15*. Basal epithelial cells are GFP+ cells. In the distal part, two fully separated GFP+ domains are located lateral to the original hemiray, one GFP+ domain *per* newly formed sister ray. As sections progress to the proximal GFP+ domain, the fluorescent domains get closer to each other, however, the proximal-most GFP domain still presents two separated GFP+ on these 6 dpa sections. Scale bar = 20μm

2. The expression domain of GFP perfectly overlaps with the *shha* expression domain

a. Comparison of the GFP fluorescent domain with *shha* domain of expression examined by *in situ* hybridization

To be able to use this *2.4shh:gfp:ABC#15* transgenic line as a tool to act on the *shha*-expressing cells, it was necessary to show that the expression pattern of GFP was actually representative of the *shha* endogenous expression in the regenerating fins.

To do so, we compared *gfp* expression to results of *in situ* hybridizations on whole mount fin regenerates at 2 dpa and 4 dpa using the *shha* probe (Fig R5). We observed that, at 2dpa, which is the onset of *shha* expression and of GFP translation, GFP fluorescent domain and *shha* expression domains are very similar (Fig R5 A). However, at 4 dpa, the fluorescent protein could be detected in a domain which was more extended on its proximal side than the domain of expression of *shha* (Fig R5 B).

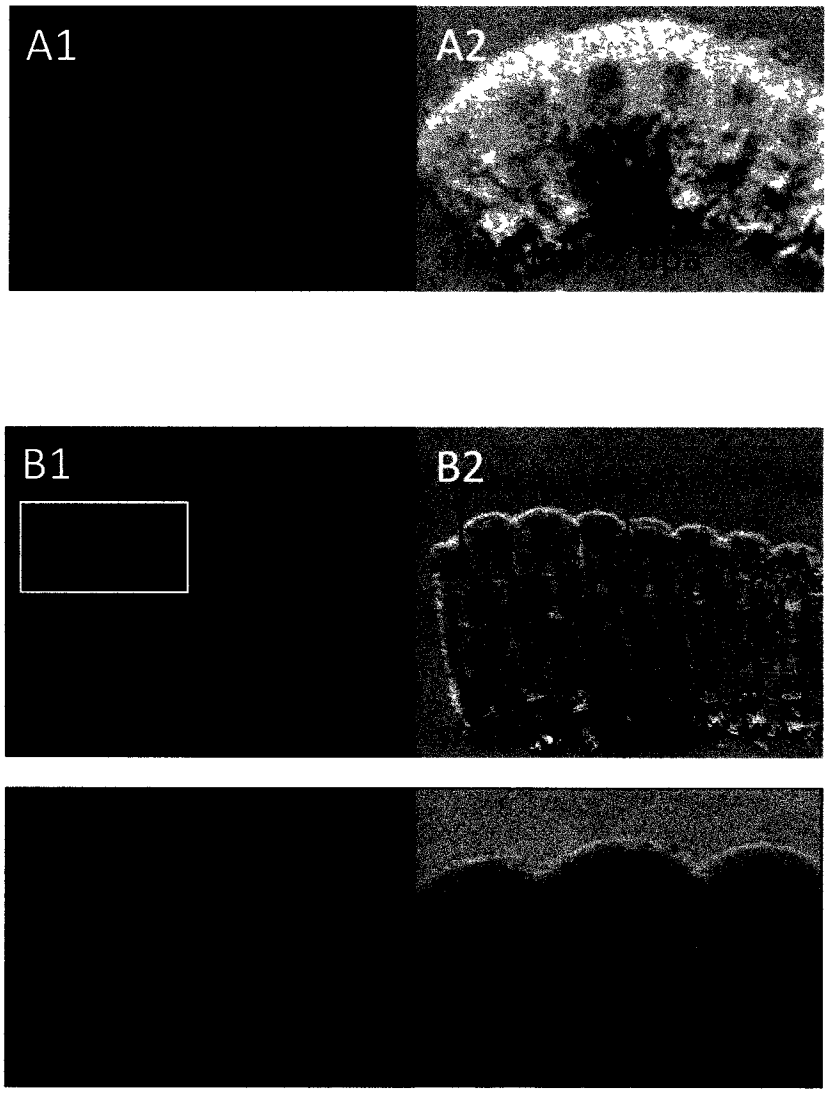

Figure R5

Figure R5: (A) *shha* mRNA and GFP+ cell distribution in a 2dpa regenerate. *shha In Situ* Hybridization (ISH) on whole mount allowed to observe a staining that is confined to the same population of cells that are GFP+ in the *2.4shh:gfp:ABC#15* line in a 2dpa regenerate. (B) *shha* mRNA and GFP+ cell distribution in a 4dpa regenerate. The *shha*-expressing domain is reduced compared to the GFP+ cell population. The GFP+ cell population is extending a little more proximally and distally in the regenerating ray than the *shha* domain of expression. The extra GFP+ cells that are not stained with *shha* probe (asterisk) are showing a very weak *gfp* signal (blue arrow).

b. Comparison of *gfp* and *shha* mRNA expression detected by *in situ* hybridization

Comparison between the GFP protein distribution and the *shha* mRNA distribution revealed a larger domain of GFP fluorescent cells than *shha* mRNA expressing cells. As the extra GFP fluorescent cells were not observed earlier (at 2 dpa) and appeared only after several days from the expression of the transgene (at 4 dpa), we hypothesized that this extra GFP signal might result from an accumulation of the GFP protein in cells that previously expressed *shha* and *gfp* transcripts.

In fact, due to possible post-translation regulation, protein distribution profile does not always recapitulate the exact domain of the gene transcription. Thus, rather than resulting from an active transcription of the transgene in these cells, the extra GFP domain would be the result of a previously transcribed and translated proteins that remain in the cells.

It is more careful, when comparing distribution pattern, to compare protein-to-protein or mRNA-to-mRNA profile, to determine, either protein distribution, or mRNA distribution, respectively. This can give a better idea about genes activity/expression profile.

As there is no Shha antibody that is commercially available, we decided to perform a profiling of *gfp* mRNA and *shha* mRNA distribution in the *2.4shh:gfp:ABC#15* regenerate. Using antisense mRNA probes for *gfp* and *shha*, we performed ISH on whole mount fin regenerates. We could see that the *gfp* mRNA and *shha* mRNA distributions were similar at 4dpa (Fig R6) and 6dpa (not shown). Thus, at 4dpa and 6dpa, the cells that are expressing *shha* and *gfp* seem to be exactly the same, confirming our hypothesis regarding the origin of the extra GFP fluorescent signal.

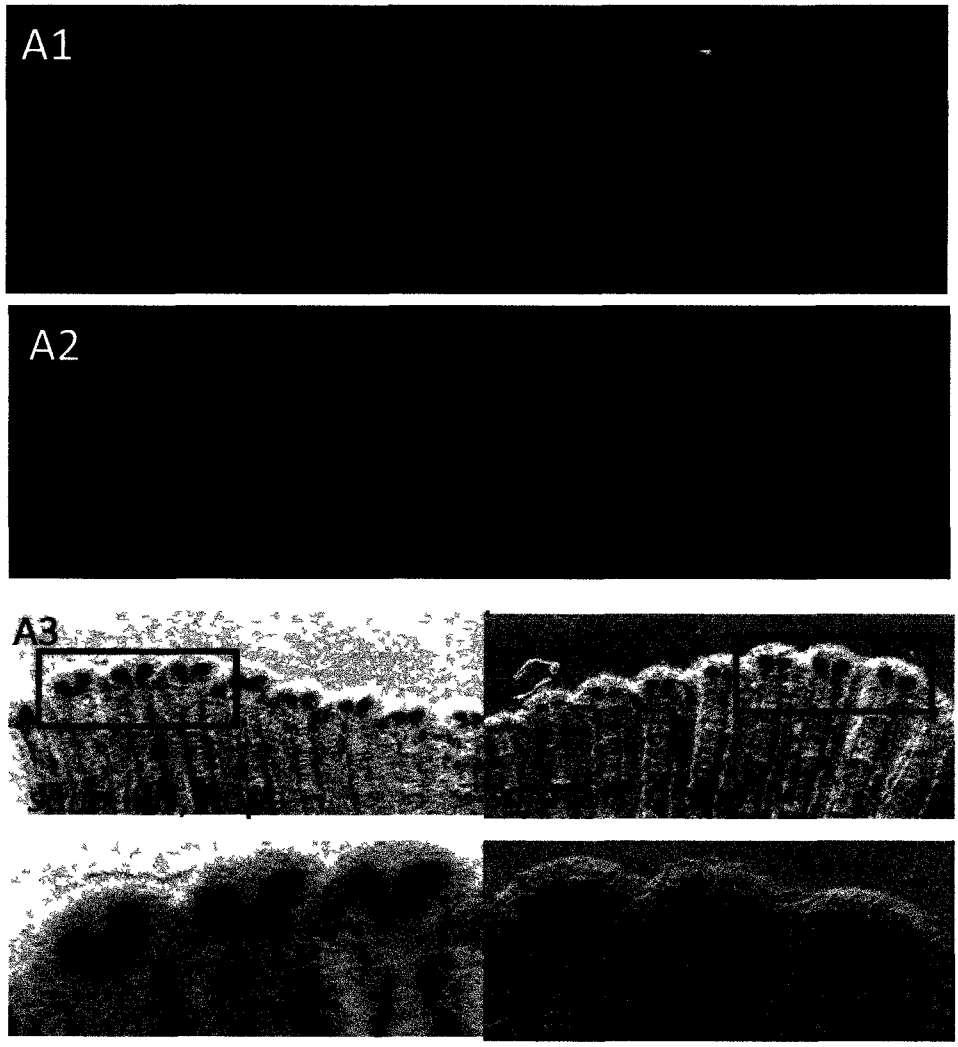

Figure R6

Figure R6: (A) *In situ* hybridization on whole-mount 4dpa regenerate with either *shha* probe or *gfp* probe allows detecting the cells that are actively expressing *shha* and *gfp* transcripts. (A1) is showing the bright field The *shha* expression domain (dorsal fin lobe) is similar to the *gfp* expression domain (ventral fin lobe). The extra GFP cells that were showing a weak fluorescent signal and were not showing *shha* mRNA, were also not detected using *gfp* probe, indicating that these cells are not undergoing active transcription of the *gfp* gene.

II. Analysis of the FGF signaling pathway and cell proliferation during branching morphogenesis

1. *fgfr1* expression pattern during branching morphogenesis suggests a cross-talk between the Fgf and Hh pathways

Cross talk between HH/FGF signaling pathways has been shown to be strongly involved in branching morphogenesis in other organs, such as the lung and the salivary gland in mice (Affolter et al., 2009). FGF signaling pathway has already been shown to be active during fin ray regeneration (Poss et al., 2000) and *fgfr1* expression was previously detected by others in longitudinal sections of 4 dpa regenerates in the distal blastema and the basal layer of the epidermis surrounding the blastema (Smith et al., 2008).

Fgfr1 has been shown to be involved in branching morphogenesis in the mouse salivary gland. In fact, as the salivary gland develops, epithelial cells bud into the surrounding mesenchyme to form a tube of proliferative epithelial cells. This bud will grow further and extend as a tubular structure within the mesenchyme. The growth is ensured by the tip of the epithelial bud. Eventually, the tip of the growing bud will invaginate to form a cleft, thus restricting the growth centers to lateral parts of the tip (see introduction for more details). At the level of the growing tip, *fgfr1*, which is involved in salivary gland branching morphogenesis, is thought to be important for transducing the Fgf signaling in the growing tip epithelium and mesenchyme, and possibly being involved in epithelial-mesenchymal interactions which are taking place during branches formation (Hoffman et al., 2002).

To address the possibility of Hh/Fgf signaling cross talks during fin ray branching morphogenesis, we performed an *in situ* hybridization (ISH) on sections of 4 dpa and 6 dpa regenerates using *Fgfr1* probe.

On transverse sections, at both 4 dpa and 6dpa, *fgfr1* expression domain consists of two sets of cells *per* ray (fig R7 A and B respectively). *fgfr1* transcripts were detected in the blastema (not shown) but also in the epithelial cells and mesenchymal cells adjacent to the basal layer of the epidermis in the differentiation zone (Fig R7). This expression pattern might suggest a role for Fgfr1 in interactions between the blastema and differentiation zones as well as in epithelial-mesenchymal interactions within the differentiation zone.

Fgf10 is a potential Fgf factor that might mediate a hypothetical cross talk between HH signaling and FGF signaling during fin ray branching morphogenesis. In fact, in the developing lung of mice, *Fgf10* has been shown to be regulated by *Shh* in order to correctly pattern branches formation (Kim et al., 2009). We performed ISH using *fgf10* antisense RNA probe in 4 dpa and 6 dpa regenerates.

No *fgf10* expression could be detected using this method (not shown). This suggests that, either *fgf10* is not expressed during fin regeneration (in this case, we will need to identify other *fgf* factor(s) that could activate the FGF pathway) or *fgf10* transcripts level in the regenerate is too low to be detected using ISH.

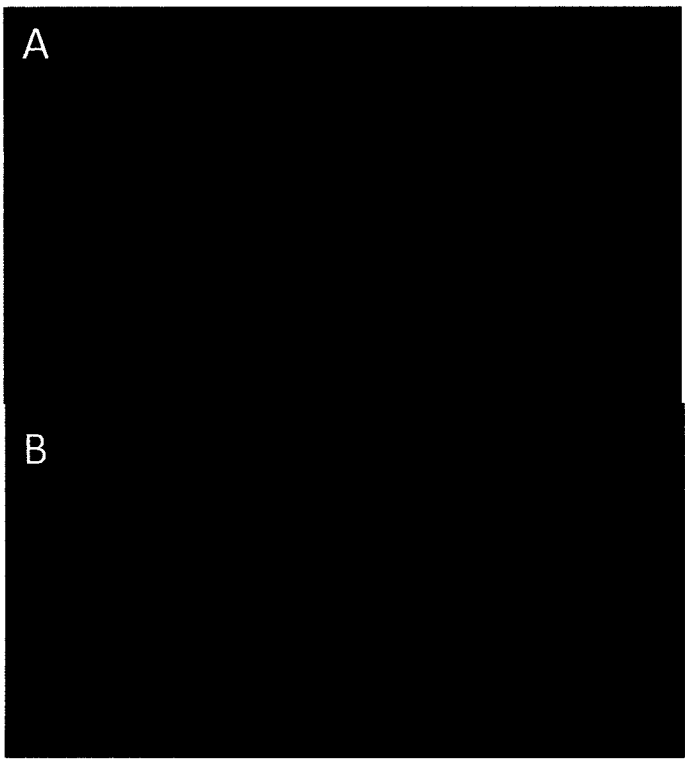

Figure R7

Figure R7: ISH on 4 dpa and 6dpa transverse sections using *fgfr1* antisense probe. (A) Expression of *fgfr1* in transverse section at 4 dpa. The basal layer of the epidermis, as well as adjacent mesenchymal cells, express *fgfr1*. The expression in the basal layer of the epidermis here is very low. (B) Expression of *fgfr1* in transverse section at 6 dpa. *fgfr1* transcripts are detected in a similar pattern at 4dpa and 6dpa. As *shha*, *fgfr1* expression domain is separated into two domains at both 4 dpa and 6 dpa. Scale bar = 20μm

2. Analysis of cell proliferation during ray branching morphogenesis

Based on the expression profile of *shha* during branching morphogenesis, as well as laser cell ablation experiment results (see introduction for further details), we think that *shha*-expressing cells are involved in branching formation. As it is established that Shh can act on the target cells as a mitogen in other branching organs such as the lung (Bellusci et al., 1997a), we wanted to test whether Shha may be involved in patterning the branching morphogenesis through inducing an increased proliferation in specific subpopulations of cells that would promote ray branching.

To visualize proliferative cells at a specific time point during branching formation, we decided to perform an immunodetection of proliferating cells using the Proliferating Cells Nuclear Antigen (PCNA) antibody on transverse sections of fin regenerates. We preferred to perform PCNA antibody staining rather than detection of BrdU incorporation for one main reason: detection of BrdU incorporation is based on the accumulation over time of bromodeoxyuridine (BrdU) within the DNA of proliferating cells, while PCNA antibody staining allows detecting the cells that are undergoing proliferation at a specific time point, rather than over an extended period. It was important for us to visualize the dynamic of cell proliferation during regeneration at a specific and precise time point,.

We performed immunostaining of transverse sections of 3dpa, 4dpa and 6 dpa fin regenerates with PCNA antibody to examine the detailed location of proliferating cells and potentially to correlate this pattern to the known *shha* expression pattern (Fig R9, R10). In the most distal sections of all examined time points, the regeneration blastema, composed of proliferative cells, was labeled using the mouse

PCNA antibody (Fig R9.A, R10.A, and R11 A). This confirmed the ability of the anti-mouse PCNA antibody to efficiently detect the zebrafish PCNA protein.

In these figures, we can determine the level of the section along the proximal-distal axis based on the population of the cells that are proliferating. The figure R8 shows PCNA staining of a 4 dpa regenerate and can be used as a reference for the two following figures (R9 and R10) to approximately determine the level of the sections along the proximal-distal axis, based on the cell types that are proliferating. The blastema region is distinguishable as the region where cells at the center of the ray are proliferating (Fig R8 A, yellow bracket); while a section in a more proximal part of the regenerate is showing a reduction in cell proliferation in the center of the ray, along with an increased proliferation in the epithelial cells (Fig R8 B, C). As proximal regenerate is typically associated with an arrest of the proliferation of the blastema cells, and an increased proliferation rate of the epidermal cells; this zone (R8 B and C) should correspond to the differentiation zone. Proximal to the blastema, differentiated cells are present. No active proliferation is detected in the mesenchymal cells located in the center of the ray in the differentiated zone at any of the considered time points. The proliferation is restricted to the multi-layered epidermis (Fig R8 D, green bracket).

In the differentiation zone of 3 dpa regenerates, the proliferative cells could be detected in a single (Fig R9 A, A', yellow arrow) or two distinct domains (Fig R9 B, C, green arrows). Based on the thickness of the bone matrix, section at the level A probably corresponds to the distal part of the 'H' shaped GFP+ positive domain in the early splitting stage, where the bone matrix is very thin or completely absent. At this

level, a single set of proliferative cells, located in the distal-most differentiation zone, was detected (see Fig R3, 3.5 dpa).

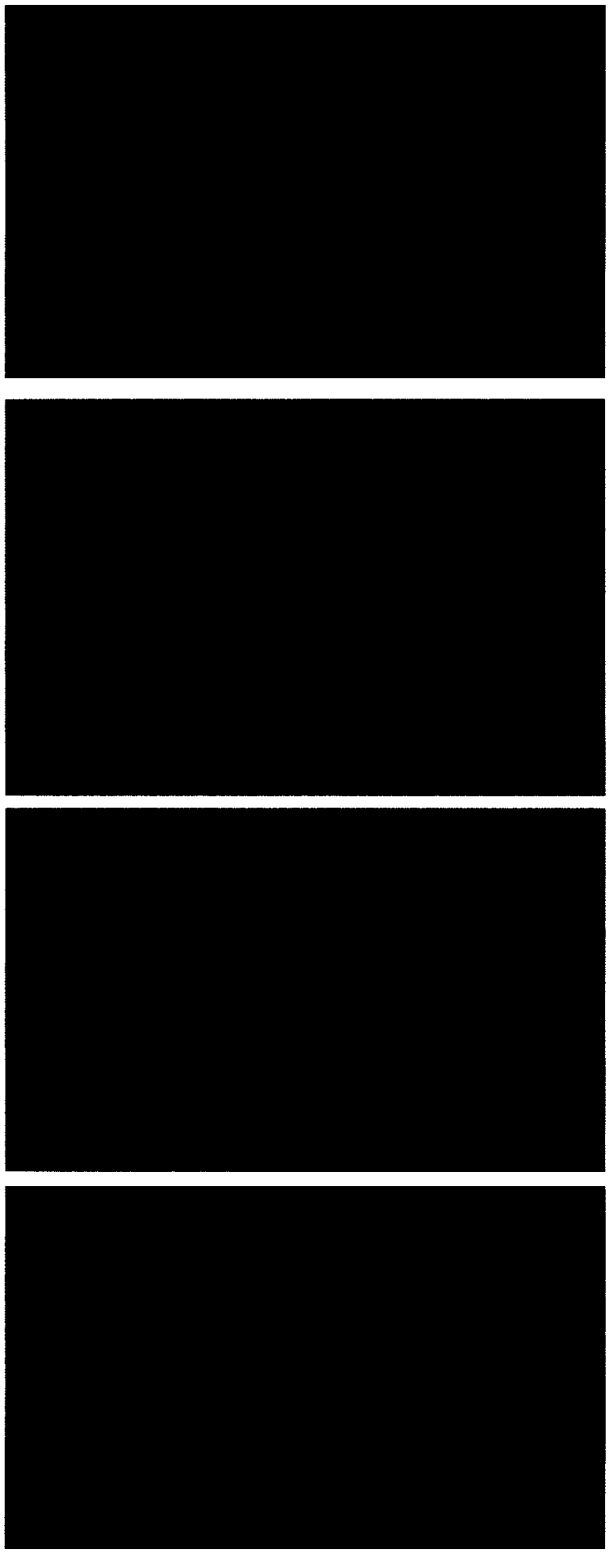
Blastema
Proximo-distal axis
Proximal
Differentiation
zone

Figure R8

Figure R8: Transverse sections through a 4 dpa regenerate, stained with PCNA antibody. The sections are shown distal to proximal. The approximate level of the sections along the proximal-distal axis can be determined based on the cell type that is undergoing proliferation. (A) Blastema cells are proliferative and are located in the center of the ray (green bracket). At the blastema level, epidermal cells are not undergoing proliferation (yellow bracket). Thus, sections that are showing a central proliferation only are sections made at the level of the blastema. (B, C) As we progress proximally, the proliferation rate of blastema cells progressively diminishes (green bracket), while epidermal cells (yellow bracket) are showing an increased proliferation rate compared to the epidermal cells at the level of the blastema (A). (D) In the proximal-most part of the regenerate, differentiation has occurred and proliferation rate is very low. The epidermal cells are the only cell type that is still proliferating at this level along the proximal-distal axis (yellow bracket). Scale bar = 20μm.

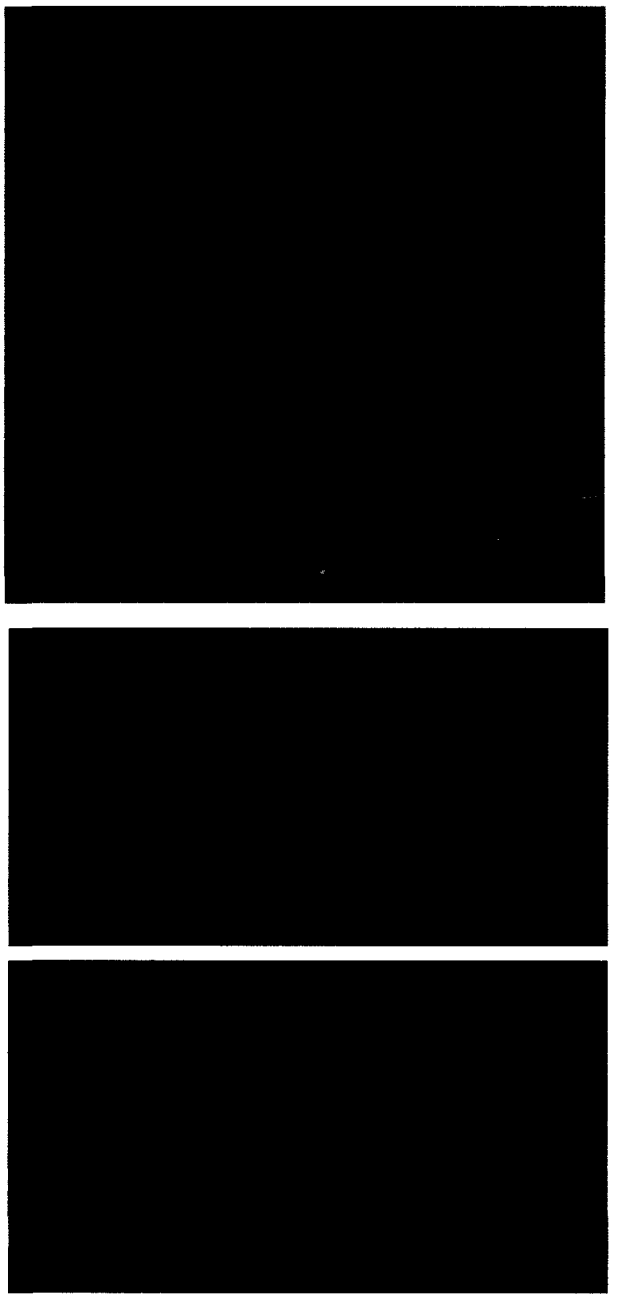
Distal
Differentiation
zone
Proximo-distal axis
Proximal
Differentiation
zone

Figure R9

Figure R9: Immunodetection of PCNA in transverse sections of a 3 dpa regenerate. The sections are all made at the level of the differentiation zone (based on the reference described in Fig R9). (A) A single set of mesenchymal cells in the differentiation zone is undergoing active proliferation (yellow arrow). This cell subpopulation is adjacent to the basal layer of the epidermis. (B, C) In different rays, two sets of mesenchymal cells belonging to the differentiation zone are undergoing active proliferation (green arrows). Bone matrix is indicated with the blue arrow. Section (A) is located more distally than (B) and (C), as it presents a thinner bone matrix. Scale bar = 20μm.

In the differentiation zone of 4 dpa regenerates, proliferation is detected in two domains flanking each hemiray (Fig R10, A, A', B, B'). The proliferative cells within this zone consist of mesenchymal cells adjacent to the basal layer of the epidermis (arrow heads), occasionally extending to lateral mesenchymal tissue toward the blood vessels (asterisk) in the interray tissue (green arrow). Cell proliferation was also detected in a few cells of the basal layer of the epidermis (Fig R10, pink arrow). In order to better visualize the proliferative cells in relation with cell distribution and bone matrix deposition in 4 dpa regenerate, we performed a double staining with anti-PCNA antibody (using a green fluorescent secondary antibody), and anti-Zns5 antibody to detect osteoblasts (using a red fluorescent secondary antibody). In order to distinguish the tissue structure, we also performed a DAPI staining, which stains the nuclei (Fig R10, C and D shown in blue). Unfortunately, the Zns-5 antibody staining seems to be incompatible with the fixation method that was used to fix the samples to efficiently perform PCNA antibody staining. Thus, we could not detect the bone matrix on the same section along with the proliferative cells. However, immunodetection of PCNA antigen, along with DAPI staining, allowed a better visualization of the tissue structure, and confirmed the observed distribution of the sub-population of cells that are proliferating in the differentiation zone.

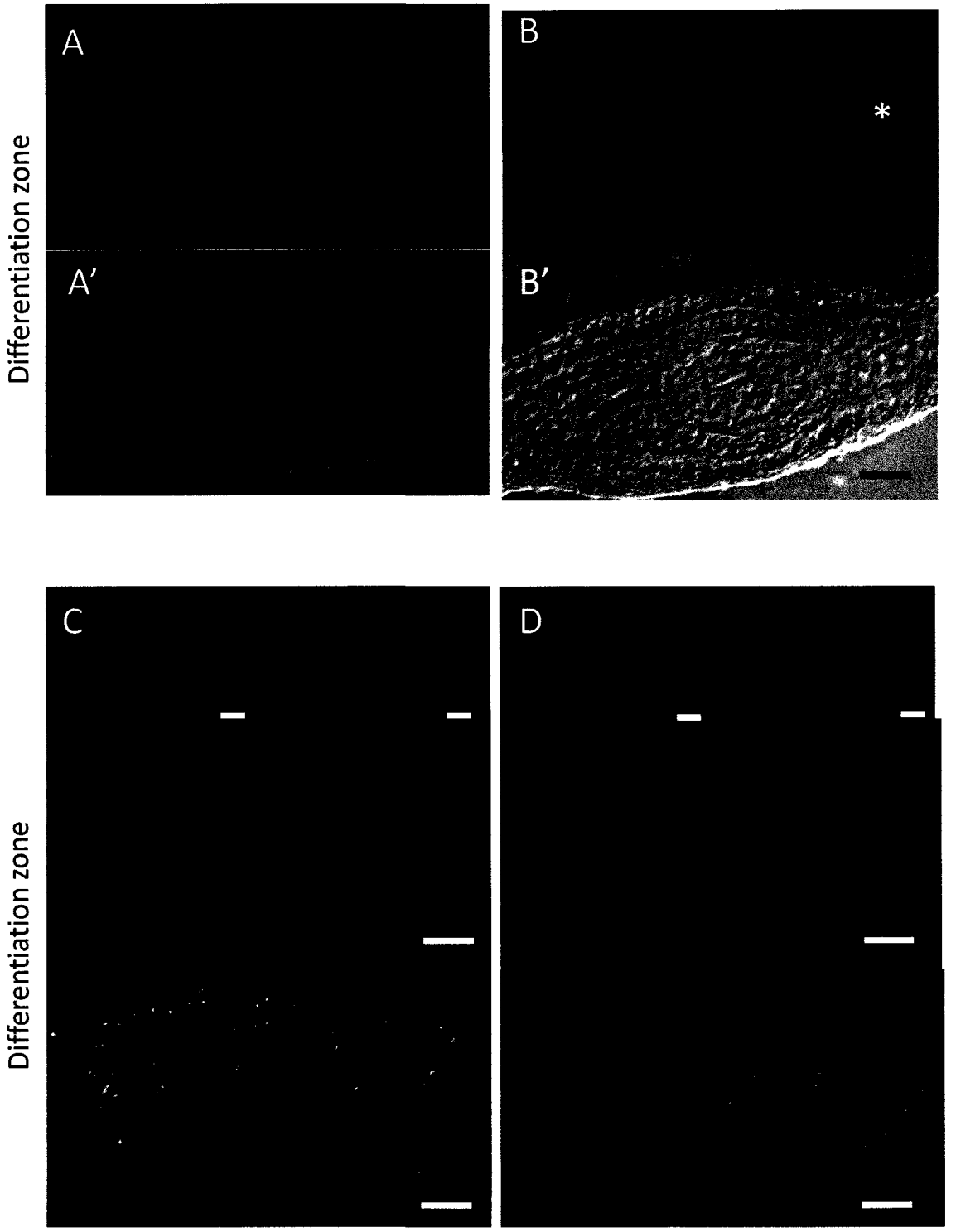

Figure R10

Figure R10: Immunodetection of PCNA in transverse section of a 4 dpa regenerate. A subpopulation of cells in the differentiation zone is undergoing active proliferation. (A, B) Proliferative cell sub-populations in the differentiation zone of two rays, stained with PCNA antibody (red fluorescence). Proliferative cells consist in two sets of mesenchymal cells flanking each hemiray (yellow arrow). These cell subpopulations are adjacent to the basal layer of the epidermis, occasionally extending in the interray mesenchyme (green arrow), toward the blood vessel (asterisk). (C, D) Sub-populations of proliferative cells in the differentiation zone of two rays, stained with PCNA antibody (green fluorescence). DAPI staining is shown in blue. Scale bar = 20μm.

We wanted to compare the distribution of the proliferative cells with the *shha*-expressing cells. As samples used for PCNA antibody staining were fixed in a solution that does not allow to conserve the GFP protein, we were not able to perform double staining (PCNA antibody and GFP antibody) on the same samples in regenerates collected from the transgenic line *2.4shh:gfp:ABC*#15, which expresses GFP protein in the *shha*-expressing cells during regeneration. Thus, we performed single staining for PCNA antibody and compared it with an ISH on 4 dpa sections using *shha* antisense probe (Fig R11, A and B). The cells that are expressing *shha* seem to be the same that are proliferating, with cell proliferation further extending on both lateral sides (asterisk). Based on bone matrix thickness, we can also ensure that the proliferative cells are located at the same level along the proximal-distal axis as the *shha*-expressing cells. However, in order to be 100% sure that *shha* expression and PCNA staining co-localize along the proximal-distal axis, we will need to optimize our antibody protocol and perform a double antibody staining with both PCNA and GFP antibody.

Figure R11

Figure R11: Immunodetection of PCNA (A) compared with *shha* ISH (B) on transverse section of a 4 dpa regenerate. Although these two sections belong to different samples, it provides us with a general idea on the respective location of both *shha*-expressing cells and the proliferative cells located at the level of the differentiation zone. The proliferative domain includes the *shha*-expressing cells (yellow arrow) and the newly differentiating osteoblasts (green arrow). The green asterisks represent blood vessels. Scale bar = 20μm.

Overall, PCNA antibody staining suggests that a sub-population of mesenchymal cells located at the level of the differentiation zone (most likely newly differentiating osteoblasts) along with interray mesenchymal tissue and occasionally including cells from the basal layer of the epidermis expressing *shha*, are undergoing active proliferation.

It has been shown that osteoblast differentiation occurs in a distal to proximal fashion: the distal-most osteoblasts (the less differentiated osteoblasts) express early differentiation markers such as *runx2a* and *runx2b*, while proximal-most osteoblasts belonging to the differentiation zone are fully differentiated, functional osteoblasts (Smith et al., 2006; Brown et al., 2009). Thus, in the differentiation zone, heterogeneous populations of osteoblasts are undergoing different steps of differentiation. We also found in the differentiation zone, some proliferative cells including cells of the basal layer of the epidermis and newly differentiating osteoblasts (Fig R10. R11). Active proliferating cells in the differentiation zone located laterally to each hemiray are still observed at 6dpa (Not shown).

We propose that the *shha*-expressing cells are maintaining the cell proliferation in the differentiation zone. By restricting the proliferative cells to the two lateral sides of the hemirays, *shha* –expressing cells are promoting the branching morphogenesis.

To assess the exact location of this population of proliferative cells, we will need to perform co-localization experiment of *shha* and *ihha* by optimizing our protocols for ISH/antibody staining.

III. Generation of a CFP-NTR transgenic line

In order to perform a long-term ablation of the *shha*-expressing cells, we proposed to generate a stable transgenic line expressing the Nitroreductase in the *shha*-expressing cells only. To generate this line, the same regulatory elements used in the *2.4shha:gfp:ABC#15* transgenic line (previously used for laser ablation experiments) were used to induce the expression of the CFP-NTR fusion protein in the *shha*-expressing cells. The construct containing the CFP-NTR fusion protein was provided to us by Dr. Stainier. The fusion protein was shown by Dr. Stainier's group to be functional in zebrafish embryos, as MTZ treatment of 24 hpf transgenic embryos expressing CFP-NTR in a specific tissue resulted in the specific ablation of the targeted cell type. Thus, this fusion allows visualizing the targeted cell population (and follow their fate to ensure that they were efficiently ablated in the MTZ treated samples), without affecting the ability of the NTR to reduce its substrate MTZ into a cytotoxic agent.

1. Transient activity of the *2.4shhtr:cfp:ntr* construct compared to the activity of the *2.4shh:gfp*

During the subcloning of the 2.4kb fragment containing the *shha* promoter, the MluI digestion resulted in the loss of 67 nucleotides at the 3' extremity of this fragment. The resulting truncated promoter (herein called *2.4shhtr*) was tested for its ability to induce the expression of *cfp:ntr* as efficiently as the full length promoter fragment, characterized by Dr. Strähle's group.

We injected 100ng/µl of either the *2.4shhtr:cfp:ntr* construct that contains the

truncated promoter fragment controlling the expression of *cfp:ntr*, or the *2.4shh:gfp* construct, graciously provided by Dr. Uwe Strähle and containing the full length promoter fragment controlling the expression of *gfp*. In stable transgenic line, we know that the latter construct drives GFP expression in the embryonic brain and the anterior part of the floor plate. A similar fluorescent pattern of the reporter gene in the brain and anterior floor plate at 24 hpf was observed in primary embryos injected with both constructs (Fig R12). No difference in the fluorescence intensity could be noticed. In addition, the percentage of fluorescent embryos was similar in the batches of embryos injected with each construct. The number of fluorescent cells in injected embryos varies from one embryo to the other, but overall, the reporter gene was expressed in the same amount of cells with both constructs. This indicates that the full length and the truncated promoter fragments have equal capacity to activate the transgene expression in the injected embryos.

We conclude that the *2.4shhtr* promoter is as efficient as the original *2.4shh* promoter in driving expression of the reporter gene.

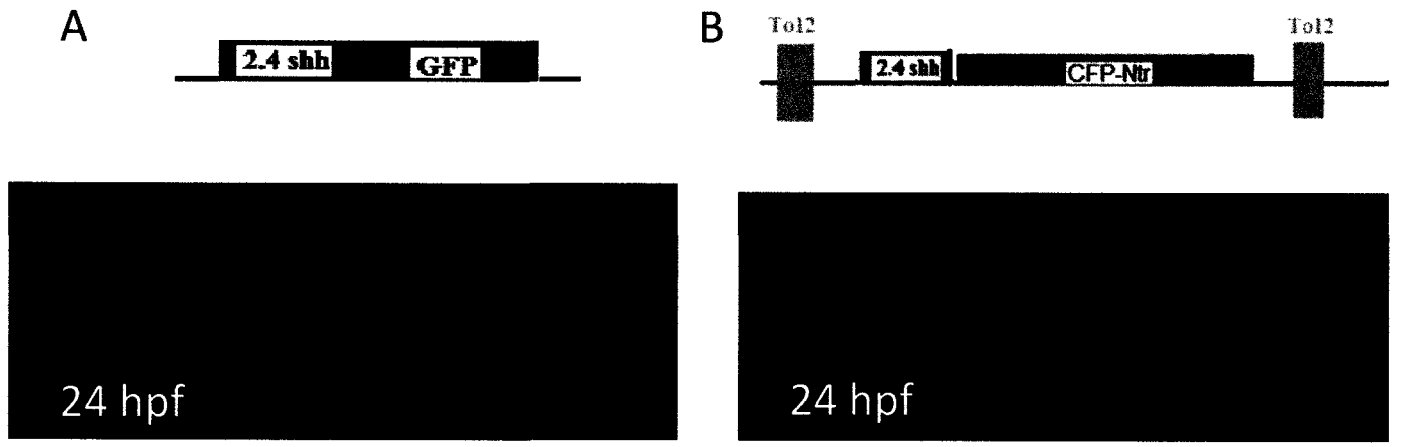
A
2.4 shh
GFP
B
Tol2
2.4 shh
CFP-Ntr
Tol2
24 hpf
24 hpf

C

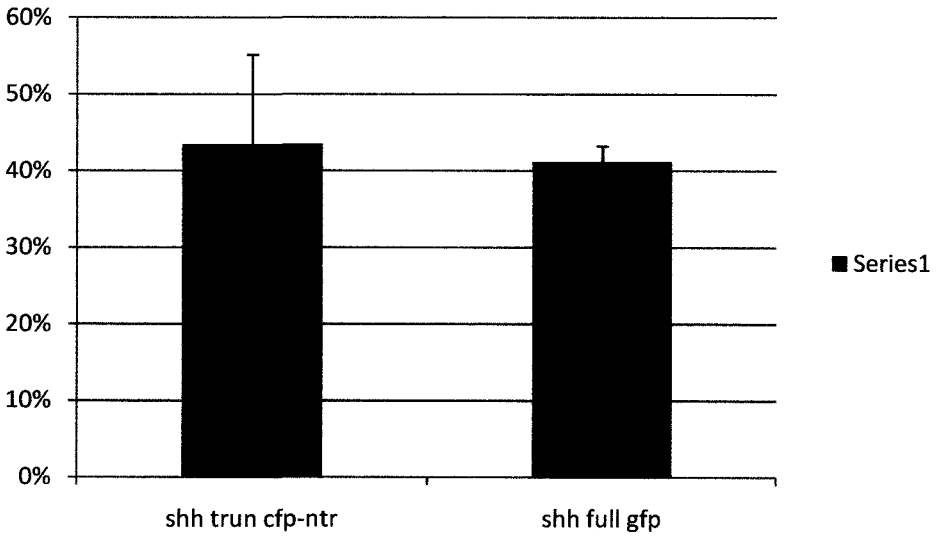
60%
50%
40%
30%
20%
10%
0%
shh trun cfp-ntr
shh full gfp
Series1

Figure R12

Figure R12: GFP fluorescence and CFP fluorescence compared in 24 hpa embryos injected with (A) the full length *shha* promoter fragment regulating the expression of the GFP reporter gene, or (B) the truncated *shha* promoter fragment that was inserted upstream of the CFP-NTR fusion protein. The pattern of fluorescence was similar in embryos injected with either of the constructs, with faint expression in the brain and expression in the floor plate. (C) The percentages of fluorescent embryos obtained following injection with either *2.4shh:gfp* or *2.4shhtr:cfp-ntr* constructs. The numbers of fluorescent embryos obtained in each batch of injections were very close.

2. Transient activity of the *2.4shha:cfp:ntr:ABC* construct

Embryos injected with the *2.4shhtr:cfp:ntr:ABC* construct, along with 50ng/µl of the *transposase* mRNA , allowed to observe the mosaic expression of CFP in the brain, floor plate and notochord (Fig. R13). These domains of expression are similar to what is observed in the stable *2.4shh:gfp:ABC#15* transgenic line. They also recapitulate the expression of the endogenous *shha* gene during embryonic development, except for the pectoral fin expression (as previously shown by Dr. Strähle's group in the stable transgenic line *2.4shha:gfp:ABC*#15).

We also observed that using the Tol2 minimal arms along with the transposase mRNA allowed reducing the mosaic expression of the reporter gene compared to primary embryos injected with constructs devoid of these sequences (Fig R13).

Thus, the construct that we made allows inducing efficiently the expression of the CFP-NTR fusion protein in *shha*-expressing cells during embryonic development.

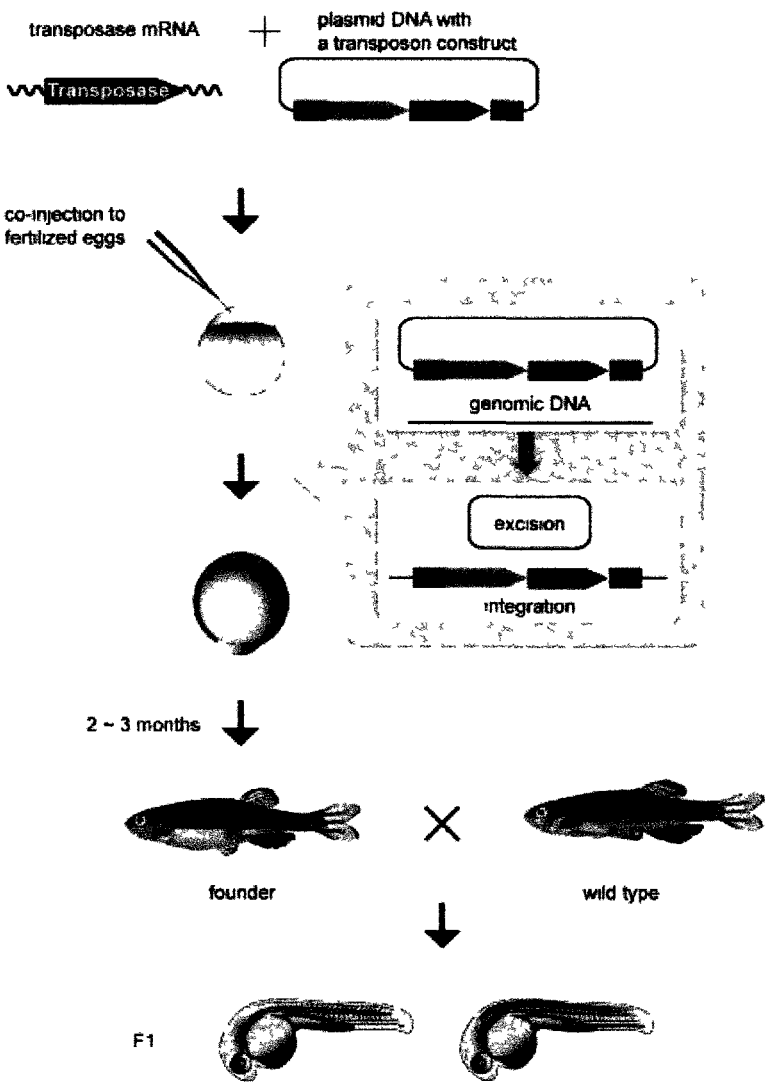

Kawakami & al 2007

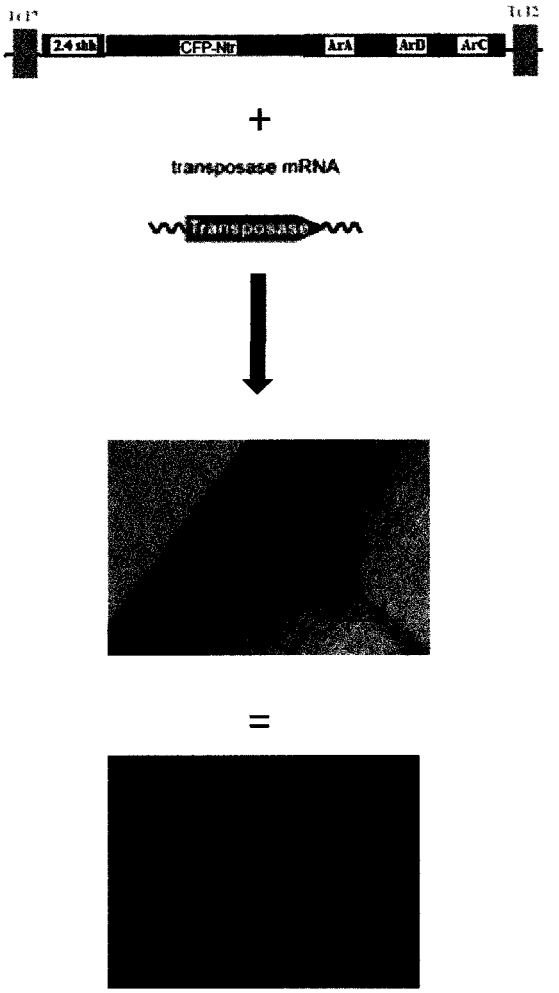

Injected with *2.4shh:cfp-ntr:ABC*

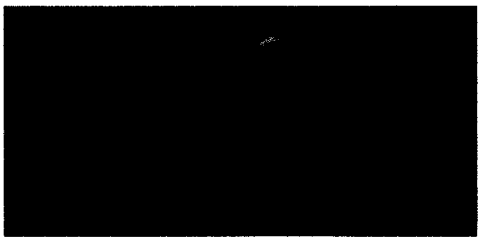

tg 2.4shh:gfp:ABC#15
(stable transgenic line)

Figure R13

Figure R13: The transient expression pattern of the *cfp* reporter gene recapitulates the expression pattern of the *gfp* reporter in the stable transgenic line *2.4shh:gfp:ABC*#15. The *2.4shha:cfp-ntr:ABC* construct was injected with the *transposase* mRNA. The transposase protein is able to recognize the tol2 minimal arms that are flanking our transgene. The transposase protein catalyses the excision of the Tol2-flanked transgene and its integration in the genome.

Embryos injected with the *2.4shh:cfp-ntr:ABC* construct, along with the *transposase* mRNA, were screened at 24 hpa for cyan fluorescence.

3. Metronidazole treatment on primary embryos: Dilution vs. Ablation

To test the activity of the NTR in our construct on primary transiently fluorescent embryos, we exposed 24 hours old fluorescent embryos to 0.2% DMSO, or 2mM, 5mM and 10mM of MTZ diluted in 0.2% DMSO. Embryos were treated for 24h, at 28.5 °C. Treated embryos were kept individually in 24 well-plates, in order to follow the variation of the fluorescence in each case, and thus be able to compare the fluorescence before and after treatment.

MTZ treated embryos showed a decrease in CFP+ cell numbers, as shown in Fig R14 A. However, DMSO treated controls also showed reduced CFP fluorescence at 48 hpf compared to 24 hpf (Fig R14). Thus, in non-treated embryos, the number of CFP+ cells decreases.

This decrease of fluorescent cells is most likely due to construct dilution during embryonic development. In fact, as we inject the embryos at one cell stage, initially, all the forming cells have equal chances to integrate the transgene in their genome. However, transgene integration does not immediately happen at the moment of injection: the injected construct remains on its circular form before its genome integration. Meanwhile, the number of cells of the fertilized embryos increases very quickly and the construct becomes diluted in the dividing cells. Some of the cells in the injected embryos will not contain any transgene sequence, resulting in the mosaic expression of the reporter gene in the injected embryos. The number of fluorescent cells observed in injected embryos varies a lot from one embryo to the other.

Thus, in injected embryos, as CFP expression is mosaic, the number of fluorescent cells that remains in the untreated embryos decreases over time. This was also observed in fish injected with the construct and subsequently treated with MTZ.

Although we did not count the initial number of fluorescent cells and compared it with the number after treatment, overall, the fluorescence before and after MTZ/DMSO treatment was not remarkably different. In order to be able to visualize the efficacy of cell ablation, we need a transgenic fish that expresses CFP in a consistent pattern allowing us to observe the reduction of fluorescence following MTZ treatment.

Thus, to efficiently ablate the *shha*-expressing cells in regenerating fins using the NTR/MTZ approach, we need to have a stable transgenic line where the reporter gene expression should recapitulate the GFP expression observed in *Tg2.4shh:gfpABC*#15. For that, we will need to have fish that integrate the construct in their germline cells. These fish will have the transgene in their gametes and will transmit it to their progeny, which will carry the transgene in all of their cells. In these progeny (which constitute the F1), we will be able to observe a complete expression pattern of the reporter gene. These fish from the F1 will be raised to adulthood, and bred to establish a stable transgenic line. If the expression pattern of the reporter *cfp* gene during embryonic development of the F1 *Tg2.4shh:cfp-ntr:ABC* is similar to the *gfp* expression in the developing *Tg2.4shh:gfpABC*#15 embryos, the expression pattern of this reporter should also be similar in adult regenerating fins. Thus, such a line could be successfully used to perform the long-term ablation of the *shha*-expressing cells in the regenerating fin rays.


0.2% DMSO
5mM MTZ in 0.2% DMSO
24 hpf (injected)
48 hpf (24h treatment)

Figure R14

Figure R14: Embryos treated for 24 h with either 5mM MTZ diluted in 0.2% DMSO, or with 0.2% DMSO only (control). Treatment started at 24 hpa. In the control embryos, as well as in the MTZ treated embryos, the number of fluorescent cells decreases over time.

4. Transgenic lines

To screen the primary (injected) fish that were raised to adulthood, we bred them with either a second primary fish, or a Wild Type fish. The embryos were observed under UV to detect CFP fluorescence at 24 hpf and 48 hpf. We considered the fish/couple as screened once we had observed beyond 300 embryos coming from this fish/couple. Among 16 fish that can be considered as 'screened', we obtained germ line transmission of the transgene for 5 adult fish. These transgenic lines show various expression patterns of the transgene, as detected *via* CFP fluorescence. The different lines are shown in the figure R15.

Line 1: At 24hpf, *2.4shh:cfp:ntr:ABC#1* showed weak fluorescence in the brain with only expression in the anterior floor plate, which resembles what is observed in the *Tg2.4shha:gfp:A* (where the *gfp* expression is regulated by the *2.4 shha* promoter fragment and the *shha* ar-A enhancer only,). The fluorescence gets weaker at 48hpf and is completely undetectable by 3dpf. The reduced expression pattern that is observed (lack of CFP expression in the notochord and posterior part of the floor plate) can result from an integration mistake. The reporter gene expression might be directed by the promoter fragment, along with only a part of the enhancers, the ar-A. The ar-B and ar-C enhancers might have been lost during the integration of the transgene. The weak fluorescent signal observed in embryos that are older than 48 hpf may result from a silencing of the reporter gene in older stages of embryonic development.

Lines 2 & 4: *2.4shh:cfp:ntr:ABC#2* and *2.4shh:cfp:ntr:ABC#4* showed, at 24hpf, an expression in the brain (weak) and in entire floor plate. However, no expression in the notochord could be detected. The fluorescence in the floor plate was maintained until 3dpf, but could not be detected later, as the pigments got more concentrated and the expression domain was internal.

Line 3: *2.4shh:cfp:ntr:ABC#3* embryos showed unspecific expression in the otic vesicle starting at 24 hpf and maintained to 6dpf. This expression pattern is most likely due to the site of integration of the transgene. Although this line is not useful for analyzing the function of *shha*-expressing cells, it could be of interest to potentially study otic vesicle regeneration in zebrafish embryos. We believe that this expression domain, along with the expression pattern obtained for both line 2 and 4, is due to the integration site of the construct in these two lines, as the transgene might have been integrated in a region that is closed to a strong promoter.

Line5: The *Tg2.4shh:cfp:ntr:ABC#5* showed a CFP expression pattern that recapitulates the expected *shha* expression in the embryos. Expression in the brain could be detected, as well as in the floor plate and notochord. Although weak in this line, the fluorescence signal can be increased through inbreeding, which increases the transgene copy number and leads to a stronger signal.


Tg 2.4shh:cfp-ntr:ABC#1, 24 hpf
Tg 2.4shh:cfp-ntr:ABC#2, 48 hpf
Tg 2.4shh:cfp-ntr:ABC#4, 48 hpf
Tg 2.4shh:cfp-ntr:ABC#3, 48 hpf

Figure R15

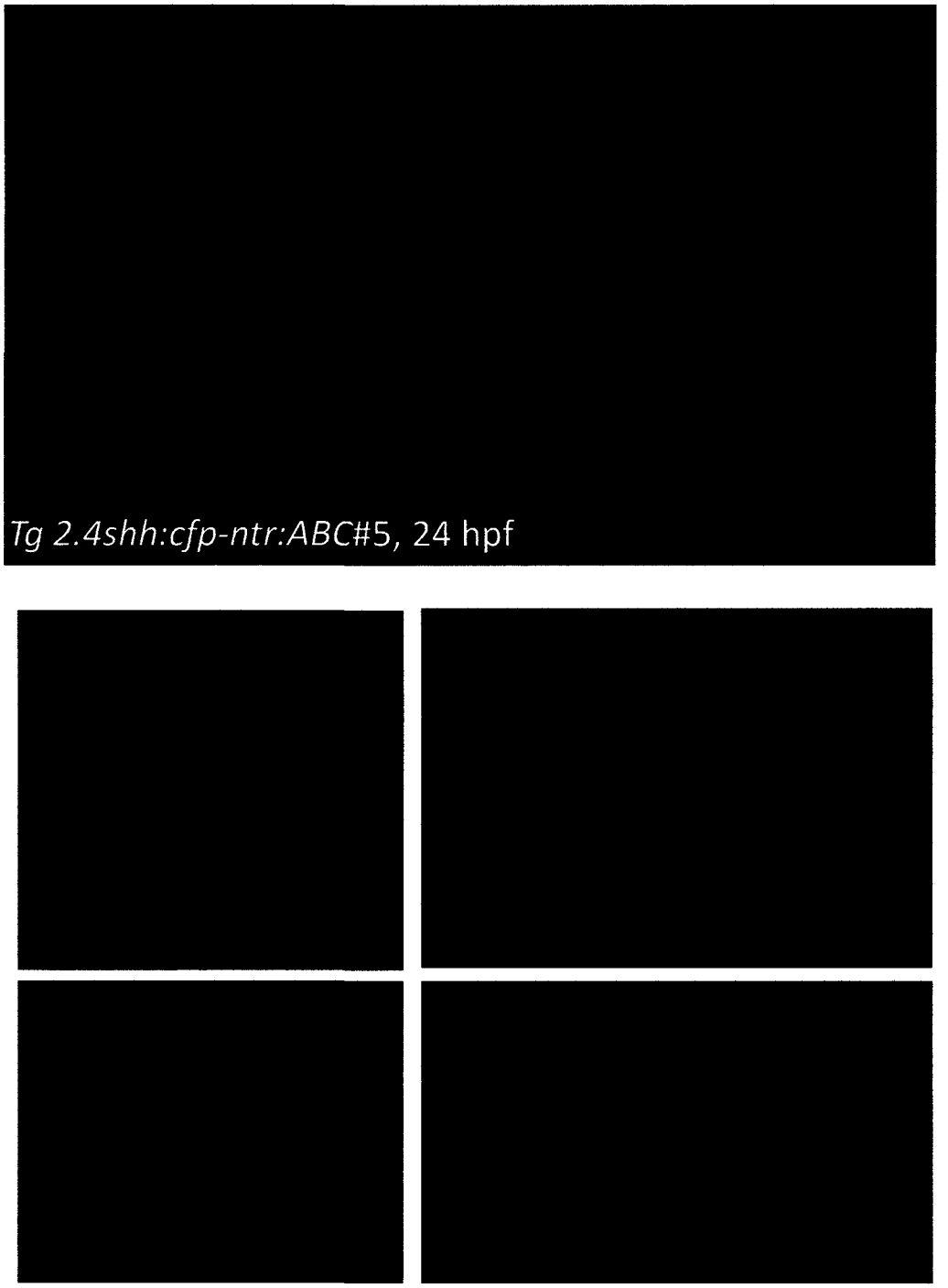

Figure R16

Figure R15 and Fig 16: Transgenic lines that were obtained. The pattern of expression differs, most likely due to integration effect. Line5 recapitulates the GFP expression in the stable transgenic line *2.4shha:gfp:ABC*#15, which makes it a valuable line to proceed to the ablation of the *shha* –expressing cells in the adult fin regenerates.

However, due to fish health issues in the fish facility, we were unable to keep any of these lines alive, as the founder fish, the embryos and the adult F1 for the line 1 died before we could proceed to the downstream analysis we were aiming for. We are currently re-injecting the *2.4shh:cfp-ntr:ABC* construct to generate the stable transgenic line expressing *cfp:ntr* in the consistent pattern at the F1 generation embryos. Only then we will be able to proceed to the analysis, consisting in fin amputation followed by assessing growth rate, branching morphogenesis (using visual assessment and also using ISH for genes known to be important for branching such as *fgf10*, *spry*, *fgfr1*), physical defect, bone defect (Alcian blue/Alizarin red staining), and osteoblasts differentiation stages (ISH for osteoblasts markers such as *runx2a*, *runx2b*, *osx*, *ssp*, *ihha*, and *col2a1*).

Discussion

The caudal fin is considered to be a good model to dissect the molecular pathways that are involved in epimorphic regeneration. The caudal fin regeneration depends on the establishment of the blastema. As they leave the blastema, undifferentiated cells undergo re-differentiation to reconstruct the lost organ. The newly formed ray first starts growing longitudinally and, later, undergoes branching.

Many organs of higher vertebrates are branched structures. The most widely studied and best characterized vertebrates branching organs are the lungs, the salivary gland, the mammary gland and the prostate. It has been suggested that conserved molecular programs are involved during branching formation of all these organs, or at least, a conserved canonical pathway that might be inducing the same events to occur during branches formation (Davies, 2002).

The objective of this study is to gain insights into the process of fin ray branching morphogenesis, and osteoblasts differentiation during fin regeneration, with a special emphasis on the role of the *shha*- expressing cells.

1. Proposed model for the separation of the *shha*- expressing cells

We precisely monitored the *shha* expression pattern during branching morphogenesis using the *2.4shhgfp:ABC#*15 zebrafish transgenic line. This line expresses *gfp* in the same cells that are expressing *shha*, as demonstrated using ISH on whole mount regenerate to assess the distribution of both *shha* and *gfp* mRNA.

GFP+ domain was a bit more extended compared to the *shha* and the *gfp* transcripts

distribution domain. We believe that the extra GFP+ cells that were not stained using *gfp* antisense probe are cells that previously expressed *gfp*, and where the *gfp* transcription has ceased. The weak fluorescent signal that is detected results from 'left-over' GFP protein. Due to its stability, GFP remains in some cells, even though *gfp* transcription does not occur anymore. Therefore, the *2.4shh:gfp:ABC*#15 line is a valuable tool to follow the expression pattern of *shha* in the fin regenerate.

Using the *2.4shh:gfp:ABC*#15 transgenic line, we were able to show that the behavior of the *shha*- expressing cell is very dynamic during the branching process, and we subsequently defined three stages that are occurring during branches formation: i) single set of *shha*- expressing cells, ii) early splitting stage and iii) heart-shape stage.

During the stage 'Single set of *shha*- expressing cells', each fin ray, including the two most lateral, non-bifurcating rays, present a unique domain of GFP+ cells. The GFP domain is located in the center of each fin ray. This single signaling center is maintained medially from 2 dpa (time at which they appear in the regenerate) to 3 dpa, with some variation between the rays (Fig D3 A). It is most likely playing a role in the ray elongation and fin growth, as inhibition of the Hh pathway in 2 dpa regenerates (*via* cyclopamine treatment) leads to a growth arrest of the regenerate (Quint et al., 2002). This mitotic effect is also supported by the presence, in some of the regenerating fins, of a lateral-most ray in which the GFP expression ceased very early during regeneration (a very weak expression is first observed and lost later). These rays are always shorter than other fin rays expressing GFP in a regular pattern (data not shown).

The 'Early splitting' phase, occurs around 3.5dpa. During this stage, *shha*-expressing cells just start to separate into two domains located laterally on each fin ray. This early

splitting is characterized by two clear and strong GFP+ domains, linked by a weaker GFP signal in the middle We also noticed that, during this phase, the separation of the GFP cells seems to be more pronounced in the proximal most part of the GFP+ domain, compared to the distal end (Fig D3 B)

shha expression is probably maintained *via* signal(s) produced by mesenchymal cells As differentiation occurs, mature osteoblasts secrete the mineralized bone matrix that accumulates in the space separating the basal layer of the epidermis at the level of the differentiation zone and the newly differentiated osteoblasts At the proximal-most part of the differentiation zone, this bone matrix is thicker compared to the newly secreted bone matrix that is located more distally Thus, proximally, where the bone matrix is thick, epithelial-mesenchymal interactions are interrupted by the bone matrix Our results support the possibility that this barrier may impair further *shha* maintenance signal, coming from the mesenchyme, to reach the target cells in the basal layer of the epidermis (Fig D3 B, bottom) In contrast, on the two lateral sides at the same level along the proximal-distal axis, and despite the thick bone matrix, the basal layer of the epidermis is still communicating with the adjacent mesenchyme (see the structure of the fin ray) The epithelial-mesenchymal interactions that are necessary to maintain the *shha* expression can still occur through these communication zones This would explain the weak *shha* expression that is observed on both sides of the ray in the proximal-most part of the *shha* expression domain (Fig D3 B, bottom) It would also explain why, at this level, the expression of *shha* is shut-off only in the central part of the hemiray, rather than being completely turned-off

The requirement of epithelial-mesenchymal interactions to maintain *shha* expression

in the basal layer of the epidermis has been proposed earlier by (Laforest et al., 1998). As we progress along the proximal-distal axis toward the distal most *shha* expression domain, the bone matrix thickness is reduced. Distal osteoblasts are either not fully differentiated, or newly differentiated and just starting to fully function as bone secreting cells. The differentiating osteoblasts are most likely not able to secrete bone matrix yet, while the newly functioning osteoblasts secrete a new bone matrix. The layer of bone that is deposited is therefore very thin at this level. In the absence of bone matrix, and perhaps in the presence of a very thin layer, epithelial-mesenchymal interactions can be maintained. The hypothetical mesenchymal signal that is necessary to maintain *shha* signal during the 'Early splitting' phase can still reach the target cells of the basal layer of the epidermis in the center of the hemiray, explaining the maintenance of the Shha signal in the distal-most GFP+ domain (Fig D3 B, top).

This idea of a physical 'barrier' that is inducing a cell separation in the proximal-most GFP+ domain is reminiscent of what is observed during salivary gland branching morphogenesis. The mice salivary gland arises from a thickening of the oral epithelium that invaginates and elongates, around E12, in the surrounding condensed mesenchymal tissue (Fig D1 A). Epithelial cells from the tip of the invaginating structure (called 'bud') are undergoing active proliferation, to ensure the elongation of the epithelial bud into the surrounding mesenchyme. The tip of the proliferative epithelial bud will eventually form a plug resulting in a cleft formation at the tip of the bud (Fig D1 B). As the cleft is formed, the proliferation is maintained at the lateral sides of the tip of the bud: the region where the plug has occurred does not proliferate. This formation of a cleft leads to the initiation of the branching (Fig D1, C).

Components of the extracellular matrix have been shown to be involved in the

formation of the plug. While they are degraded on the lateral sides of the bud, both Collagen (synthesized by mesenchymal cells under the influence of epithelial factors) (Bernfield, 1970), and Glycosaminoglycans (GAGs), which are macromolecules composing the extracellular matrix, accumulate in the median part of the bud (Spooner et al., 1985). Fibronectin, an extracellular matrix glycoprotein, is also transiently expressed in the center of the tip of the epithelial bud during the formation of the cleft. Fibronectin is required for correct patterning of the branches in the developing salivary gland (Sakai et al., 2003) (Fig D1, B). This matrix accumulation acts as a cellular constraint, which directs cell proliferation toward the two lateral edge of the epithelial bud. (Grobstein and Cohen, 1965; Bernfield and Banerjee, 1982) (Fig D1 B and C). This orientated proliferation results in the formation of the branches. As these two newly formed branches continue to be the site of active proliferation at their tip, they elongate, and later undergo the same process, leading to the formation of a tree-like structure (Fig D1 C).

In the fin rays, a similar physical barrier phenomenon might result in the proximal cleft formation in the *shha* domain during the 'Early splitting' phase. Shha might induce cell proliferation, while secreted bone matrix acts as a plug, restricting cell proliferation to lateral edge of the hemiray, thus leading to the formation of a cleft.

A short split was also observed in the distal-most *shha* expression domain. However, this splitting is not as pronounced as the proximal one. As no bone, or a very thin layer of bone is present at this level, the faint separation that is observed can be due to other factors that are also involved in 'Heart shape' stage and that will be discussed herein (Fig D3 B, top).

The 'Heart-shape' stage is characterized by the maintenance of the proximal split

observed in 'Early splitting' (Fig D3 C, bottom) This initial cell separation is reinforced, distally, by a larger separation of the *shha* expression domain Because most of the organs that form branches in vertebrates do so *via* a signal that is generated by the mesenchymal tissue and that is acting on the 'branching-epithelial cells', we believe that the branching signal involved in the 'Heart shape' stage in the regenerating ray is generated by mesenchymal cells The mesenchymal signal might act on the epithelial cells and induce the splitting in the *shha* expression domain (Fig D3 C, top)

The distal splitting is most likely due to a secreted factor that either 1) turns off the Shha pathway in the distal part of the *shha* expression domain, but only in the cells located in the central part of the *shha*-expression domain, and/or 2) maintains the Shha signal only on the lateral sides of the GFP+ domain

The Shha inhibiting signal, acting on the distal-most *shha* domain, if such a signal exists, would be secreted by 1) cells from the proximal blastema (just distal to the *shha*-expressing cells level), and 2) cells from the adjacent mesenchyme, at the same level as the distal-most *shha*-expressing cells, but restricted to the central part of the adjacent mesenchyme Mesenchymal signal will inhibit the epithelial *shha* in the central domain, thus inducing a separation of the *shha*-expressing cells (Fig D3, C top)

In contrast, the Shha maintaining signal on the lateral side of the distal-most *shha* domain, if such a signal exists, would be secreted by mesenchymal cells located at the same level as the distal-most *shha*-expressing cells, but lining on both lateral sides of the *shha* expression domain, either in the ray, or in the surrounding interray tissue (Fig D3 C, factor X, and Y, respectively)

Another hypothesis will be a combination of both maintenance signal acting on lateral part of the *shha* domain and an inhibiting signal in the central part of the *shha* domain.

Potential candidate genes for a virtual *shha* maintenance signal are members of the Fgf signaling, as Fgf/Shh cross talks were shown to be strongly involved during branching morphogenesis in both salivary gland and lung (see Introduction for details, and Figure D2 for synthesis of lung branching morphogenesis process).

In the regenerating fin ray, we were able to detect *fgfr1* transcripts in the distal blastema, but also in the basal epithelial layer and the newly differentiating osteoblasts. *Fgfr1*, which is expressed in the mesenchyme and epithelium of the mice salivary gland at E.13, was shown to be important for branches formation, as oligonucleotides knockdown of *Fgfr1* in culture of salivary gland tissue results in the reduction of the branching morphogenesis (Hoffman et al., 2002). Although the role of Fgfr1 during regenerate outgrowth remains unknown, it is possible that Fgfr1 may be involved in epithelial-mesenchymal interactions. Direct results of these interactions would be the activation of the *shha* expression, and therefore directing the patterning of the branching morphogenesis. To further understand the role of *fgfr1* during fin regeneration and shed the light on its potential involvement in HH/FGF cross-talk, more precise co-localization experiments will be required (*fgfr1* expression profile compared with *shha* and *ihha* expression profile). Also, we will need to assess how *fgfr1* expression is affected in rays in which *shha*–expressing cells have been removed?

Fgf10 is an Fgf factor that was linked to branches patterning. It is playing a key role, along with *Shh*, in patterning the branches formation in the developing lung.

Mesenchymal Fgf10 acts as chemoattractant on the targeted epithelial cells. A correct distribution of *Fgf10* in the lung bud is crucial for the correct patterning of the branches (Fig D2). The spatial distribution of *Fgf10* is controlled *via* Shh (Kim et al., 2009) (Fig D2).

In the fin regenerate, we used *fgf10* antisense RNA probe to assess the expression profile of *fgf10* during branching morphogenesis. However, we could not detect any expression using ISH, indicating that, either *fgf10* is not expressed in the regenerate, or ISH is not sensitive enough to detect the amount of *fgf10* transcripts present in the regenerate. If *fgf10* is expressed in the regenerate, variations of its expression during fin regeneration may be assessed using qRT-PCR. If no *fgf10* expression can be detected, other Fgf factors should be investigated.

In order to establish a proper lung and salivary gland patterning in mice, the distribution of *Shh* needs to be finely tuned during branching morphogenesis. Very often, a feed-back loop is involved in controlling the expression pattern of *Shh* during branching morphogenesis (see Introduction for details).

The expression pattern of *Shh* in the lung is controlled by Hhip, that downregulates *Shh* in the central part of the bud (Chuang et al., 2003) (Fig D2). Interestingly, *hhip* expression was detected in the central part of the newly formed osteoblats (Jing Zhang, unpublished results). This suggests that, similarly to the lung model, a local inhibition of the Hedgehog pathway in the medial part of the newly formed hemiray is taking place during ray branching morphogenesis. We therefore suggest that *shha* central downregulation is involved in patterning the fin rays branches. In the branching ray, Hhip could be mediating the distal split of the *shha* expression domain in 'Early splitting' stage, and the pronounced cell separation in the 'Heart shaped'

stage of branching morphogenesis in the fin ray (Fig D3 B and C, respectively).

In contrast to other rays, the lateral ray of the fin is surrounded by only one interray. It has previously been shown that these rays are able to bifurcate if grafted in a 'bifurcation-prone' environment (surrounded by two interrays), suggesting that their natural location neighboring a single interray can be the reason of the non-bifurcation of these rays (Murciano et al., 2002). While we observed that some of the lateral-most, non-bifurcating rays are undergoing the 'Early splitting' stage, none of them undertook the 'Heart shape' stage for *shha* expression. These rays rather present a unique *shha* expression domain that resembles half of the *shha* expression domain as seen for the rays that bifurcate, recalling 'half-heart'. It is possible that the neighboring interray, through producing a *shha* maintenance signal (represented as Factor Y in the schema Fig D3, C), restricts the expression of *shha* on both lateral extremities of the ray. As the lateral-most ray has a single neighboring inter-ray tissue, the hypothetical inter-ray *shha* maintenance signal is produced on a unique side of the lateral hemiray. Thus, *shha* expression is induced only in the inter-ray-neighboring side of the lateral ray. This hypothesis is supported by the observation of *shha* expression on the interray-neighboring lateral side of the lateral-most ray.

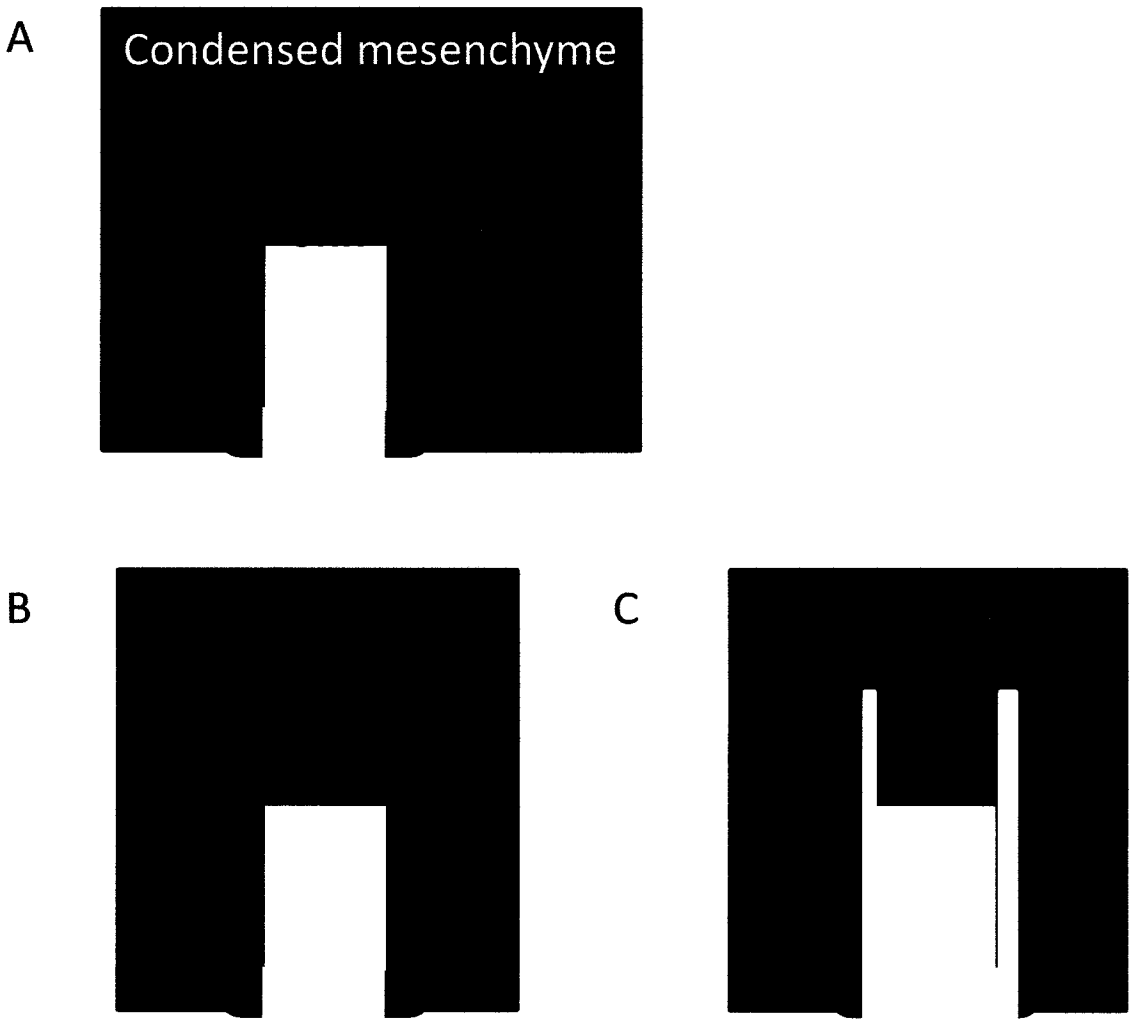

Figure D1: cleft formation during salivary gland branching moprhogenesis

Figure D1: Branching morphogenesis in the salivary gland. (A) The initiation of the salivary gland morphogenesis is ensured by a budding of the epithelial cells (red) in the surrounding mesenchymal tissue (blue). Epithelial cells at the tip of the bud express *Shh*, which promotes cell proliferation and bud elongation within the mesenchyme (yellow arrows). (B) Extracellular matrix (Fibronectin, GAG and Col) accumulates in the central part of the growing bud (green arrow), forming a plug (brown). The plug impairs further bud elongation in the central region, while proliferation and growth are maintained on both lateral sides (yellow arrows). (C) The formation of the cleft, combined with the maintained lateral cell proliferation, leads to the formation of proliferating epithelial cells. These two 'buds' further elongate within the mesenchyme (yellow arrows) and eventually undergoes the same process to form the final tree-like structure (not represented).

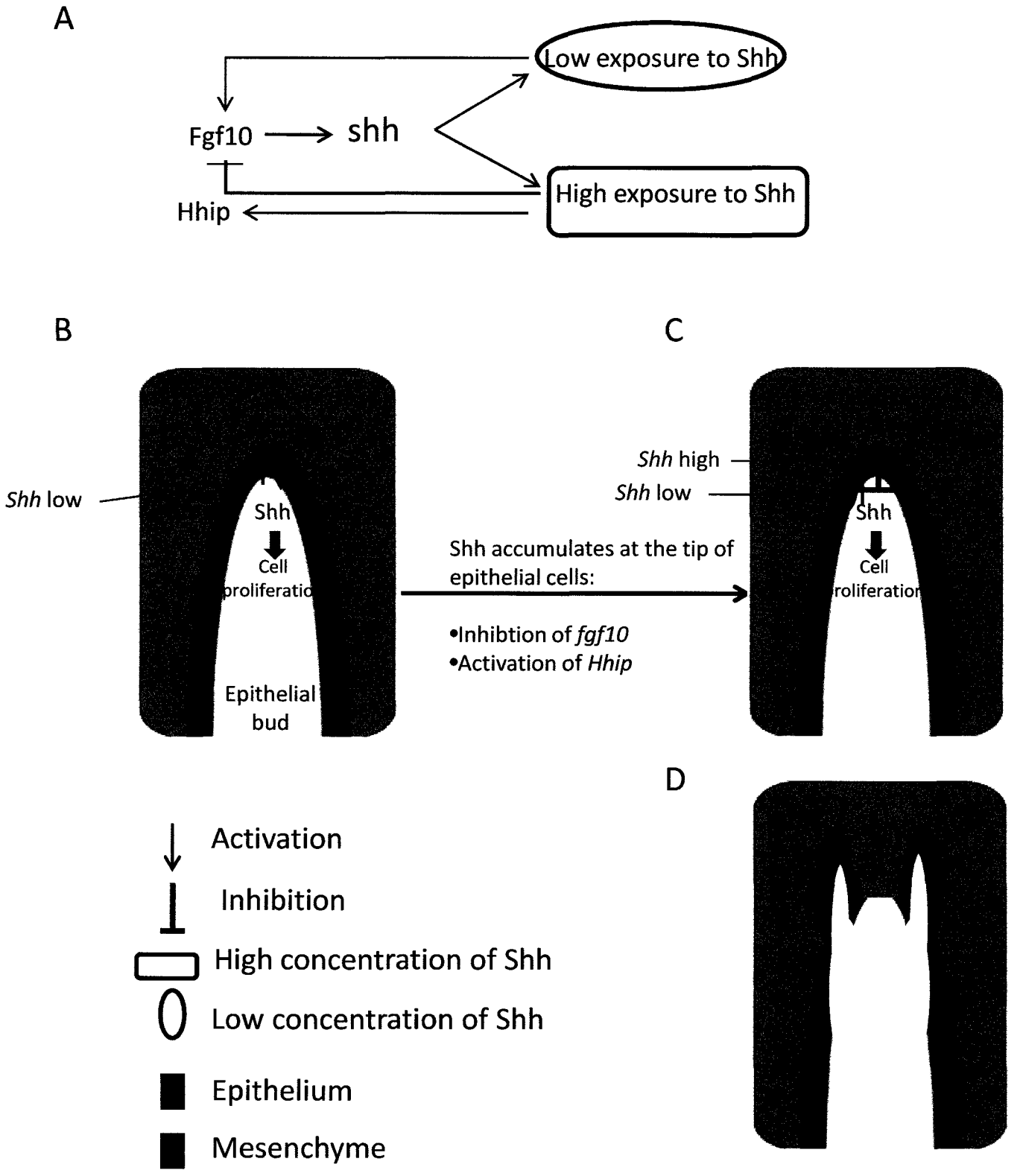

Figure D2: Lung branching morphogenesis

Figure D2: Branching morphogenesis in the developing lung. (A) Simplified diagram showing the effect of low and high concentration of Shh secreted by epithelial cells on mesenchymal cells. Epithelial cells express *Shh*, which, at low doses, positively regulates *Fgf10* expression in the neighbouring mesenchyme, while it negatively regulates its expression at high level. Mesenchymal cells exposed to high doses of Shh also express Hhip, which is the natural inhibitor of *Shh*. (B) In the lung bud, Fgf10 activates *Shh* expression in the epithelial cells located at the tip of the bud. It also induces epithelial cells proliferation and acts as chemo-attractant, thus ensuring the growth of the bud. Low doses of Shh initially secreted promote the expression of mesenchymal *Fgf10* (blue circle). (C) Accumulation of the secreted amount of Shh eventually leads to a 'Shh High dose': mesenchymal cells centrally located are exposed to high level of Shh, which negatively regulates *Fgf10* and stimulates the expression of Hhip (yellow box). Meanwhile, lateral mesenchymal cells surrounding the epithelial bud are exposed to a low level of Shh, thus maintaining the *Fgf10* expression laterally (blue circle). (D) Localized expression of *Fgf10* induces the restriction of the expression of *Shh* on both lateral sides of the bud, and localized cell growth, which leads to branching morphogenesis.

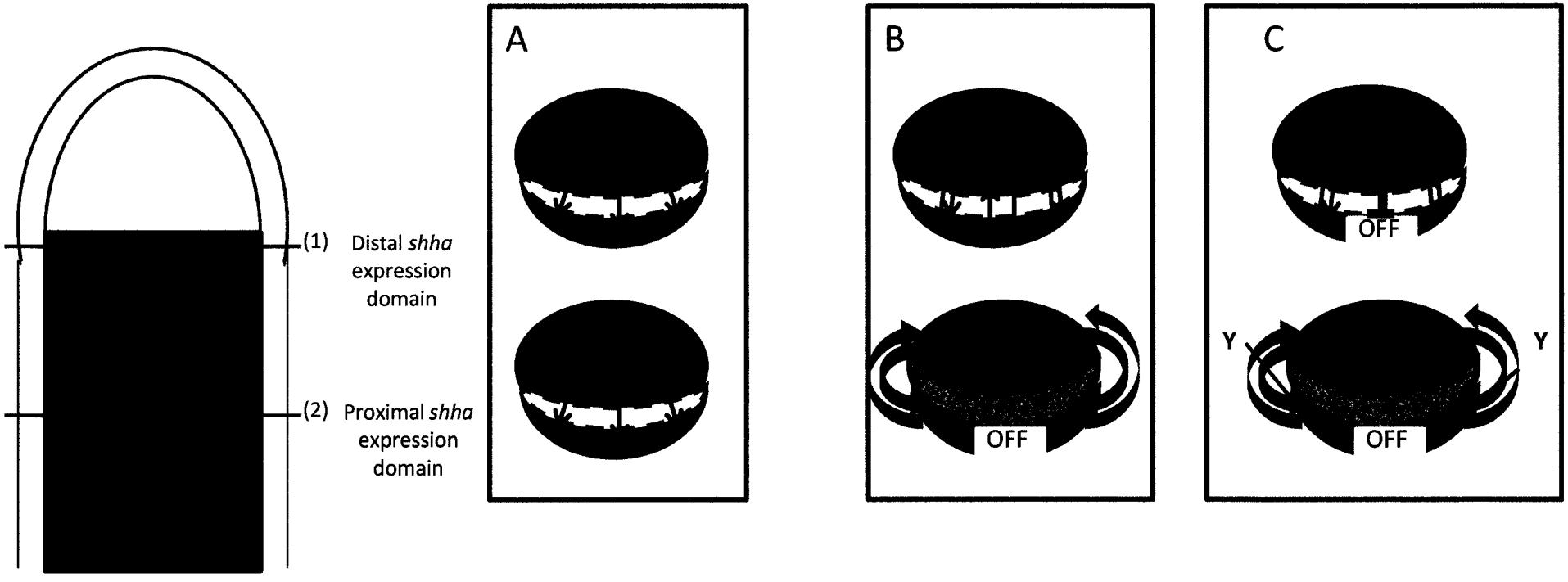

Figure D3: Proposed model for branching morphogenesis in the regenerating fin ray

Figure D3: Schematic representation of the proposed model for branching morphogenesis in the regenerating fin ray. On the left is represented the *shha*–expression domain, with transverse section at the distal level (1) and proximal level (2).

(A) At 2 dpa, a hypothetical factor X secreted by mesenchymal cells (red) activates the expression of *shha* in the basal layer of the epidermis (green), which in turn helps maintaining factor X expression. These epithelial-mesenchymal interactions are possible at this time point because of the very thin/absent bone matrix at this level along the proximal-distal axis.

(B) As Shha concentration increases, the mesenchymal cells in the centre of the domain are exposed to a high level of Shha, which activates the expression of *hhip*. High concentration of Shha also inhibits the expression of *factorX*. However, the expression level of *hhip* is not high enough to completely inhibit the expression of *shha*. This situation results in the short splitting observed in the distal part of the *shha* expression domain (A, top). At the proximal level of the *shha* expression domain (bottom), the osteoblasts are secreting a bone matrix that did accumulate and forms a thick bone, impairing the epithelial-mesenchymal interaction to occur. Thus, at this level, Factor X is not able to activate the epithelial *shha* expression. However, on the two lateral sides of the hemiray, the epithelium is still communicating with the mesenchymal cells (see hemiray structure FigR1). Thus, on the lateral sides at the proximal level, *shha* expression is maintained by Factor X and *vice versa* (red arrow indicates a signal from the mesenchyme to the epithelium, green arrow indicates a signal from the epithelium to the mesenchyme).

(C) shha accumulates and eventually, its concentration is high enough to completely turn off *factor X* expression in the central mesenchymal cells *Hhip* expression also contributes to shut-off *shha* expression, which leads to the large splitting that is observed at 4 5 dpa during the 'Heart-shape' stage (top, OFF) The mesenchymal cells located at the two lateral sides of the hemiray are exposed to a low concentration of Shha, thus maintaining *factor X* expression, and inducing the expression of *shha* in the basal layer of the epidermis located on the lateral sides of the hemiray (top) The joint action of maintaining *shha* expression on the lateral sides and inhibiting it in the central part of the expression domain leads to the formation of the 'Heart-shape' expression domain Y represents a hypothetical factor secreted by interray mesenchymal cells that would also promote the expression of *shha* on the lateral sides At the proximal level, a mechanism similar to what was previously described in (B, proximal) takes place to maintain *shha* on lateral sides of the hemiray only (bottom) In fact, epithelial-mesenchymal interactions are not interrupted on lateral sides at this level, allowing Factor X to maintain the expression the *shha* This situation does not apply to the central region, where epithelial-mesenchymal interations are impaired by the bone matrix

2. *shha* expression domain splitting is required for patterning branching morphogenesis: effect on osteoblasts differentiation and/or on cell proliferation?

Laser ablation of *shha*-expressing cells has demonstrated that the transient absence of *shha*-expressing cells from the regenerate leads to a delay in branches formation. How *shha*-expressing cells are involved in promoting branches formation remains not clear?

Previous studies have shown that, in the fin ray, *shha* is able to induce ectopic bone deposition through the induction of its downstream target *bmp2b*. However, ectopic bone deposition was only observed in interray mesenchyme, suggesting that *shha* is able to induce mesenchymal cells to differentiate into osteoblasts (Smith et al., 2006). During branching morphogenesis, the down-regulation of *shha* in the central part of the hemiray may be inducing a restriction of *bmp2b* expression in adjacent mesenchymal cells, on both lateral sides of the hemiray. As *bmp2b* is not expressed in the central hemiray anymore, osteoblasts differentiation no longer occurs medially, restricting the differentiation of the osteoblasts on lateral sides. This directed site of osteoblasts differentiation may promote branches formation. Thus, *shha* might be promoting a 'localized osteoblasts differentiation' through restricting *bmp2b* expression to lateral sides.

This hypothesis is supported by expression profile analysis of *collagen10a1 (col10a1),* which is expressed in both epithelial and mesenchymal cells in the differentiation zone, and *dlx5a,* which is expressed in the newly differentiated osteoblasts, extending further medially in the mesenchymal tissue (Jing Zhang, unpublished data). These

markers are expressed in a single set of cells, located medially to the hemiray, until 5 dpa. At 5 dpa, shortly after the *shha*-expressing cells have undertaken the 'Heart shape' stage, osteoblasts separate in two distinct domains (Fig D4). This suggests a chronological succession of events, starting with *shha*-expressing cells separation, followed by osteoblasts separation, with the first event possibly inducing the second. In fact, the osteoblasts separation appears to be dependent on the *shha*-expressing cells separation: analysis of the expression pattern of *col10a1* and *dlx5a* in the rays in which *shha*–expressing cells were ablated, and that showed a delayed branching morphogenesis, has shown that osteoblasts separation is also delayed. In fact, in the 6 dpa ablated rays, 3 days after the ablation of the *gfp*-expressing cells, the *col10a1*-expressing cells, as well as the *dlx5a*-expressing cells are still observed in a single domain (Fig D4 B). The osteoblasts separation in control rays normally occurs at 5 dpa, one day after the separation of *shha*-expressing cells. As the osteoblasts separation is delayed when the *shha*-expressing cells are temporarily removed from the regenerate, *shha*-expressing cells might direct osteoblasts separation. Their temporary absence results in a delayed 'separation signal', that explains the delayed osteoblasts separation and bifurcation.

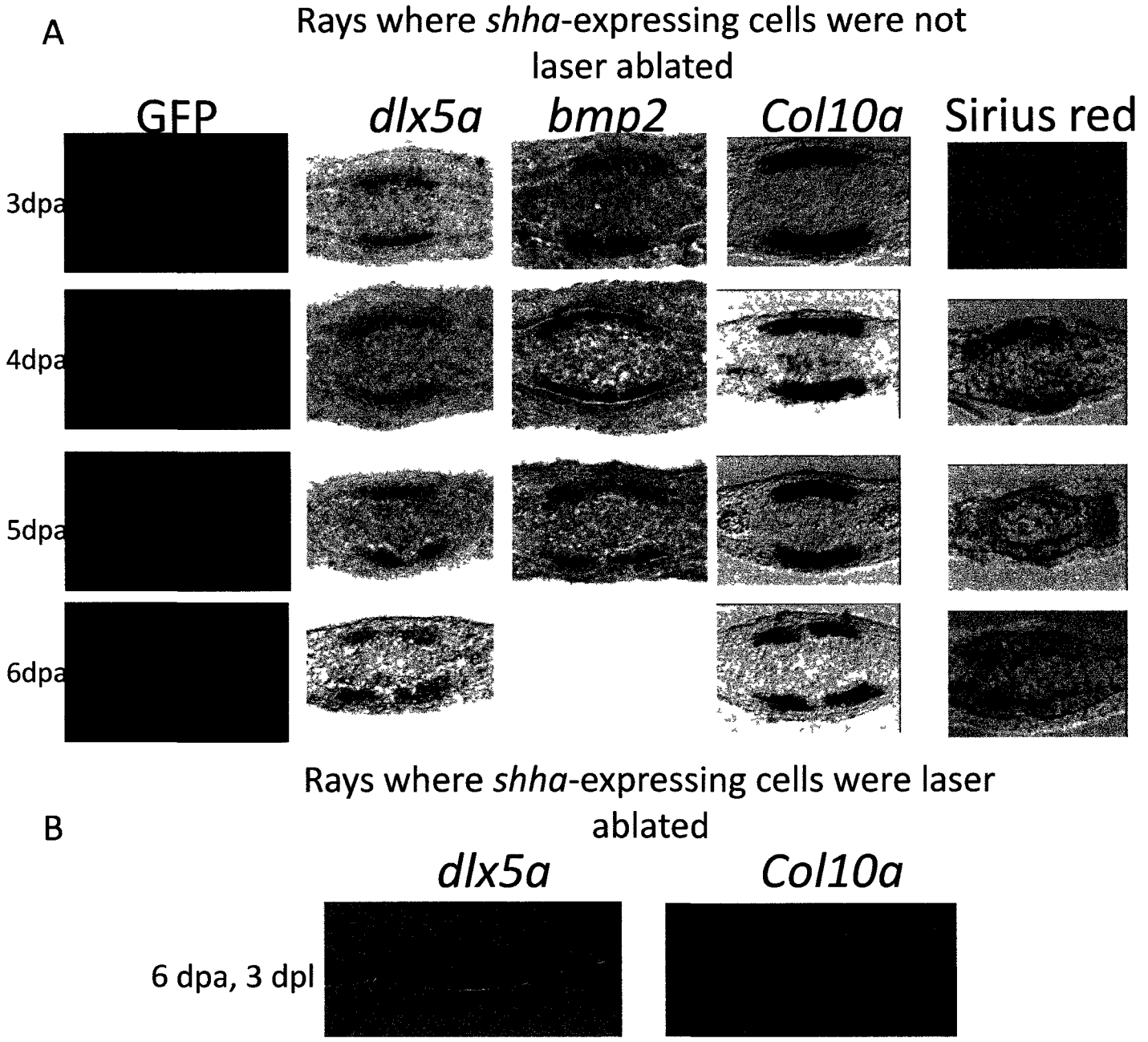

Figure D4: Gene expression analysis in rays in which *shha*-expressing cells were not (A) or were (B) ablated

Figure D4: Gene expression analysis in rays in which *shha*-expressing cells were not (A) or were (B) ablated, in *Tg 2,4shha:gfp:ABC#*15 regenerates.

(A) Time course analysis of GFP expression, and of genes expressed in the newly differentiated osteoblasts (*dlx5a*) only, or in both newly differentiated osteoblasts and *shha*-expressing cells (*bmp2b* and *col10a*). Pico Sirius red staining allows to visualize the bone matrix. At 3 and 4 dpa, *shha*–expressing cells form a unique domain of expression (as seen with GFP expression). At 5dpa this domain separates into two subgroups. The separation of the newly differentiated osteoblasts (c.f. *dlx5a*, *bmp2b* and *col10a*) occurs at 6 dpa . (B) Expression analysis of *dlx5a* and *col10a* in the laser-ablated rays, at 6 dpa shows the absence of cell separation normally occurring at this time point (6dpa, A).

What we call 'separation signal' can actually be a signal that directs osteoblasts differentiation, osteoblasts proliferation or osteoblasts migration toward the source of *shha*-expressing cells.

One hypothesis to explain the delayed growth could be that, *shha*-expressing cells direct osteoblasts progenitor's proliferation, rather than interfering with the differentiation of osteoblasts. In other organs, Shh has been shown to possess a mitotic activity (Johnson et al., 1996; Towers et al., 2008). Similarly, during zebrafish caudal fin regeneration, the Hh pathway has already been shown to be required for the maintenance of the regenerate outgrowth. The positive effect of the Hh pathway on cell proliferation rate has also previously been shown, as Hh inhibition *via* cyclopamine treatment leads to regenerate growth arrest and inhibition of blastema cells proliferation (Quint et al., 2002).

During branching morphogenesis, we were able to demonstrate that blastema cells are not the only cell population that is undergoing active proliferation in the regenerate: a subpopulation of cells, more proximal than the blastema, belonging to the differentiation zone mesenchyme, extending toward the interray mesenchyme and occasionally including cells from the basal layer of the epidermis, is also actively proliferating. These cells are located at the same level along the proximal-distal axis as the *shha*–expressing cells. At 3dpa, 4 dpa and 6dpa, the proliferation rate was shown to be higher on the two lateral sides of the ray, in mesenchymal cells that are adjacent to the basal layer of the epidermis. At these time points, *shha* –expression is also restricted to the lateral sides of the hemirays. Thus, this pattern of cell proliferation, which correlates with the distribution of the Shha activity, suggests a link between the Hh signaling pathway and the proximal cells proliferation. Through

inducing a site-directed proliferation, Hh might regulate branching morphogenesis, as it might induce cell proliferation restricted to both lateral sides of the ray. When, *shha*-expressing cells are present in a single domain, they would induce osteoblasts proliferation in a single domain fashion, ensuring the longitudinal outgrowth of the ray. As *shha*-expressing cells separate, they induce lateral cell proliferation only. Medially located osteoblasts are deprived from a Shh pro-mitotic signal and stop to proliferate, while lateral osteoblasts, that are still receiving a Shh signal, keeps proliferating, leading to branching formation. This hypothesis is supported by the proliferation analysis done in the fin regenerate.

However, as the method of fixation used to perform the PCNA antibody staining seems to affect the GFP protein conformation (fluorescence is lost and GFP antibody binding is no longer efficient), we are not able, yet, to precisely localize the proliferative cells in relation to the *shha* –expressing cells. We will need to optimize our antibody staining protocol (for immunodetection of GFP, performed in the *2.4shha:gfp:*ABC#15 transgenic line) to adapt it to the PCNA antibody staining in order to visualize both populations of cells (proliferative cells and *shha*-expressing cells).

3. Future direction: to identify new genes that are potentially regulating the branching morphogenesis

We have demonstrated that the *shha*-expressing cells are involved in the branches formation during fin ray regeneration. As demonstrated using the laser ablation experiments, we think that this cell population is directing the branching morphogenesis initiation, and is necessary to maintain this process.

To identify genes that are differentially regulated in the *shha*-expressing cells during

the branching morphogenesis process, and that might be participating to the branching, we want to perform a microarray analysis on these cells. To identify genes involved in the branching process, we will consider the 2 dpa time point as our 'reference', since it shows a single set of *shha*-expressing cells and should not be expressing branching inducing genes yet. We will sort the GFP+ cells in 2 dpa regenerates from the *2.4shh:gfp:ABC* #15 line, along with the two time points that are considered to be important for the branching patterning: 3.5 dpa ('Early splitting') and 4.5 dpa (Heart shape). The genetic profile of the GFP+ cells at these time points will be compared with the gene expression of the 2 dpa GFP+ cells. Thus, we will be able to identify the genes that are differentially regulated during 'Early splitting' and 'Heart shape' stages. We already tested several protocols for cell trypsinisation (to sort the GFP+ cells) in the fin rays and determined the appropriate parameters that allow an efficient cell separation while conserving the cellular integrity, the GFP signal and the mRNA of the cells (see **Appendix** for details).

4. Long-term ablation using the NTR/MTZ: future perspective

As mentioned earlier, laser cell ablation did not allow long-term ablation of the *shha*-expressing cells. To assess this long-term effect, we opted for the NTR/MTZ mediated cell ablation. We did not explore the possibility of using morpholino knock-down of the *shha* gene for two reasons: 1) the morpholino effects are also transient, and thus does not allow to down-regulate the *shha* expression for a long-term, and 2) as *shha* is expressed in the basal layer of the epidermis, and as the morpholino injection in the fin is done in the blastema followed by electroporation, the chances that the morpholino would diffuse from the blastema, through the

basement membrane and the newly secreted bone matrix to reach the targeted cells are very low. As the targeted cell population is very spatially restricted (one layer of cells surrounding each hemiray), it will be very hard to inject directly within this cell population. Thus, cell ablation seems to be the only method that would allow inhibiting the Shh pathway from the fin regenerate. NTR/MTZ is based on the establishment of a transgenic line in which the expression of the transgene (the *nitroreductase* gene) is specifically induced in the targeted cell population. The NTR itself is not harmful for the expressing cells, and has the ability to convert its substrate, the MTZ, into a cytotoxic agent. Thus, following the addition of the MTZ, the targeted cell population will be able to convert the MTZ into a cytotoxic agent and to undergo apoptosis. We wanted to establish a stable transgenic line in which the NTR expression during regeneration will be restricted to the *shha*-expressing cells. Once the line will be obtained, cell ablation will be easily achieved. As long as the fish are kept in MTZ, the absence of the *shha*-expressing cells should be maintained. As MTZ was shown to efficiently diffuse through embryonic tissue to reach internal organs (pancreas, liver and heart) (Curado et al., 2007), the diffusion of the MTZ through fin tissue should be easily achieved. However, if the MTZ is unable to reach target cell population through diffusion, we will need to directly inject it in the fin regenerate.

We will proceed to the downstream analysis on the *shha* –expressing cells ablated rays once the MTZ long-term ablation protocol will be set-up: we will use the proper concentration of MTZ to efficiently ablate all the *shha*-expressing cells for up to the longest exposure time that can be tolerated by the fish. We will analyze the regenerate morphology (assessing the growth rate, the branching morphogenesis and the bone matrix thickness), the proliferation profile in the differentiation zone and the gene expression profile. We will perform ISH for markers of the osteoblasts differentiation

(*runx2a*, *runx2b*, *osx*, *ihha*), genes from the Fgf pathway (*fgfr1*, *fgf10*, *fgf8*) and Wnt pathway (*wnt5a*, *lef1*) to identify potential cross talks that are taking place between the Hh pathway and other pathways, and also genes that we will identify as differentially regulated during branching morphogenesis process in the fin using the microarray profiling, (see **3. Future direction)**

To conclude, we have demonstrated that *shha* expression is differentially regulated during branching morphogenesis process and that its expression pattern characterizes distinct stages of the branch formation process Based on the *shha* expression profile during branching morphogenesis, along with PCNA staining, we propose a branching morphogenesis model in which *shha*-expressing cells are directing the branching morphogenesis, through inducing a site-directed cell proliferation This hypothesis seems to be in agreement with what is known about the mitotic activity of Shh and previously suggested role of the Hh pathway in maintaining the regenerate outgrowth It also allows formulating a plausible interpretation of the branching delay that is observed in the rays in which *shha*-expressing cells were temporarily removed However, this hypothesis needs to be further confirmed, by doing precise co-localization experiments, and by assessing the proliferation rate and proliferation profile in rays in which the *shha*-expressing cells would have been removed One way to assess co-localization of *shha* expression and proliferative cells would be to optimize the double antibody staining with PCNA and GFP antibody, or set-up a protocol for double *in situ* hybridization using fluorescent probes for *shha* and markers of cell proliferation, such as *cyc-D*

We also set up a protocol to trypsinize cells from fin regenerates, which will be used to sort the *shha*-expressing cells and to identify novel genes that are differentially

regulated in these cells to influence the branching morphogenesis. This will be done using the microarray approach.

The long-term ablation system using the MTZ is in progress, and we are generating the stable transgenic line by re-injecting our construct in zebrafish embryos. This ablation system will be of a great help to elucidate the role of the *shha*-expressing cells, allowing us to increase our sample numbers, but also to conduct different types of downstream analysis in a reproducible fashion.

Together, the microarray results, as well as results obtained from the long-term ablation of the *shha*-expressing cells, will allow us to better understand the fin ray branching morphogenesis process, and either confirm, or infirm our proposed hypothesis. In a larger perspective, this project will allow to identify novel regulator of, and better understand, the branching morphogenesis process in different organs that undergo branching.

References

Abler LL, Mansour SL, Sun X. 2009. Conditional gene inactivation reveals roles for Fgf10 and Fgfr2 in establishing a normal pattern of epithelial branching in the mouse lung. Dev Dyn 238:1999-2013.

Abzhanov A, Rodda SJ, McMahon AP, Tabin CJ. 2007. Regulation of skeletogenic differentiation in cranial dermal bone. Development 134:3133-3144.

Affolter M, Zeller R, Caussinus E. 2009. Tissue remodelling through branching morphogenesis. Nat Rev Mol Cell Biol 10:831-842.

Akimenko MA, Mari-Beffa M, Becerra J, Geraudie J. 2003. Old questions, new tools, and some answers to the mystery of fin regeneration. Dev Dyn 226:190-201.

Altaner C. 2008. Prodrug cancer gene therapy. Cancer Lett 270:191-201.

Andersson ER, Lendahl U. 2009. Regenerative medicine: a 2009 overview. J Intern Med 266:303-310.

Avaron F, Hoffman L, Guay D, Akimenko MA. 2006. Characterization of two new zebrafish members of the hedgehog family: atypical expression of a zebrafish indian hedgehog gene in skeletal elements of both endochondral and dermal origins. Dev Dyn 235:478-489.

Aza-Blanc P, Lin HY, Ruiz i Altaba A, Kornberg TB. 2000. Expression of the vertebrate Gli proteins in Drosophila reveals a distribution of activator and repressor activities. Development 127:4293-4301.

Becerra J, Montes GS, Bexiga SR, Junqueira LC. 1983. Structure of the tail fin in

teleosts. Cell Tissue Res 230:127-137.

Bellusci S, Furuta Y, Rush MG, Henderson R, Winnier G, Hogan BL. 1997a. Involvement of Sonic hedgehog (Shh) in mouse embryonic lung growth and morphogenesis. Development 124:53-63.

Bellusci S, Grindley J, Emoto H, Itoh N, Hogan BL. 1997b. Fibroblast growth factor 10 (FGF10) and branching morphogenesis in the embryonic mouse lung. Development 124:4867-4878.

Bernfield M, Banerjee SD. 1982. The turnover of basal lamina glycosaminoglycan correlates with epithelial morphogenesis. Dev Biol 90:291-305.

Bernfield MR. 1970. Collagen synthesis during epitheliomesenchymal interactions. Dev Biol 22:213-231.

Bridgewater JA, Knox RJ, Pitts JD, Collins MK, Springer CJ. 1997. The bystander effect of the nitroreductase/CB1954 enzyme/prodrug system is due to a cell-permeable metabolite. Hum Gene Ther 8:709-717.

Bridgewater JA, Springer CJ, Knox RJ, Minton NP, Michael NP, Collins MK. 1995. Expression of the bacterial nitroreductase enzyme in mammalian cells renders them selectively sensitive to killing by the prodrug CB1954. Eur J Cancer 31A:2362-2370.

Brittijn SA, Duivesteijn SJ, Belmamoune M, Bertens LF, Bitter W, de Bruijn JD, Champagne DL, Cuppen E, Flik G, Vandenbroucke-Grauls CM, Janssen RA, de Jong IM, de Kloet ER, Kros A, Meijer AH, Metz JR, van der Sar AM, Schaaf MJ, Schulte-Merker S, Spaink HP, Tak PP, Verbeek FJ,

Vervoordeldonk MJ, Vonk FJ, Witte F, Yuan H, Richardson MK. 2009. Zebrafish development and regeneration: new tools for biomedical research. Int J Dev Biol 53:835-850.

Broughton G, 2nd, Janis JE, Attinger CE. 2006. The basic science of wound healing. Plast Reconstr Surg 117:12S-34S.

Brown AM, Fisher S, Iovine MK. 2009. Osteoblast maturation occurs in overlapping proximal-distal compartments during fin regeneration in zebrafish. Dev Dyn 238:2922-2928.

Bryant SV, Endo T, Gardiner DM. 2002. Vertebrate limb regeneration and the origin of limb stem cells. Int J Dev Biol 46:887-896.

Burglin TR. 2008. The Hedgehog protein family. Genome Biol 9:241.

Byrd N, Becker S, Maye P, Narasimhaiah R, St-Jacques B, Zhang X, McMahon J, McMahon A, Grabel L. 2002. Hedgehog is required for murine yolk sac angiogenesis. Development 129:361-372.

Chamoun Z, Mann RK, Nellen D, von Kessler DP, Bellotto M, Beachy PA, Basler K. 2001. Skinny hedgehog, an acyltransferase required for palmitoylation and activity of the hedgehog signal. Science 293:2080-2084.

Chuang PT, Kawcak T, McMahon AP. 2003. Feedback control of mammalian Hedgehog signaling by the Hedgehog-binding protein, Hip1, modulates Fgf signaling during branching morphogenesis of the lung. Genes Dev 17:342-347.

Curado S, Anderson RM, Jungblut B, Mumm J, Schroeter E, Stainier DY. 2007.

Conditional targeted cell ablation in zebrafish: a new tool for regeneration studies. Dev Dyn 236:1025-1035.

Curado S, Stainier DY, Anderson RM. 2008. Nitroreductase-mediated cell/tissue ablation in zebrafish: a spatially and temporally controlled ablation method with applications in developmental and regeneration studies. Nat Protoc 3:948-954.

Currie PD, Ingham PW. 1996. Induction of a specific muscle cell type by a hedgehog-like protein in zebrafish. Nature 382:452-455.

Davies JA. 2002. Do different branching epithelia use a conserved developmental mechanism? Bioessays 24:937-948.

Dessaud E, McMahon AP, Briscoe J. 2008. Pattern formation in the vertebrate neural tube: a sonic hedgehog morphogen-regulated transcriptional network. Development 135:2489-2503.

Dohle E, Fuchs S, Kolbe M, Hofmann A, Schmidt H, Kirkpatrick CJ. Sonic hedgehog promotes angiogenesis and osteogenesis in a coculture system consisting of primary osteoblasts and outgrowth endothelial cells. Tissue Eng Part A 16:1235-1237.

Dyer MA, Farrington SM, Mohn D, Munday JR, Baron MH. 2001. Indian hedgehog activates hematopoiesis and vasculogenesis and can respecify prospective neurectodermal cell fate in the mouse embryo. Development 128:1717-1730.

Eblaghie MC, Reedy M, Oliver T, Mishina Y, Hogan BL. 2006. Evidence that autocrine signaling through Bmpr1a regulates the proliferation, survival and

morphogenetic behavior of distal lung epithelial cells Dev Biol 291 67-82

Echelard Y, Epstein DJ, St-Jacques B, Shen L, Mohler J, McMahon JA, McMahon AP 1993 Sonic hedgehog, a member of a family of putative signaling molecules, is implicated in the regulation of CNS polarity Cell 75 1417-1430

Ekker SC, Ungar AR, Greenstein P, von Kessler DP, Porter JA, Moon RT, Beachy PA 1995 Patterning activities of vertebrate hedgehog proteins in the developing eye and brain Curr Biol 5 944-955

Entesarian M, Matsson H, Klar J, Bergendal B, Olson L, Arakaki R, Hayashi Y, Ohuchi H, Falahat B, Bolstad AI, Jonsson R, Wahren-Herlenius M, Dahl N 2005 Mutations in the gene encoding fibroblast growth factor 10 are associated with aplasia of lacrimal and salivary glands Nat Genet 37 125-127

Farzan SF, Singh S, Schilling NS, Robbins DJ 2008 The adventures of sonic hedgehog in development and repair III Hedgehog processing and biological activity Am J Physiol Gastrointest Liver Physiol 294 G844-849

Fuse N, Maiti T, Wang B, Porter JA, Hall TM, Leahy DJ, Beachy PA 1999 Sonic hedgehog protein signals not as a hydrolytic enzyme but as an apparent ligand for patched Proc Natl Acad Sci U S A 96 10992-10999

Gardiner DM, Endo T, Bryant SV 2002 The molecular basis of amphibian limb regeneration integrating the old with the new Semin Cell Dev Biol 13 345-352

Geraudie J, Monnot MJ, Brulfert A, Ferretti P 1995 Caudal fin regeneration in wild type and long-fin mutant zebrafish is affected by retinoic acid Int J Dev Biol

39:373-381.

Grobstein C, Cohen J. 1965. Collagenase: effect on the morphogenesis of embryonic salivary epithelium in vitro. Science 150:626-628.

Han M, Yang X, Farrington JE, Muneoka K. 2003. Digit regeneration is regulated by Msx1 and BMP4 in fetal mice. Development 130:5123-5132.

Han M, Yang X, Taylor G, Burdsal CA, Anderson RA, Muneoka K. 2005. Limb regeneration in higher vertebrates: developing a roadmap. Anat Rec B New Anat 287:14-24.

Ho L, Alman B. Protecting the hedgerow: p53 and hedgehog pathway interactions. Cell Cycle 9:506-511.

Hoffman MP, Kidder BL, Steinberg ZL, Lakhani S, Ho S, Kleinman HK, Larsen M. 2002. Gene expression profiles of mouse submandibular gland development: FGFR1 regulates branching morphogenesis in vitro through BMP- and FGF-dependent mechanisms. Development 129:5767-5778.

Hsu CC, Hou MF, Hong JR, Wu JL, Her GM. Inducible male infertility by targeted cell ablation in zebrafish testis. Mar Biotechnol (NY) 12:466-478.

Hynes M, Stone DM, Dowd M, Pitts-Meek S, Goddard A, Gurney A, Rosenthal A. 1997. Control of cell pattern in the neural tube by the zinc finger transcription factor and oncogene Gli-1. Neuron 19:15-26.

Ingham PW, McMahon AP. 2001. Hedgehog signaling in animal development: paradigms and principles. Genes Dev 15:3059-3087.

Jaskoll T, Abichaker G, Witcher D, Sala FG, Bellusci S, Hajihosseini MK, Melnick M 2005 FGF10/FGFR2b signaling plays essential roles during in vivo embryonic submandibular salivary gland morphogenesis BMC Dev Biol 5 11

Jaskoll T, Leo T, Witcher D, Ormestad M, Astorga J, Bringas P, Jr, Carlsson P, Melnick M 2004 Sonic hedgehog signaling plays an essential role during embryonic salivary gland epithelial branching morphogenesis Dev Dyn 229 722-732

Johnson RL, Rothman AL, Xie J, Goodrich LV, Bare JW, Bonifas JM, Quinn AG, Myers RM, Cox DR, Epstein EH, Jr, Scott MP 1996 Human homolog of patched, a candidate gene for the basal cell nevus syndrome Science 272 1668-1671

Kim HR, Richardson J, van Eeden F, Ingham PW Gli2a protein localization reveals a role for Iguana/DZIP1 in primary ciliogenesis and a dependence of Hedgehog signal transduction on primary cilia in the zebrafish BMC Biol 8 65

Kim N, Yamamoto H, Pauling MH, Lorizio W, Vu TH 2009 Ablation of lung epithelial cells deregulates FGF-10 expression and impairs lung branching morphogenesis Anat Rec (Hoboken) 292 123-130

Krauss S, Concordet JP, Ingham PW 1993 A functionally conserved homolog of the Drosophila segment polarity gene hh is expressed in tissues with polarizing activity in zebrafish embryos Cell 75 1431-1444

Laforest L, Brown CW, Poleo G, Geraudie J, Tada M, Ekker M, Akimenko MA 1998 Involvement of the sonic hedgehog, patched 1 and bmp2 genes in patterning of the zebrafish dermal fin rays Development 125 4175-4184

Lee Y, Hami D, De Val S, Kagermeier-Schenk B, Wills AA, Black BL, Weidinger G, Poss KD. 2009. Maintenance of blastemal proliferation by functionally diverse epidermis in regenerating zebrafish fins. Dev Biol 331:270-280.

Mackie EJ, Ahmed YA, Tatarczuch L, Chen KS, Mirams M. 2008. Endochondral ossification: how cartilage is converted into bone in the developing skeleton. Int J Biochem Cell Biol 40:46-62.

Mari-Beffa M, Palmqvist P, Marin-Giron F, Montes GS, Becerra J. 1999. Morphometric study of the regeneration of individual rays in teleost tail fins. J Anat 195 (Pt 3):393-405.

Maun HR, Wen X, Lingel A, de Sauvage FJ, Lazarus RA, Scales SJ, Hymowitz SG. The hedgehog pathway antagonist 5E1 binds hedgehog at the pseudo-active site. J Biol Chem.

Mesnil M, Piccoli C, Tiraby G, Willecke K, Yamasaki H. 1996. Bystander killing of cancer cells by herpes simplex virus thymidine kinase gene is mediated by connexins. Proc Natl Acad Sci U S A 93:1831-1835.

Morgan TH. 1901. Regeneration and Liability to Injury. Science 14:235-248.

Morrisey EE, Hogan BL. Preparing for the first breath: genetic and cellular mechanisms in lung development. Dev Cell 18:8-23.

Muller F, Chang B, Albert S, Fischer N, Tora L, Strahle U. 1999. Intronic enhancers control expression of zebrafish sonic hedgehog in floor plate and notochord. Development 126:2103-2116.

Murciano C, Fernandez TD, Duran I, Maseda D, Ruiz-Sanchez J, Becerra J,

Akimenko MA, Mari-Beffa M. 2002. Ray-interray interactions during fin regeneration of Danio rerio. Dev Biol 252:214-224.

Nakatani Y, Nishidate M, Fujita M, Kawakami A, Kudo A. 2008. Migration of mesenchymal cell fated to blastema is necessary for fish fin regeneration. Dev Growth Differ 50:71-83.

Nusslein-Volhard C, Wieschaus E. 1980. Mutations affecting segment number and polarity in Drosophila. Nature 287:795-801.

Okubo T, Knoepfler PS, Eisenman RN, Hogan BL. 2005. Nmyc plays an essential role during lung development as a dosage-sensitive regulator of progenitor cell proliferation and differentiation. Development 132:1363-1374.

Patel VN, Rebustini IT, Hoffman MP. 2006. Salivary gland branching morphogenesis. Differentiation 74:349-364.

Pepicelli CV, Lewis PM, McMahon AP. 1998. Sonic hedgehog regulates branching morphogenesis in the mammalian lung. Curr Biol 8:1083-1086.

Pisharath H, Rhee JM, Swanson MA, Leach SD, Parsons MJ. 2007. Targeted ablation of beta cells in the embryonic zebrafish pancreas using E. coli nitroreductase. Mech Dev. 124(3):218-29

Poleo G, Brown CW, Laforest L, Akimenko MA. 2001. Cell proliferation and movement during early fin regeneration in zebrafish. Dev Dyn 221:380-390.

Poss KD, Keating MT, Nechiporuk A. 2003. Tales of regeneration in zebrafish. Dev Dyn 226:202-210.

Poss KD, Shen J, Nechiporuk A, McMahon G, Thisse B, Thisse C, Keating MT. 2000. Roles for Fgf signaling during zebrafish fin regeneration. Dev Biol 222:347-358.

Quint E, Smith A, Avaron F, Laforest L, Miles J, Gaffield W, Akimenko MA. 2002. Bone patterning is altered in the regenerating zebrafish caudal fin after ectopic expression of sonic hedgehog and bmp2b or exposure to cyclopamine. Proc Natl Acad Sci U S A 99:8713-8718.

Raya A, Consiglio A, Kawakami Y, Rodriguez-Esteban C, Izpisua-Belmonte JC. 2004. The zebrafish as a model of heart regeneration. Cloning Stem Cells 6:345-351.

Reginelli AD, Wang YQ, Sassoon D, Muneoka K. 1995. Digit tip regeneration correlates with regions of Msx1 (Hox 7) expression in fetal and newborn mice. Development 121:1065-1076.

Ribes V, Balaskas N, Sasai N, Cruz C, Dessaud E, Cayuso J, Tozer S, Yang LL, Novitch B, Marti E, Briscoe J. Distinct Sonic Hedgehog signaling dynamics specify floor plate and ventral neuronal progenitors in the vertebrate neural tube. Genes Dev 24:1186-1200.

Roelink H, Augsburger A, Heemskerk J, Korzh V, Norlin S, Ruiz i Altaba A, Tanabe Y, Placzek M, Edlund T, Jessell TM, et al. 1994. Floor plate and motor neuron induction by vhh-1, a vertebrate homolog of hedgehog expressed by the notochord. Cell 76:761-775.

Rohatgi R, Milenkovic L, Scott MP. 2007. Patched1 regulates hedgehog signaling at the primary cilium. Science 317:372-376.

Sakai T, Larsen M, Yamada KM. 2003. Fibronectin requirement in branching morphogenesis. Nature 423:876-881.

Sasaki H, Nishizaki Y, Hui C, Nakafuku M, Kondoh H. 1999. Regulation of Gli2 and Gli3 activities by an amino-terminal repression domain: implication of Gli2 and Gli3 as primary mediators of Shh signaling. Development 126:3915-3924.

Scherz PJ, McGlinn E, Nissim S, Tabin CJ. 2007. Extended exposure to Sonic hedgehog is required for patterning the posterior digits of the vertebrate limb. Dev Biol 308:343-354.

Shao J, Qian X, Zhang C, Xu Z. 2009. Fin regeneration from tail segment with musculature, endoskeleton, and scales. J Exp Zool B Mol Dev Evol 312:762-769.

Smith A, Avaron F, Guay D, Padhi BK, Akimenko MA. 2006. Inhibition of BMP signaling during zebrafish fin regeneration disrupts fin growth and scleroblasts differentiation and function. Dev Biol 299:438-454.

Smith A, Zhang J, Guay D, Quint E, Johnson A, Akimenko MA. 2008. Gene expression analysis on sections of zebrafish regenerating fins reveals limitations in the whole-mount in situ hybridization method. Dev Dyn 237:417-425.

Sobkow L, Epperlein HH, Herklotz S, Straube WL, Tanaka EM. 2006. A germline GFP transgenic axolotl and its use to track cell fate: dual origin of the fin mesenchyme during development and the fate of blood cells during regeneration. Dev Biol 290:386-397.

Spooner BS, Bassett K, Stokes B. 1985. Sulfated glycosaminoglycan deposition and processing at the basal epithelial surface in branching and beta-D-xyloside-inhibited embryonic salivary glands. Dev Biol 109:177-183.

St-Jacques B, Hammerschmidt M, McMahon AP. 1999. Indian hedgehog signaling regulates proliferation and differentiation of chondrocytes and is essential for bone formation. Genes Dev 13:2072-2086.

Towers M, Mahood R, Yin Y, Tickle C. 2008. Integration of growth and specification in chick wing digit-patterning. Nature 452:882-886.

Tucker AS. 2007. Salivary gland development. Semin Cell Dev Biol 18:237-244.

Varjosalo M, Taipale J. 2008. Hedgehog: functions and mechanisms. Genes Dev 22:2454-2472.

Vidal P, Dickson MG. 1993. Regeneration of the distal phalanx. A case report. J Hand Surg Br 18:230-233.

Vortkamp A, Lee K, Lanske B, Segre GV, Kronenberg HM, Tabin CJ. 1996. Regulation of rate of cartilage differentiation by Indian hedgehog and PTH-related protein. Science 273:613-622.

Westerfield M. 1995. The zebrafish Book. University of Oregon Press.

White JA, Boffa MB, Jones B, Petkovich M. 1994. A zebrafish retinoic acid receptor expressed in the regenerating caudal fin. Development 120:1861-1872.

Xie J, Murone M, Luoh SM, Ryan A, Gu Q, Zhang C, Bonifas JM, Lam CW, Hynes M, Goddard A, Rosenthal A, Epstein EH, Jr., de Sauvage FJ. 1998. Activating

Smoothened mutations in sporadic basal-cell carcinoma. Nature 391:90-92.

Xu Q, Guo L, Moore H, Waclaw RR, Campbell K, Anderson SA. Sonic hedgehog signaling confers ventral telencephalic progenitors with distinct cortical interneuron fates. Neuron 65:328-340.

Yokoyama H. 2008. Initiation of limb regeneration: the critical steps for regenerative capacity. Dev Growth Differ 50:13-22.

Yuasa T, Kataoka H, Kinto N, Iwamoto M, Enomoto-Iwamoto M, Iemura S, Ueno N, Shibata Y, Kurosawa H, Yamaguchi A. 2002. Sonic hedgehog is involved in osteoblast differentiation by cooperating with BMP-2. J Cell Physiol 193:225-232.

Zhang J, Wagh P, Guay D, Sanchez-Pulido L, Padhi BK, Korzh V, Andrade-Navarro MA, Akimenko MA. Loss of fish actinotrichia proteins and the fin-to-limb transition. Nature 466:234-237.

Zhao XF, Ellingsen S, Fjose A. 2009. Labelling and targeted ablation of specific bipolar cell types in the zebrafish retina. BMC Neurosci 10:107.

Zhu AJ, Scott MP. 2004. Incredible journey: how do developmental signals travel through tissue? Genes Dev 18:2985-2997.

Zunich SM, Douglas T, Valdovinos M, Chang T, Bushman W, Walterhouse D, Iannaccone P, Lamm ML. 2009. Paracrine sonic hedgehog signalling by prostate cancer cells induces osteoblast differentiation. Mol Cancer 8:12.

Appendix

Appendix I : Synthesis of the antisense RNA probes

List of the restriction enzymes used to linearize each plasmid and the appropriate RNA polymerase needed to synthesize the antisense RNA probes.

Plasmid's name	Vector	Size of the probe	Restriction enzyme used to linearize	RNA polymerases
Shh	pBS	2.5kb	EcoRI	T7
GFP	pDrive	0.7kb	XhoI	T7

Appendix II: Sequences of the primers used for different sub-cloning

1. ***2.4shh* promoter fragment from the original *2.4shh:gfp:AC* construct:**

- Forward primer: GTGTAGCAGAACTACGTCTG
- Reverse primer: TGGCTAGCAGGGTTTCTCG

2. **ar-A and ar-C enhancers sequence from the *2.4shh:gfp:AC* construct:**

- Forward primer: AACGTGGAGGGCCCGACGGATGAG
- Reverse primer: ACCTTCGCTAGCTTTGTGTGAGATGAAG

3. ***2.4shh:cfp-ntr* fragment from the *2.4shh:cfp-ntr* construct:**

- Forward primer: TTGTCGACGAATTGAGATTGTGTAGC
- Reverse primer: CTGTCGACTTCGGCGTATTGGTT

4. ***gfp* fragment from the *2.4shh:gfp* construct:**

- Forward primer: ATGAGTAAAGGAGAAGAACTTTTCA
- Reverse primer: TTTGTATAGTTCATCCATGCCA

Appendix III: Maps of the different constructs

Insertions of the original plasmid constructs that were used

2 4shh gfp AC

2 4shh gfp B

Tol2_MCS-*cfp-ntr*

T2-beta-globin-sp72

Intermediate constructs made during the different sub-cloning

*2.4shh*pDrive

arA-arCpDrive

arA-arB-arCpDrive

ABC-T2sp72

2.4shh:cfp-ntr

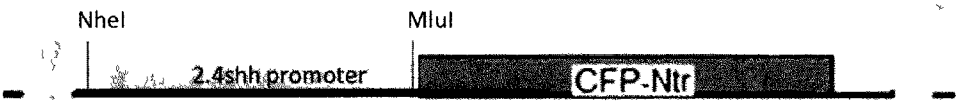

*2.4shh:cfp-ntr*pDrive

Final construct

2 4shh cfp-ntr ABC

Appendix IV: Protocol for the trypsinization of fin regenerates

Fin regenerates were collected at the desired time point, and transferred in 1.5 ml eppendorf tube, filled with 1xPBS. PBS was carefully removed and replaced with 0.5% Trypsin and 1mM EDTA in 1xPBS. Samples were incubated at 28.5 °C for 45 minutes, and triturated with a 200µl pipette every 15 minutes. The digestion was stopped by adding a solution of CaCl2 to a final concentration of 1mM, and Calf Serum (CS) to a final concentration of 10%. Both CaCl2 and Calf Serum were added to the mixture in the eppendhorf tube (adjusted according to the volume of PBS/trypsin added initially). Cells were centrifuged 3 minutes at 3000 rpm, and resuspended in 1%CS in 1xPBS. Filter the samples using Partec Cell Trics disposable filters (this step is recommended by the FACS facility, to avoid impurities that could damage the cell-sorting machine). In an ice box, take the samples to the MO-flow facility in the general hospital (contact informations: Paul Oleynic, poleynic@ohri.ca, Eye building (Critical care wing) on the 5th floor, phone extension is 73916)

The authorizations to reproduce figures from published papers were obtained from respective publishers. The official documents are available at the Department of Cellular and Molecular Medicine, Faculty of Medicine, University of Ottawa, or from the thesis author upon request.